Development and Validation of the Control Loops for the Haptic Interfaces of a Standard Manual Wheelchair Simulator

by

Ary Druva PIZARRO-CHONG

THESIS PRESENTED TO ÉCOLE DE TECHNOLOGIE SUPÉRIEURE IN PARTIAL FULFILLMENT FOR A MASTER'S DEGREE WITH THESIS IN ENGINEERING, CONCENTRATION IN HEALTH TECHNOLOGIES
M.A.Sc.

MONTREAL, JANUARY 5, 2021

ÉCOLE DE TECHNOLOGIE SUPÉRIEURE
UNIVERSITÉ DU QUÉBEC

BOARD OF EXAMINERS

THIS THESIS HAS BEEN EVALUATED

BY THE FOLLOWING BOARD OF EXAMINERS

Mr. Félix Chénier, Thesis Supervisor
Department of Systems Engineering at École de Technologie Supérieure

Mr. Rachid Aissaoui, President of the Board of Examiners
Department of Systems Engineering at École de Technologie Supérieure

Mr. François Routhier, External Evaluator
Department of Rehabilitation at Université Laval

THIS THESIS WAS PRESENTED AND DEFENDED

IN THE PRESENCE OF A BOARD OF EXAMINERS AND PUBLIC

ON DECEMBER 16, 2020

AT ÉCOLE DE TECHNOLOGIE SUPÉRIEURE

ACKNOWLEDGMENTS

I would like to thank, first and foremost, my thesis supervisor, Prof. Félix Chénier, without whom none of the work conducted in this thesis would have been possible. I learnt so much, not only about manual wheelchair simulators, but also about how to conduct research and how to develop an engineering prototype. For that, I am profoundly grateful. What's more, I will always remember his unwavering support during trying times, when I felt I would not have the strength to complete this thesis. I will always appreciate his kindness, his understanding and his never-ending encouragement.

I would also like to thank Prof. Rachid Aissaoui, director of the Movement Analysis Laboratory at the CRCHUM and the Health Technologies Laboratory at ETS where the manual wheelchair simulator is housed. His invigorating discussions offered fuel for my own inner discussions and understanding of the wheelchair-user and simulator systems.

I would like to thank Prof. Hironao Yamada for having graciously accepted to host me in his laboratory at Gifu University in Japan during the summer of 2018. I would like to thank the MITACS organization for having awarded me the MITACS-Japan Summer Research Award in 2018, which allowed me to go to Japan and conduct research on Prof. Yamada's manual wheelchair simulator. I would like to thanks my friends and labmates at the Human Support Systems laboratory for a great summer 2018: Huu Hung Ha, Masumi Nagata, Yuichiro Suzuki.

I would like to Prof. François Routhier for having accepted to be a member of the jury and to evaluate my thesis. I sincerely appreciate the time he took out of his busy schedule for this task.

I would also like to thank research associates Aiman Feghoul and Amir Chitour for their help when modifying the hardware and software, and during testing of the simulator. I would also like to thank Yolène Rosello, data coordinator at the LIO, and Marta Strzelczak, ethics officer

at the LIO, for the many helpful discussions regarding data and ethics for the wheelchair simulator project.

I would like to thank the Jewish Community Foundation, the Najman Family and Ruth Najman for providing me with a scholarship to pursue my research. My wish is that this research will one day help your daughter and other people with spinal cord injuries live a pain-free life.

I would like to thank my fellow labmates for technical and non-technical discussions, including Alberto, Ali, Bilal, Chandra, Iris, Sara S., Sarra B. and Valentin.

I would like to thank two people, Sara I. and Birte K., who hold a special place in my heart. Without the magical moments we shared together I would not as happy as I am today and would not have the strength to accomplish all that I accomplish. A handful of people played a very important role in my life, but unfortunately the winds of life led us on different paths: Ali, Kira, Lixian, Ioannis, Rixta, Zhenya. A special thanks to Maude who with her affectionate touch helped me stay calm, cool and collected during the stressful final stretches of my thesis. I would like to thank my close friends, in Montreal and abroad, who made difficult times more bearable and good times more joyful: Ghaiss (Giorgio), Siamak (Sam Abbas Fathi), Omer, Yoyo, Charlotte, Simona, Corinna, Anne-Mari. Some of you I've known for fifteen years, and some only six months, but the bond of friendship remains indelible. And I am especially grateful to Ana Maria for sharing with me the experience of dance and love during these difficult times.

Turning to my family, I would like to thank my favorite uncle, Gonzalo, and my late grandmother Mamá Chela, both of whom showered me with a tremendous amount of tenderness and warmth. Finally, I would like to thank my parents, Rosa and Humberto, for their support throughout my life.

Développement et validation des boucles de contrôle pour les interfaces haptiques d'un simulateur de propulsion en fauteuil roulant manuel standard

Ary Druva PIZARRO-CHONG

RÉSUMÉ

Il y a environ 47,000 utilisateurs de fauteuils roulants manuels (FRM) au Québec, et 155,000 au Canada. 30 à 70% des utilisateurs de FRM commencent à souffrir de douleurs chroniques aux articulations des membres supérieurs dans les cinq premières années d'utilisation. Pour investiguer cette problématique en laboratoire, notre équipe a développé un simulateur de fauteuil roulant manuel. Les capteurs de force utilisés sont des roues instrumentées qui remplacent les roues originelles du fauteuil, ce qui limite le degré de réalisme du simulateur.

L'objectif du travail était d'accroître ce degré de réalisme, en remplaçant le capteur de force qui est utilisé actuellement. Pour ce faire, une cellule de force à six axes a été placée sous le fauteuil roulant. Ensuite, une boucle de contrôle par admittance a été développée pour contrôler l'interaction moment-vitesse des roues-arrière du fauteuil. Une acquisition de données pilote a été effectuée sur un sujet sain pour évaluer le degré de réalisme de la propulsion. Des deux côtés, les moments de propulsion maximaux M_{zmax} (Nm), la force maximale appliquée F_{TOTmax} (N), le temps de poussée T_P (s) et le temps de recouvrement T_R (s) ont été calculés et comparés, et ce, dans les trois conditions ci-après: sur le sol (SS), sur simulateur contrôlé par les roues instrumentées (RI) et sur simulateur contrôlé par la cellule de force (CF).

Les résultats confirment les hypothèses de recherche : la boucle de contrôle est stable, c'est-à-dire que la vitesse réelle des roues suit la vitesse désirée. La comparaison des paramètres biomécaniques donne les résultats suivants: pour M_{zmax}, la différence entre SS et CF est petite, alors qu'elle est grande entre SS et RI. Quant à F_{TOTmax} et T_P, les différences entre SS et CF et entre SS et RI sont toutes les deux considérées grandes. Pour T_R, les différences entre SS et CF et entre SS et RI sont considérées petites dans les deux cas.

En conclusion, il semble que la propulsion sur simulateur contrôlé par la cellule de force soit légèrement plus proche de la propulsion sur le sol que celle contrôlée par des roues instrumentées. On pourrait expliquer ce résultat par le fait que le mouvement du tronc affecte le dynamique des roues, un mouvement qui est pris en compte par la cellule de force mais pas par les roues instrumentées.

Mots-clés : robotique de la réadaptation, interface haptique, fauteuil roulant, simulateur, réalisme

Development and validation of the control loops for the haptic interfaces of a standard manual wheelchair propulsion simulator

Ary Druva PIZARRO-CHONG

ABSTRACT

There are about 47,000 manual wheelchair (MWC) users in Quebec, and 155,000 in Canada. Research indicates that 30 to 70% of them begin feeling chronic pain in the upper limb joints within the first five years of use. To investigate this issue in the laboratory, our team has developed a manual wheelchair simulator that uses instrumented wheels as force sensors. These wheels replace the wheelchair's original wheels, thus limiting the degree of realism of the simulator.

The objective of this work was to increase this degree of realism, by replacing the force sensors used currently. To this effect, a six-axes force cell was placed underneath the wheelchair. An admittance control loop was developed to control the moment-velocity interaction of the wheelchair's rear wheels. Data gathering was conducted with one healthy subject to evaluate the level of realism of wheelchair propulsion. On both sides, maximum propulsive moments M_{zmax} (Nm), maximum applied force F_{TOTmax} (N), push time P_T (s) and recovery time R_T (s) were calculated and compared between three conditions: on the ground (OG), on the simulator controlled by the instrumented wheels (SW) and on the simulator controlled by the force cell (FC).

Results confirm the research hypotheses: the control loop is stable, meaning that the real speed follows the desired speed. Comparison of biomechanical parameters is as follows: regarding M_{zmax}, the difference between conditions OG and FC is small, whereas that between OG and SW is large. With regards to F_{TOTmax} and T_P, differences between OG and FC, and between OG and SW are both large. For T_R, differences between OG and FC and between OG and SW are both small.

In conclusion, it seems that propulsion on the simulator controlled by a force cell may be slightly closer to propulsion on the ground than that on a simulator controlled by instrumented wheels. This could be explained by the fact that the movement of the trunk of the user affects the dynamics of the wheelchair-user system. This effect is captured by the force cell, but not by the Smartwheels.

Keywords: rehabilitation robotics, haptic interface, wheelchair, simulator, realism

TABLE OF CONTENTS

Page

LIST OF TABLES

Page

LIST OF FIGURES

Page

LIST OF ABREVIATIONS

1D	One-dimensional
2D	Two-dimensional
3D	Three-dimensional
ANOVA	Analysis of variance
CAD	Computer aided design
CEAL	Challenging environment assessment laboratory
COP	Center of pressure
CRCHUM	Centre de recherche du centre hospitalier de l'université de Montréal
ETS	École de technologie supérieure
FBD	Free body diagram
FC	Force cell
H1	Hypothesis 1
H2	Hypothesis 2
HC	Point of hand contact
HR	Point of hand release
IMU	Inertial measurement unit
KTK	Kinesiology toolkit
LIO	Laboratoire de recherche en imagerie et orthopédie
MEF	Mechanical effective force
MWC	Manual wheelchair
MWCU	Manual wheelchair user
O_2	Oxygen gas

OG	Overground
PD	Proportional-derivative
PI	Proportional-integral
PID	Proportional-integral-derivative
ROD	Requirement related to overground dynamics
RRCF	Requirement to conduct research and to provide clinician feedback
RSF	Requirement related to sensory feedback
SW	Smartwheel
UCL	Université catholique de Louvain
VE	Virtual environment
WC	Wheelchair
WMS	Wheelmill system

LIST OF SYMBOLS

μ_{caster}	Friction coefficient at the caster-ground interface
μ_{rear}	Friction coefficient at the rear-wheel-ground interface.
arm_L	Moment arm (left side)
arm_R	Moment arm (right side)
$a_{trunk/wc,frame}$	Acceleration of the trunk, arms and head with respect to the wheelchair frame, in the x-direction.
$a_{wc,frame}$	Acceleration of the MWC frame
a_x	Acceleration of the wheelchair-user system in the x-direction.
$\vec{F}_{air}$	Air resistance
$\vec{F}_{prop}$	Propulsion force applied by the ground on the wheels
$\vec{F}_{roll,rear}$	Rolling resistance of the rear wheel
$\vec{F}_{roll,caster}$	Rolling resistance of the front caster
$\vec{F}_{weight}$	Weight of the wheelchair-user system
$F_{APP,L,SW}$	Force applied on the left handrim, as measured by the Smartwheel
$F_{APP,R,SW}$	Force applied on the right handrim, as measured by the Smartwheel
F_r	Force radial to the pushrim
F_{roll}	Force of rolling resistance
F_t	Force tangential to the pushrim
F_{TOT}	Total resultant force
F_{TOTmax}	Maximum Force applied by the MWCU on the handrim during a push cycle
F_x	Force applied by the MWCU on the handrim, in the horizontal direction

F_y	Force applied by the MWCU on the handrim, in the vertical direction
$F_{Y,FC}$	Force measured by the force cell in the horizontal direction
$F_{yL,FC}$	Equivalent calculated horizontal force (left side), obtained from the measurement of the force cell
$F_{yR,FC}$	Equivalent calculated horizontal force (right side), obtained from the measurement of the force cell
F_z	Force applied by the MWCU on the handrim, in the direction along the wheel axis
G_f	Amplifier gain
k_P	Proportional gain
k_I	Integral gain
k_{FF}	Feedforward gain
k_{RT}	constant (includes the ratio of the radii of wheelchair wheels to rollers and a motor constant)
m	half of the total combined mass of the wheelchair and user
$M_{app,i}$	Moment of the applied force F_{prop} at the handrim by the user
$M_{F,i}$	Moment of rolling resistance
m_{trunk}	Half of the mass of the trunk
$m_{wc,frame}$	Half of de la masse of the MWC frame
M_x	Moment applied by MWCU about the x-axis
M_y	Moment applied by MWCU about the y-axis
M_z	Moment applied by MWCU about the wheel axis
$M_{Z,FC}$	Moment measured by the force cell
M_{zL}	Moment applied by MWCU about the wheel axis (left side)
M_{zLmax}	Maximum moment applied by MWCU about the wheel axis during a push cycle (left side)

$M_{zL,SW}$	Moment applied by MWCU about the wheel axis and measured by the Smartwheel (left side)
M_{zmax}	Maxmum moment applied by MWCU about the wheel axis during a push cycle
M_{zR}	Moment applied by MWCU about the wheel axis (right side)
M_{zRmax}	Maximum moment applied by MWCU about the wheel axis during a push cycle (right side)
$M_{zR,SW}$	Moment applied by MWCU about the wheel axis and measured by the Smartwheel (right side)
m/s	meters per second
N	Newton
Nm	Newton-meter
P_T	Push time
R_T	Recovery time
r_H	Radius of the handrim
S_{ij}	Term in the Sensitivity matrix
$u_{FF,L}$	Control input from the feedforward controller (left side)
$u_{FF,R}$	Control input from the feedforward controller (right side)
V	Volts
V_{fexec}	Excitation voltage
VO2max	maximum oxygen uptake

INTRODUCTION

There are about 65 million manual wheelchair users (MWCU) worldwide, representing about 1% of the world population (World Health Organization, 2008). The numbers are 10 million wheelchair users in developed countries (New Disability, 2002), 155,000 in Canada (Shields, 2004), and 47,000 in Quebec (Camirand et al., 2010) this last number representing a proportion of 0.5% of the population.

Manual wheelchairs (MWC) are prescribed to people who suffer from a congenital condition (e.g., spina bifida), have suffered trauma (e.g., a spinal cord injury, an amputation), have difficulty moving after the onset of a medical condition (e.g, multiple sclerosis, polio, stroke), or suffer from incapacity due to old age (Kaye et al., 2000). A wheelchair is a necessary mobility aid which allows the aforementioned people to participate in society (daily activities, work, education, social life) (Rushton et al., 2010).

However, piloting a wheelchair requires complex capacities including vision, balance, force, spatial perception, and orientation (Grant et al., 2004). As such, two important issues have come to light regarding the use of manual wheelchairs: (i) chronic injuries, and (ii) lack of training. About 50% of users are sustaining chronic injuries within the first five years of use (Paralyzed Veterans of America, 2005). The injuries noted are: shoulder pain (59% of patients with tetraplegia, 63% of patients with paraplegia), carpal tunnel syndrome, elbow tendonitis (Curtis et al., 1999). With regards to training (which could potentially reduce the rate of injuries), it is not being provided at a level deemed necessary by world health bodies (World Health Organization, 2008).

i. Issues regarding research into wheelchair propulsion biomechanics and physiology, and chronic injuries

Manual wheelchair users push their wheelchairs 2000 to 3000 times a day, for more than 10 hours, as part of their daily activities (Warms et al., 2008). Wheelchair propulsion utilizes the shoulder and wrist areas of the upper limbs. The long-term use of a manual wheelchair has

been shown to lead to injury in these areas (Brose et al., 2008; Curtis et al., 1999; Paralyzed Veterans of America, 2005). Surveys of manual wheelchair users show the prevalence of shoulder pain to be between 31% and 73% (Boninger et al., 2002).

The human shoulder requires the soft tissue structures to retain the balance of the joint, keeping the humeral head near the acromion and the glenoid during functional activities. The rotator cuff, containing a group of muscles and tendons, plays a very important role in stabilizing the glenohumeral joint (Rankin et al., 2011). High pressure transmitted across the subacromial area during wheelchair propulsion may contribute to the large number of problems in the shoulder in paraplegics (Bayley, Cochran, & Sledge, 1987). The repetitive nature of wheelchair propulsion may be a cause in upper-extremity pain and injury.

Identifying shoulder pathology in MWCUs is an important step in understanding wheelchair propulsion mechanics and may assist in identifying the factors that contribute to pathology. Improved knowledge of shoulder pathology and associated mechanics may lead to efforts to prevent the pathology (Finley & Rodgers, 2004).

There is still a need to better understand propulsion biomechanics, and how this leads to pain and injury (Koontz et al., 2012). To improve the quality of life of manual wheelchair users in both a daily and sports setting (and also to improve wheelchair design), reliable and valid measures of wheelchair propulsion are necessary (de Groot et al., 2014). These measurements can be made in the field (everyday propulsion) or in the laboratory on either a treadmill or a wheelchair ergometer.

Field-based testing present researchers with the least standardized but most externally valid conditions in which to study wheelchair propulsion. Considering the importance of wheelchair settings on performance, it is important that the user be tested in his personal wheelchair (van der Woude et al., 2006). For this reason, it would be preferable to run experiments in the field. However, studies on wheelchair propulsion are difficult to conduct in the natural environment for several reasons. Equipment may not operate as desired in such an environment (Wu, 2013).

It is problematic to collect physiological, kinetic, or kinematic data without changing the wheelchair in terms of mass and configuration. Experimental conditions and the number of variables to be accounted for are difficult to control, reducing the repeatability of such measures. Moreover, the movement of the wheelchair with respect to the environment makes it difficult to make measurements (van der Woude et al., 2001).

All lab-based modalities provide considerable advantages for researchers investigating wheeled mobility, when compared to overground testing (de Klerk, Vegter, Goosey-Tolfrey, et al., 2020). They allow detailed physiology and biomechanics studies to be conducted under controlled conditions while the wheelchair-user system is stationary (Niesing et al., 1990). Therefore, manual wheelchair propulsion research today is still mostly done in the laboratory. The devices used in laboratories, take the shape of treadmills, integrated ergometers and rollers ergometers (Wu, 2013). Each will be defined and detailed in the literature review.

The choice of equipment is important because a laboratory should allow for accurate measurements and simulate wheelchair driving as realistically as possible. In an exhaustive review on comparisons between overground propulsion and wheelchair ergometers, De Klerk et al. (2020) concluded that the Wheelchair Ergometer testing environment was not yet able to closely emulate overground conditions.

It is important that results obtained using these devices be ecologically valid, meaning they represent what happens in the field. This way, studies performed in the laboratory can lead to recommendations that are reliable. The closer the device can replicate environmental conditions (meaning the more realistic the simulator), the more ecologically valid it is.

ii. Issues regarding manual wheelchair training

As mentioned previously, a wheelchair is a useful tool to improve the participation in society of people with lower limb disorders. However, even though people can potentially benefit from the use of a wheelchair, there is no guarantee they will be able to do safely and efficiently on their own. When not used properly, a wheelchair can actually have the opposite effect and be

detrimental to the user's wellbeing, when measured in terms of life satisfaction and community participation (Hosseini et al., 2012). Moreover, wheelchairs can lead to chronic (Akbar et al., 2010) and acute (Chen et al., 2011) overuse injuries.

Therefore, it is important for wheelchair users to receive appropriate training when first being prescribed a wheelchair. This way they can learn the skills necessary to the safest and most efficient use their wheelchair possible. These skills include propulsion techniques, transfers and maneuvering around physical barriers (Morgan et al., 2017).

Rehabilitation professionals have developed standardized wheelchair skills training programs, such as the Wheelchair Skills Program. Current evidence suggests that these programs are effective for manual wheelchair users undergoing rehabilitation (MacPhee et al., 2004; Worobey et al., 2016) and for power wheelchair users (Kirby, Miller, et al., 2015). Many positive effects stem directly from an individual possessing a better set of wheelchair skills. For example, researchers have observed increased wheelchair use (Hoenig et al., 2005), increased rate of return to work (Velzen et al., 2012) and increased participation (Phang et al., 2011), amongst others.

Despite the benefits and necessity of wheelchair training programs, these are still not administered as a standard part of rehabilitation to new wheelchair users. In Canada, the United States and the United Kingdom, the prevalence of training programs ranges from 11 to 55% (Kirby, Wang, et al., 2015).

The World Health Organization recommends that training be given when a wheelchair is prescribed (World Health Organization, 2008). This recommendation is hardly followed, as attested by the proportion of training programs in the three developed countries mentioned above. Lack of time and lack of resources are the two reasons cited most frequently when it comes to explaining why the administration of training programs is low (Best et al., 2015).

The use of a wheelchair training simulator, which is a less conventional training tool, may help address the aforementioned lack of time and resources. A simulator may be used to supplement traditional skills training and it may present some other advantages. It may require less time to

switch or modify tasks, integrate self-guided exploration and independent practice and provide automatic real-time performance feedback (Rizzo & Kim, 2005). In this scenario, the user/trainee may be able to operate the simulator safely and receive feedback with little intervention from the therapist.

A simulator would give health professionals who provide this training a tool to evaluate, early on, the level of ability of the user (Grant et al., 2004). A simulator could help a user learn skills, but it can only be useful if those skills can be transferred to real life. The degree of realism of simulation in virtual-reality-based training systems has been shown to be correlated to the degree at which skills are transferred to real life (Arlati et al., 2019).

iii. Realism of stationary devices for the evaluation and training of manual wheelchair propulsion

In the previous sections, we have explained how manual wheelchair laboratory devices could become a valuable tool for the community of manual wheelchair users: researchers can use the devices to improve their knowledge of shoulder pathology, and clinicians can use them as a training tool with which to teach manual wheelchair skills. Nonetheless, despite their potential benefits, laboratory devices cannot be truly useful unless the simulation of propulsion has a high degree of realism.

Researchers have investigated the biomechanical and physiological aspects of wheelchair propulsion on laboratory devices. The results of that research points to those aspects that contribute most to the realism of simulation of manual wheelchair propulsion. All of these aspects contribute to the validity of research results obtained on those devices and they improve the degree to which skills learnt on them are transferred to real life.

People perceive their environment via their senses. The highest level of realism of a simulation is obtained by stimulating all of the user's senses, i.e. touch (force feedback), vision, vestibular and hearing (Pithon et al., 2009).

The following are important aspects of laboratory devices and will be further detailed in the literature review. The devices should:

- match the altered sense of effort needed to propel a wheelchair in a straight line, over varying surfaces and slope conditions
- accurately detect the rotation of the driving wheels
- provide a sophisticated algorithm that translates wheel rotation into virtual wheelchair movement
- allow wheelchair users to use their own wheelchairs (the platform must have the flexibility to accommodate wheelchairs from a range of manufactures)
- provide force feedback and stimulate the human vestibular system
- simulate collisions with virtual objects in a manner that is analogous to that encountered in reality
- provide high quality virtual real time graphics and the right choice of visual interface
- integrate auditory perception
- provide fast communications between the platform and the virtual reality host so that interaction is near real-time

As will be detailed in the literature review, existing laboratory devices do not, at present, comply with all the design requirements for high realism and there is room to improve their level of realism (de Klerk, Vegter, Goosey-Tolfrey, et al., 2020).

iv. Work presented in this thesis

The Laboratoire de recherche en Imagerie et Orthopédie (LIO) (located at the Centre de Recherche du Centre Hospitalier de l'Université de Montréal, CRCHUM) and the Health Technologies Laboratory at the École de Technologie Supérieure (ETS) are, jointly, a collaborative laboratory located in Montreal, Canada whose researchers aim, amongst many other research projects, to better understand human locomotion. The research team has built a manual wheelchair simulator (henceforth called the LIO Simulator) that is built upon the principles of haptic robotics. The main goal of the research program was to develop a tool for investigation into, and training of, propulsion techniques of manual wheelchair users (Chénier,

2012). It is shown in Figure 0.1. It simulates the dynamic behavior of a wheelchair and its user (the wheelchair-user system) on level ground, and links the forces applied by the user on the handrims to the velocity of the wheels via a haptic interface. Nonetheless, the dynamic behavior is not fully accurately simulated because the simulator does not take into account the effect of the movement of the user and the user's trunk on the trajectory of the wheelchair.

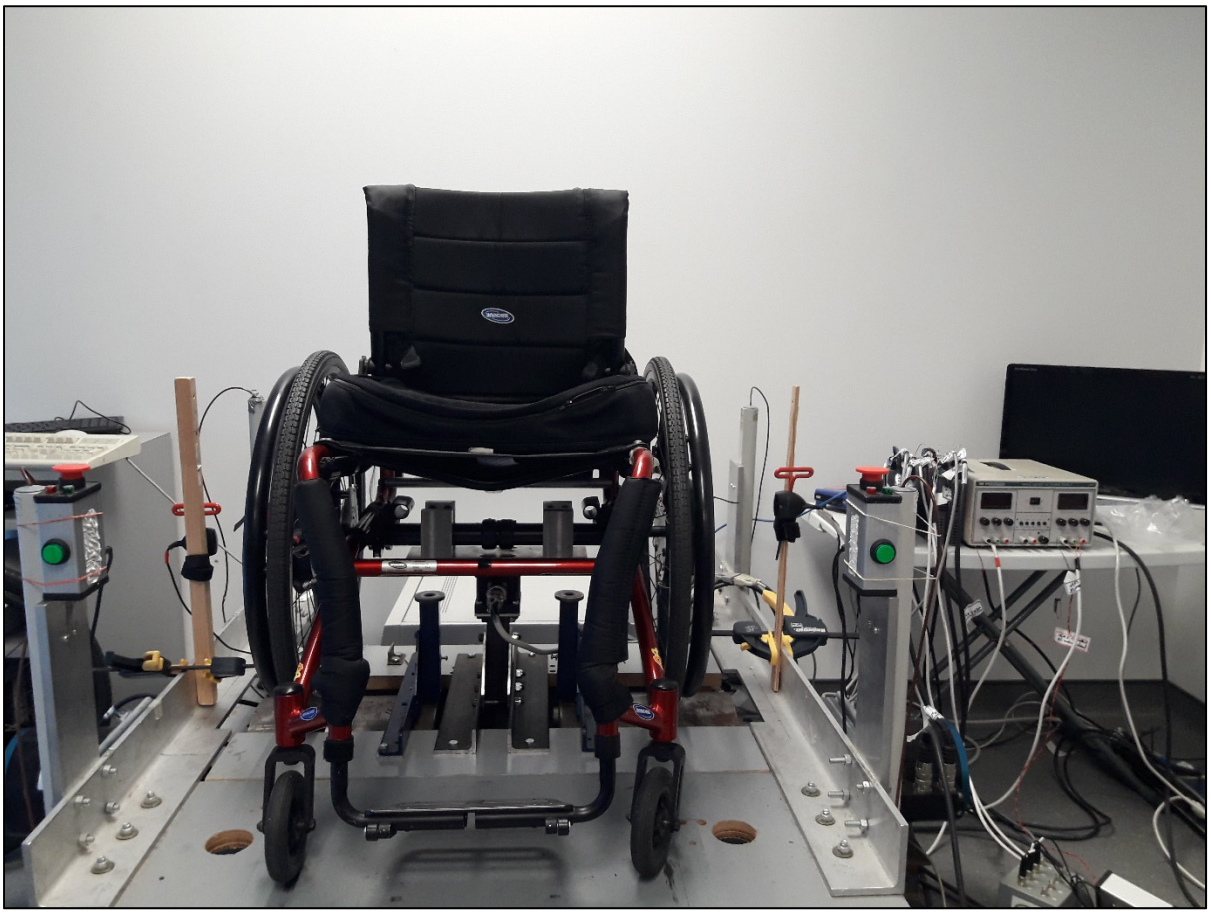

Figure 0.1 The LIO manual wheelchair simulator housed at the CRCHUM (Montreal, Canada)

The simulator was built with motorized rollers so that it can use the user's wheelchair, it can use a curvilinear model of wheelchair propulsion, and it can provide biofeedback. It has high ecological validity because it does not make assumptions usually made when designing a wheelchair simulator: e.g, straight-line propulsion, no contribution from castors to the dynamics of the wheelchair (Chénier et al., 2014). It uses, as force and moment sensors, two

instrumented wheels called Smartwheels (which were developed by Three Rivers Holdings LLC, a now-defunct company which was based out of Mesa, Arizona, United States). These wheels replace the wheelchair's original wheels, which are different in geometry and rigidity from the user's wheelchair, thus affecting the realism of simulation. Moreover, the replacement of the wheelchair wheels is a complex operation that can be time-consuming. The removal of this step would maximize the time patients spend with therapists.

The work presented in this thesis is an attempt to improve upon the realism of the LIO Simulator and to ease its use in a clinical setting by removing the step of replacing the wheels. We seek to use the user's wheelchair without any modification (more specifically, by not replacing the original wheels) and take into account more fully the wheelchair-user system dynamics that occur during propulsion (more specifically, the contribution of the movement of the user's trunk). With this aim, we developed a new control system for this simulator, which uses a force cell instead of the instrumented wheels as the force and moment sensor.

The thesis is written as follows. Chapter 1 is the literature review, placing the foregoing problem in context. We describe several existing stationary devices used to measure manual wheelchair propulsion, including the LIO Simulator, along with the extent of their ecological validity. Chapter 2 lists the objectives for this project, the research hypotheses and the approach used to achieve said objectives. Chapter 3 is a description of the experimental methodology, relating on the one hand the design of the force cell and tests to validate it, and on the other hand the design and development of the control loop and the tests run to validate its design (evaluation of its stability and evaluation of the realism of the simulator). Chapter 4 describes the results obtained. In Chapter 5, we discuss the results obtained during the experimental phase. The conclusion summarizes the work performed in this thesis.

CHAPTER 1

LITERATURE REVIEW

1.1 Overground wheelchair propulsion

We begin by describing the movement of a manual wheelchair on the ground, in a straight line. Figure 1.1 shows a wheelchair user propelling her wheelchair.

Figure 1.1 Wheelchair user at two points of propulsion (on the left: beginning of the push, on the right: end of the push) (Johansson & Chinworth, 2012)

Manual wheelchair propulsion patterns vary depending on the individual. However, they can be analyzed as follows. The propulsion pattern is made up of several push cycles. The push cycle is comprised of the push phase and the recovery phase (refer to Figure 1.2). The push phase starts when the user grips the handrim (HC, point of hand contact) and propels it. The push phase ends when the user lets go of wheel (HR, point of hand release). At this same point, the recovery phase starts and ends when the user once again grips the wheel at the next HC, completing a push cycle.

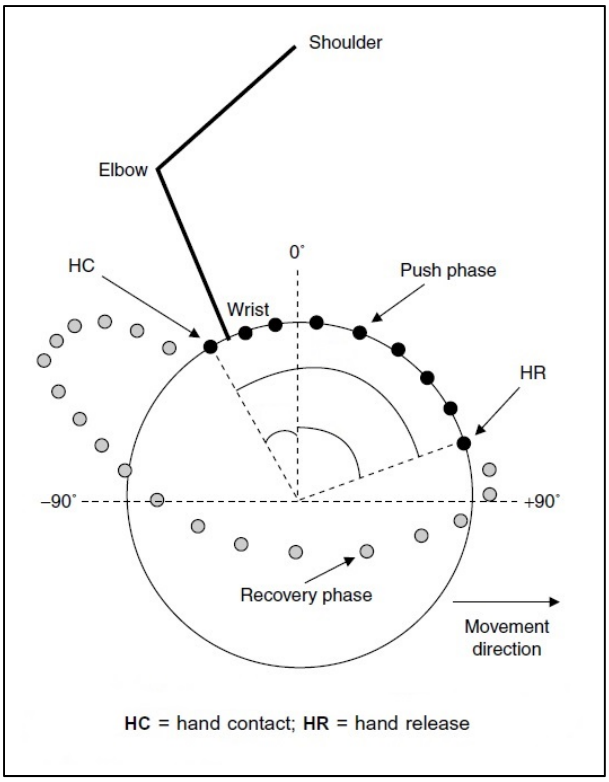

Figure 1.2 Parameters of wheelchair propulsion technique (Y. Vanlandewijck et al., 2001)

1.2 Models of overground wheelchair propulsion

In order to simulate the dynamics of a wheelchair moving over a surface, it is necessary to have a mathematical model of the wheelchair in its environment.

1.2.1 One-dimensional model

Figure 1.3 shows a physical model of wheelchair propulsion on a straight line, for one half of the wheelchair.

We can derive a one-dimensional equation of this model by applying Newton's Second Law of Motion to the free-body diagram of the wheelchair-user system:

$$\sum \vec{F} = m\vec{a} \tag{1.1}$$

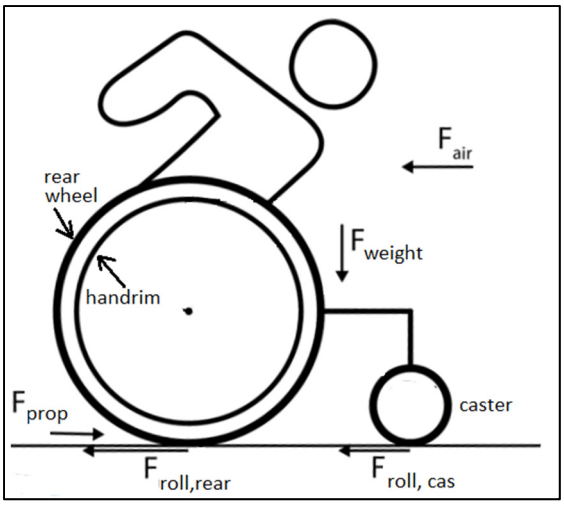

Figure 1.3 Physical model of the wheelchair-user system

We consider that the user is rigidly attached to the wheelchair and does not move within it.

m is half of the total combined mass of the wheelchair and user

$\vec{a}$ is the acceleration of the center of mass of the wheelchair-user system

$\sum \vec{F}$ is the sum of all of the individual forces applied to one half of the wheelchair-user system. They are (Niesing et al., 1990): $\vec{F}_{prop}$, $\vec{F}_{air}$, $\vec{F}_{roll,\ rear}$, $\vec{F}_{roll,\ caster}$, $\vec{F}_{weight}$ and are detailed below.

- $\vec{\boldsymbol{F}}_{\mathbf{prop}}$ is the propulsion force applied by the ground on one wheel (either the left or right wheel).

  The user applies a force on the handrim, which we call F_{tot}. F_{tan} is the part of F_{tot} in the plane of the wheel. F_{tan} creates a moment M_z around the wheel axle. F_{prop} is a reaction from the ground to the application of M_z.

- $\vec{\boldsymbol{F}}_{\mathbf{air}}$ is the air resistance $F_{air} = ½.\rho.(V_{air} - V_{wc})^2.A.C_d$

  where ρ is the air density, V_{air} is the air speed, V_{wc} is the speed of the wheelchair (F_{air} depends on the sign of $(V_{air} - V_{wc})$), A is the cross-sectional area of the wheelchair-user system, C_d is the drag coefficient.

- $\vec{\boldsymbol{F}}_{\mathbf{roll,rear}}$ is the rolling resistance of the rear wheels $F_{roll,rear} = \mu_{rear}N_{rear}$

  where μ_{rear} is the coefficient of rolling resistance at the interface of the rear tire-surface it contacts and depends on the rear tire material, surface material and the pressure of the air in the rear tire

N_{rear} is the reaction force from the ground (perpendicular to the ground) at the point the rear wheel meets the ground.

- $\vec{F}_{roll,caster}$ is the rolling resistance of the front casters $F_{roll,caster} = \mu_{caster} N_{caster}$

  where μ_{caster} is the coefficient of rolling resistance at the interface of the caster-surface it contacts and depends on the caster material, surface material and the pressure of the caster.

  N_{caster} is the reaction force from the ground (perpendicular to the ground) at the point where the caster meets the ground.

- $\vec{F}_{weight}$ is the weight of the wheelchair-user system $F_{weight} = mg$

  where g is the gravitational constant $g = 9.81 m/s^2$

The resulting force can then be expressed as:

$$\sum \vec{F} = \vec{F}_{prop} - \vec{F}_{air} - \vec{F}_{roll,rear} - \vec{F}_{roll,caster} - \vec{F}_{weight} \quad (1.2)$$

Substituting (1.2) into (1.1) we obtain:

$$\vec{F}_{prop} - \vec{F}_{air} - \vec{F}_{roll,rear} - \vec{F}_{roll,caster} - \vec{F}_{weight} = m\vec{a} \quad (1.3)$$

At velocities less than 2 m/s, F_{air} is less than 1 N (Frank & Abel, 1991), so we can neglect it. In addition, $\vec{F}_{weight}$ has no horizontal component on level ground.

Equation (1.3) reduces to, in the x-direction:

$$F_{prop} - F_{roll,rear} - F_{roll,caster} = ma_x \quad (1.4)$$

where a_x is the acceleration of the wheelchair-user system in the x-direction.

1.2.2 One-dimensional model with trunk

When a user who has abdominal control is propelling his wheelchair, he will usually move his trunk from the backrest to an angled position closer to the ground, as shown on Figure 1.4. This movement can happen because of a reaction force applied from the wheelchair backrest or seat onto the person. According to Newton's Third Law, there is an equal and opposite force onto the wheelchair from the user. This force has a quantifiable effect on the dynamics of the wheelchair, as described below.

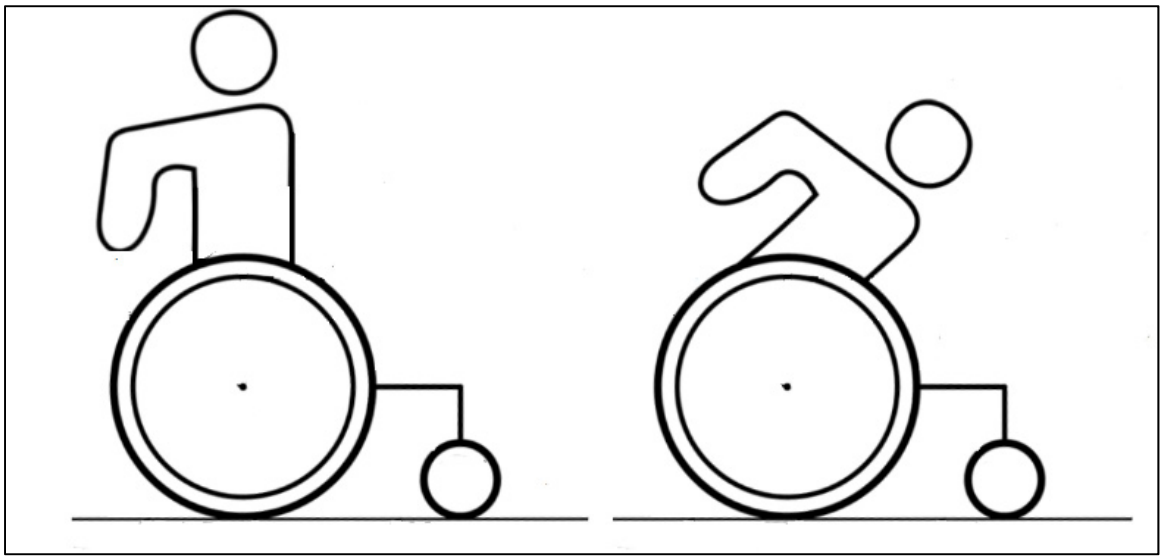

Figure 1.4 Trunk movement during manual wheelchair propulsion

The one-dimensional model of Eq. (1.4) can be further refined in order to account for movement of the trunk during the propulsion cycle described above (Chénier et al., 2016). The movement of this mass can be modeled as a force which influences the acceleration of the rest of the wheelchair. The physical model under consideration is now the one shown on Figure 1.5, which is a free-body diagram of forces imparted on the wheelchair frame in the x-direction. Notice that air resistance has been neglected, because we assume a wheelchair speed of less than 2 m/s.

Here the trunk is replaced by the force F_{trunk} applied by the trunk onto the frame of wheelchair. In the horizontal direction:

$$F_{trunk} = m_{trunk} a_{trunk/(wc,frame)} \tag{1.5}$$

m_{trunk} is half of the mass of the trunk

$a_{trunk/wc,frame}$ is the acceleration of the trunk, arms and head with respect to the wheelchair, in the x-direction.

We now look at the wheelchair frame which is isolated in the free-body diagram of Figure 1.5.

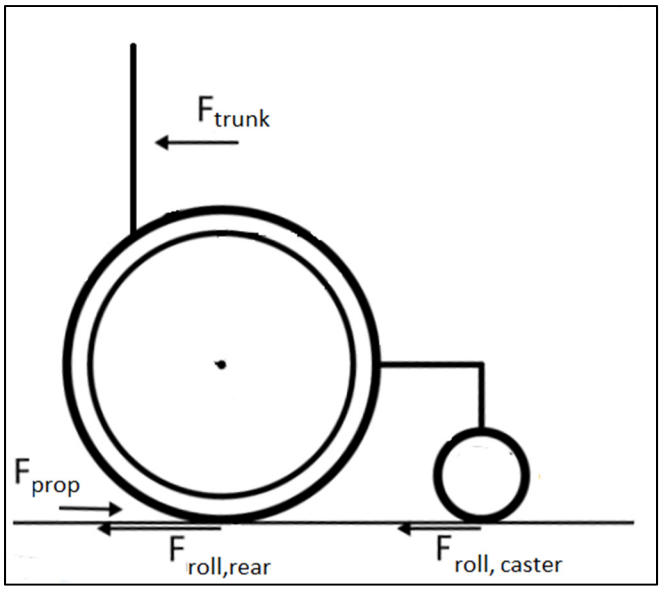

Figure 1.5 Physical model of the wheelchair frame,
taking trunk movement into account

Applying Newton's Second Law of Motion:

$$F_{prop} - F_{roll,rear} - F_{roll,caster} - F_{trunk} = m_{wc,frame} a_{wc,frame} \quad (1.6)$$

where:

$m_{wc,frame}$ is the half of the mass of the wheelchair frame

$a_{wc,frame}$ is the acceleration of the wheelchair frame

Inserting **Erreur ! Source du renvoi introuvable.** into (1.6), we obtain:

$$F_{prop} - F_{roll,rear} - F_{roll,caster} - m_{trunk} a_{trunk/wc,frame} = m_{wc,frame} a_{wc,frame} \quad (1.7)$$

Our goal is to improve the LIO simulator by simulating Equation (1.7) on it.

We should mention a further refinement of the one-dimensional model is possible. This involves the fact that the distribution of rolling resistance between the casters and the rear wheels depends upon the proportion of the weight of the user that is bearing upon the said casters and wheels (Bascou et al., 2013; Kurt et al., 2008; Sauret et al., 2012). Figure 1.6 s**Erreur ! Source du renvoi introuvable.**hows the geometry of the wheelchair (with respect to the distribution of mass) used to describe its effect on rolling resistance.

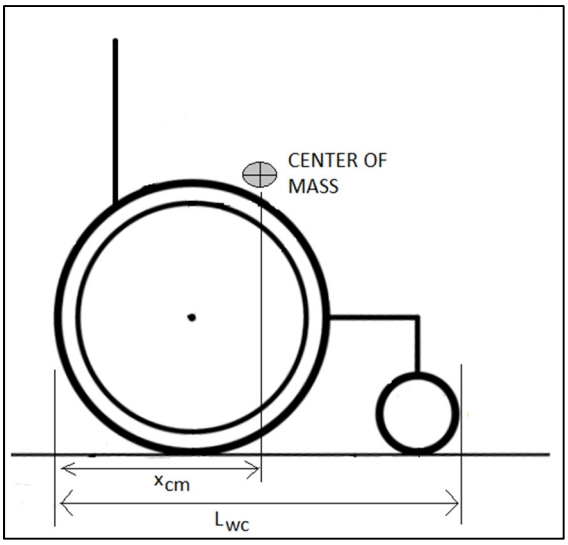

Figure 1.6 Wheelchair geometry to account
for distribution of rolling resistance

Unpacking the rolling resistances, we obtain the following descriptions:

$$F_{roll,caster}(x_{cm}) = \mu_{caster}.mg.\frac{x_{cm}}{L_{wc}} \tag{1.8}$$

and

$$F_{roll,rear}(x_{cm}) = \mu_{rear}.mg.\left(1 - \frac{x_{cm}}{L_{wc}}\right) \tag{1.9}$$

where x_{cm} is the x-position of the center of mass, L_{wc} is the distance between the back of the rear wheel and the front of the caster, m is half the total mass of the wheelchair-user system.

Reprising equation (1.7) and taking into account that the rolling resistances are a function of the position of the center of mass of the wheelchair-user system,

$$F_{prop} - F_{roll,rear}(x_{cm}) - F_{roll,caster}(x_{cm}) - m_{trunk}a_{trunk/wc,frame} = m_{wc,frame}a_{wc,frame} \tag{1.10}$$

Inserting Eqs (1.8) and (1.9) into (1.10), we obtain:

$$F_{prop} - \mu_{rear}.mg.\left(1 - \frac{x_{cm}}{L_{wc}}\right) - \mu_{caster}.mg.\frac{x_{cm}}{L_{wc}} - m_{trunk}a_{trunk/wc,frame} = m_{wc,frame}a_{wc,frame} \tag{1.11}$$

Ideally, on the simulator, we would try to simulate Eq. (1.11) but we could only do so if we could measure or estimate the location of the center of mass of the wheelchair-user system. On the LIO Simulator, we do not do so at this time. We will therefore attempt to simulate Eq. (1.7).

Simulating the dynamics of overground propulsion is only one part involved in the realism of manual wheelchair simulators. Other aspects are also important, and all together constitute design requirements for high realism of stationary devices for the evaluation of wheelchair propulsion. Those are detailed in the next section.

1.3 Design requirements for high realism of manual wheelchair simulators

A manual wheelchair simulator is a highly realistic device that can be used for training and for research of manual wheelchair propulsion. Such a device is said to have high ecological validity. Ecological validity is defined as the extent to which the conclusions of a research study can be generalized to the settings and situations in which the phenomenon under study would naturally occur (*Ecological Validity in Psychology*, 2020).

One could divide the design requirements for this electromechanical machine into three categories. The first two are related to the realism (i.e. the ecological validity) of the device. The third are criteria related to ergometers.

The first requirements concern the implementation of the overground dynamics (the physical forces) of a manual wheelchair on a stationary device. For example, the device could try to implement Eq. (1.7). In addition to the dynamics, the second set of design requirements that the device must meet relates to ergonomics and sensory feedback. The third set of requirements is related to measurements of parameters for research.

The next few sections are a list of requirements based on research on manual wheelchair simulators, with regards to highly realistic simulations (Arlati et al., 2019; de Klerk, Vegter, Goosey-Tolfrey, et al., 2020; Grant et al., 2004; Harrison et al., 2004; Pithon et al., 2009).

1.3.1 Requirements related to the implementation of Overground Dynamics (ROD)

The ergometer must provide a realistic simulation of manual wheelchair propulsion. A simulation with fidelity to overground propulsion can be obtained by fulfilling the requirements below.

ROD1. The device must provide a realistic simulation of the linear inertia of the wheelchair user system (mass of the wheelchair-user system x acceleration of the wheelchair-user system) (Chénier et al., 2015; Crichlow, 2011)
ROD2. The device should take into account the influence of the trunk on the dynamics of the wheelchair-user system (Mason et al., 2014).
ROD3. The device must provide proper simulation of friction due to rolling resistance. The value of this force is dynamic because it depends on the surface on which the wheelchair rolls, on pressure of the air in the rear tires, and on the weight bearing down on each rear wheel and on each caster (Sauret et al., 2012).
ROD4. The simulator must provide adequate simulation of friction due to air resistance. This is neglected in almost all simulators reviewed (Arlati et al., 2019; de Klerk, Vegter, Goosey-Tolfrey, et al., 2020), because the assumption is that the wheelchair is going slower than 2 m/s. However, this is not the case in strong winds or when simulating wheelchair racing. At 5 m/s, aerodynamic drag can represent about 90% of resistance forces (Forte et al., 2016).
ROD5. There must be realistic simulation of ascending slopes (Klaesner et al., 2014)
ROD6. There must be realistic simulation of descending slopes (Klaesner et al., 2014)
ROD7. There must be realistic simulation of cross-slopes (Klaesner et al., 2014)
ROD8. linear paths must be modeled (1D model of wheelchair propulsion). The sophistication of the algorithm that translates wheel rotation into virtual wheelchair movement can be crucial in determining the realism of the simulation (Bentaleb et al., 2019; Grant et al., 2004; Niesing et al., 1990)
ROD9. Curvilinear paths must be modeled (2D model of wheelchair propulsion) (Bando et al., 2004; Chénier, 2012)

ROD10. Paths that go out of the plane of the ground (e.g., when performing wheelies, managing curbs or tipping over) must be modeled (3D model of wheelchair propulsion) (Crichlow, 2011)

1.3.2 Requirements related to Sensory Feedback (RSF)

This part of the ecological validity of manual wheelchair simulators is concerned with the degree to which all of the subject's senses are stimulated. It relates to the fidelity with which the device reproduces the following aspects of manual wheelchair use: ergonomics, haptic feedback, proprioceptive feedback. visual feedback and auditory feedback. For propulsion to be representative of that in the real world, the subject propelling must be immersed in an environment comparable to the one he is used to in reality. The following requirements provide him or her with such an environment.

RSF1. The simulator must respect the ergonomic properties of the wheelchair-user interface, which entails the full use of the user's wheelchair (same wheels, seat height and camber) (Lakomy et al., 1987)
RSF2. The simulator must provide haptic feedback at the wheels on the basis of the interaction with the environment (rolling resistance, ascending and descending slopes, collisions with objects). The effect of varying surface characteristics on rolling resistance is a fundamental physical limitation on manual wheelchair operation (Chénier, 2012; Grant et al., 2004; Harrison et al., 2004)
RSF3. The ergometer must provide proprioceptive feedback (this provides cues to the user with respect to his position and orientation in space). This can be provided with the use of a platform in order to simulate ascending, descending and cross-slopes (Bando et al., 2004; Klaesner et al., 2014) and vibrations due to ground roughness (Pouvrasseau et al., 2017).
RSF4. The simulator must provide visual cues by using a large screen (Bentaleb et al., 2019; Harrison et al., 2004) or a head-mounted display (Bando et al., 2004). The choice of visual interface and the quality of the virtual real time graphics, which are important for user perception, has an impact on user's immersion. Graphics quality and realism are immediately

perceived by users, and may have a large impact on an interface as a learning tool (Pithon et al., 2009).

RSF5. The simulator must provide auditory feedback, replicating sounds from the environment (Harrison et al., 2004). Sound may be coupled with visual feedback to motivate subjects in their learning task. Auditory perception may have a positive effect on the sense of immersion (Pithon et al., 2009).

1.3.3 Requirements specifically to conduct Research (RCR)

An ergometer must be able to measure parameters that are representative of manual wheelchair propulsion.

RCR1. With regards to biomechanical parameters, an ergometer must measure tangential, radial and medio-lateral forces of the hand on the handrims, and torques around the vertical and horizontal axes, and around the axes of the wheels (Chénier et al., 2018; Mason et al., 2014).

RCR2. The ergometer must be able to reliably measure the output power on the wheels (Chénier et al., 2018; Mason et al., 2014), which is calculated from the measurement of torque around the wheel axle and the wheel angular speed.

RCR3. The ergometer must be able to measure reaction forces of the seat and backrest and the lower body and trunk (Niesing et al., 1990).

RCR4. The ergometer must be able to measure physiological parameters, e.g.: aerobic power output, O_2 uptake, heart rate (Chénier et al., 2018; Devillard et al., 2001; Lakomy et al., 1987; Mason et al., 2014)

RCR5. The ergometer must provide the possibility of analyzing the effect of different wheelchair configurations (Crichlow, 2011; Faupin et al., 2008; Klaesner et al., 2014; Niesing et al., 1990)

In this section, we drew a list of requirements for the realism of stationary manual wheelchair propulsion devices. In the next section, we will take a look at the different devices that have

been used to evaluate manual wheelchair propulsion, and how each type of device measures up against the requirements.

1.4 Review of stationary devices for the evaluation of manual wheelchair propulsion

Several types of devices, whose aim was the evaluation of manual wheelchair propulsion, have been used, designed and built. They could be divided into the following four categories: treadmills, integrated ergometers, roller ergometers and wheelchair simulators. A major common thread for the biomechanical measurement of wheelchair propulsion, either in the field or amongst all four of the stationary modalities mentioned, is the use of the instrumented wheel called the Smartwheel. This device is also used to measure parameters for the work in this thesis. It is pertinent to describe the functioning of Smartwheels at this point as it will help to elucidate the inner workings of the laboratory devices that we will subsequently describe.

1.4.1 Smartwheels

1.4.1.1 Characteristics of Smartwheels

Smartwheels are instrumented wheels that were previously commercially available. One of them is shown on Figure 1.7**Erreur ! Source du renvoi introuvable.**. Smartwheels replace the wheelchair's original wheels and measure directly the forces applied by the user on the handrim. The Smartwheel software can display real-time plots of tangential force and speed along with a set of calculated variables including peak force, push length, and cadence. However, the display cannot isolate variables or show performance targets, making it difficult for users to understand what and how much they should improve. Smartwheels were available in fixed wheel diameters, ranging from 22" to 26" (Cooper, 2009).

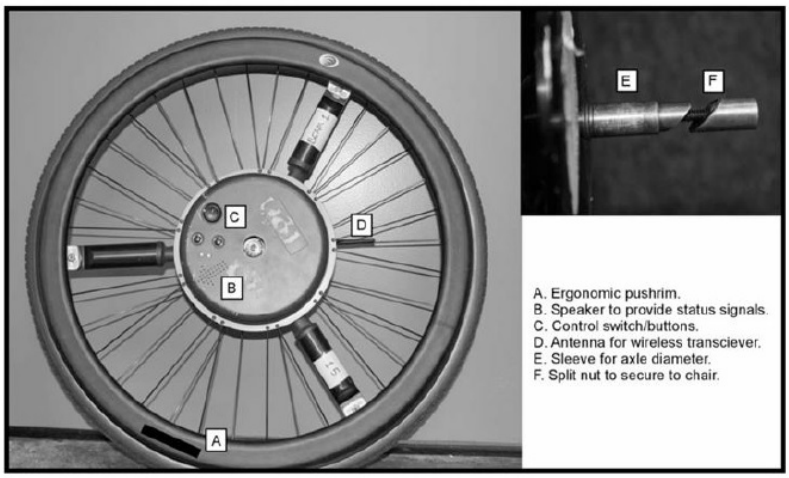

Figure 1.7 Smartwheel (Cooper, 2009)

The raw data obtained via the Smartwheels depends on whether it was obtained on the ground or on an ergometer. However, there are similar characteristics to both types of acquisitions that will be detailed shortly. Figure 1.8 shows Smartwheels mounted on a wheelchair on the ground and Figure 1.9 shows Smartwheels mounted on a wheelchair on the LIO simulator.

Figure 1.8 Smartwheels on a wheelchair
on the ground

Figure 1.9 Smartwheels on a wheelchair
on the LIO simulator

Smartwheels perform data gathering involving a spatial-temporal variable (the angle of rotation of the wheel) and the following six kinetic variables applied at the handrims: F_x, F_y, F_z, M_x, M_y, M_z. The latter are shown on Figure 1.10, and are described below.

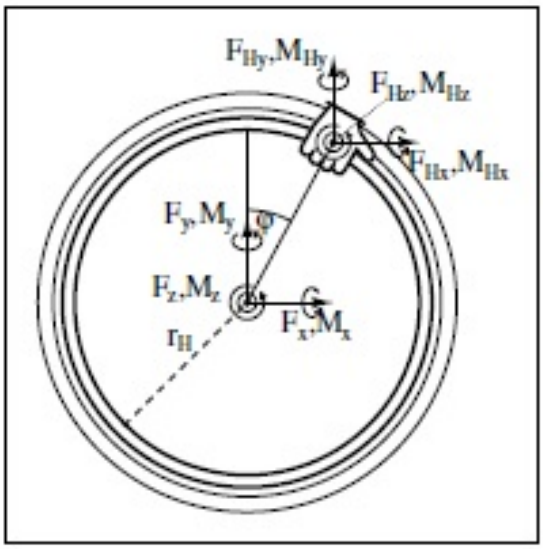

Figure 1.10 Forces and moment on a
wheelchair wheel (Chénier, 2012)

F_Y is the force applied vertically on the pushrim and F_X is the force applied anteriorly (both of these forces are in the plane of the wheel). F_Z is the force out of the plane of the wheel. M_X and M_Y are moments about the center of the wheel, along the x and y axes respectively. M_Z is the moment about the axis of rotation of the wheels and is the moment responsible for angular acceleration of the wheel. The direction of the axes are shown on Figure 1.11 (Three Rivers Holdings LLC, 2010). Other quantities can be derived from these measurements, including F_t (force tangential to the pushrim), F_r (force radial to the pushrim), and the total resultant force F_{TOT}.

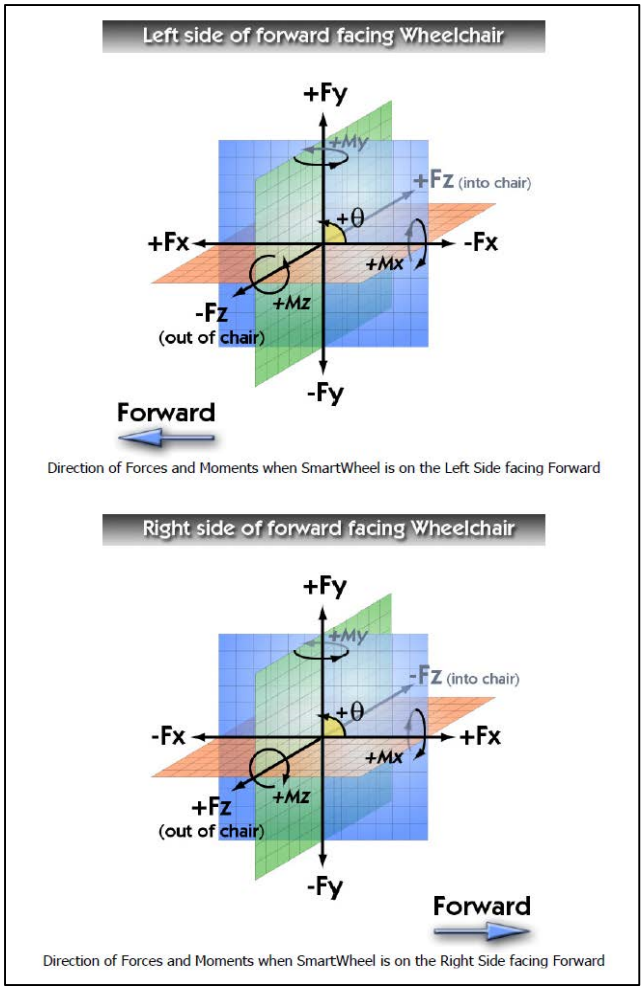

Figure 1.11 Direction of the Smartwheel axes
(Three Rivers Holdings LLC, 2010)

1.4.1.2 Smartwheel biomechanical parameter measurements on the ground

This section details how the Smartwheels mounted on the wheelchair on the ground provide their data. The Smartwheels connect via WiFi to a laptop dedicated to data acquisition with the Smartwheels. The data is processed in real-time and shown in a Windows dialogue box showed on Figure 1.12.

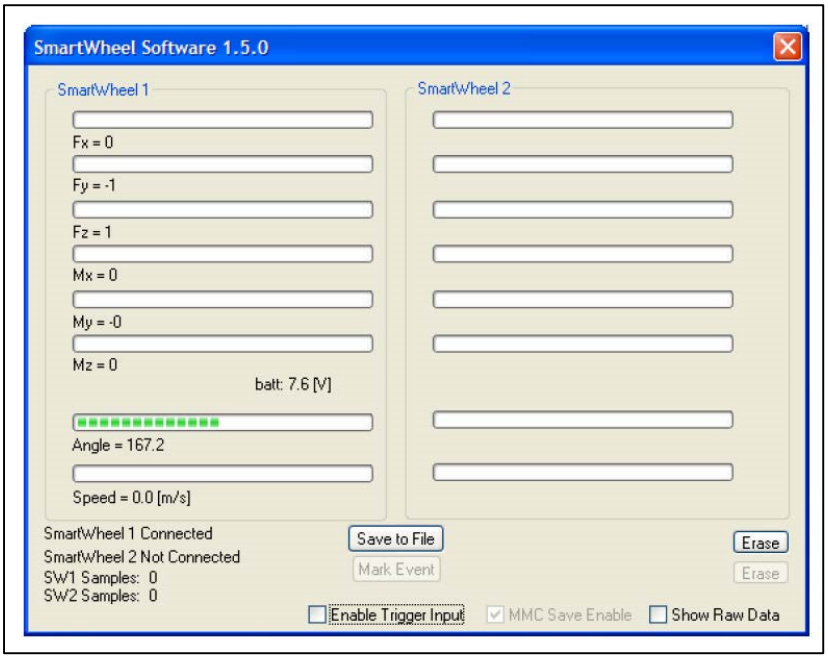

Figure 1.12 Smartwheels laptop: researcher dialog

The raw data contains sinusoidal or constant offsets that are due to the weight of the handrim that is applied in a dynamic direction due to the rotating wheel. The software provided by Three Rivers Holdings removes the offsets before outputting the data. The data is recorded at the end of a trial run as a csv file.

1.4.1.3 Smartwheel biomechanical parameter measurements on an ergometer

The older Smartwheels that are installed on the LIO Simulator are connected directly to the ergometer's computer and transmit raw data via RS232 ports. Figure 1.13 shows an example

of an interface between the output of the Smartwheels mounted on the ergometer and a computer (a MATLAB/Simulink model).

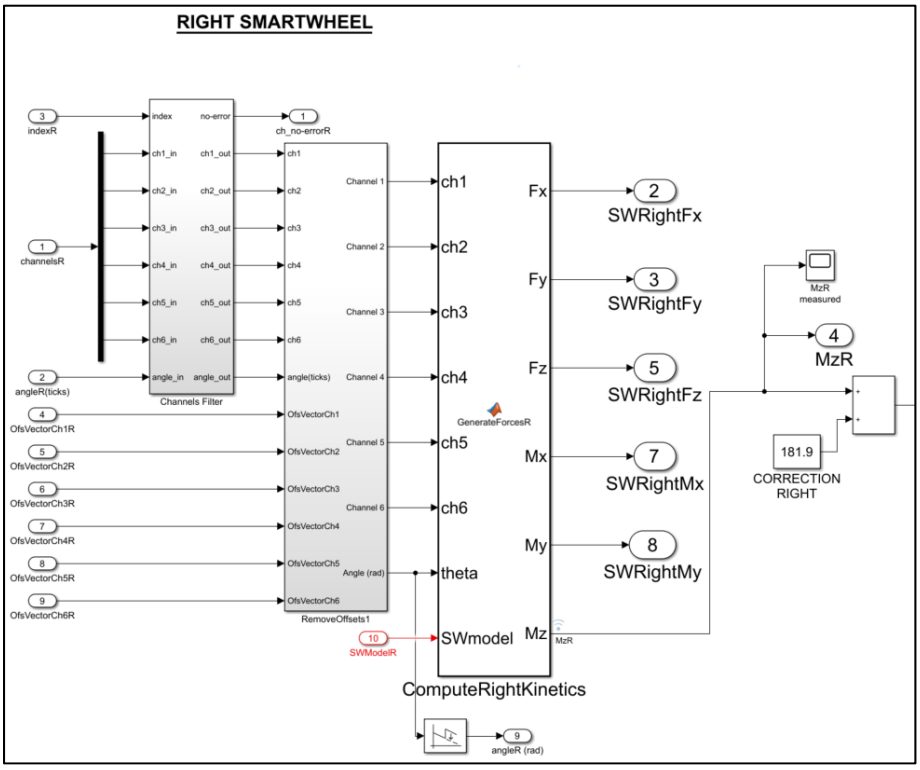

Figure 1.13 Interface between a Smartwheel output and a MATLAB model

The raw measurements taken by the Smartwheel enter the MATLAB model through the "ComputeRightKinetics" block. This block outputs measurements of F_x, F_y, F_z and M_x, M_y, M_z. These values contain offsets from the actual value, so they will require processing before being recorded.

The propulsion moments measured by the Smartwheels in this setting have an offset (which is about 180 Nm for $M_{zL,SW}$ and about -180 Nm for $M_{zR,SW}$) which must be corrected to 0 before the values are used as inputs to the mathematical model. The correction block is on the right of the Simulink model of Figure 1.13. The exact value of the offset changes every time the Smartwheels are turned on and off, and consequently must be updated once before the experiments begin.

Figure 1.14 shows the $M_{zR,SW}$ signal before correction, and Figure 1.15 shows the same signal after correction.

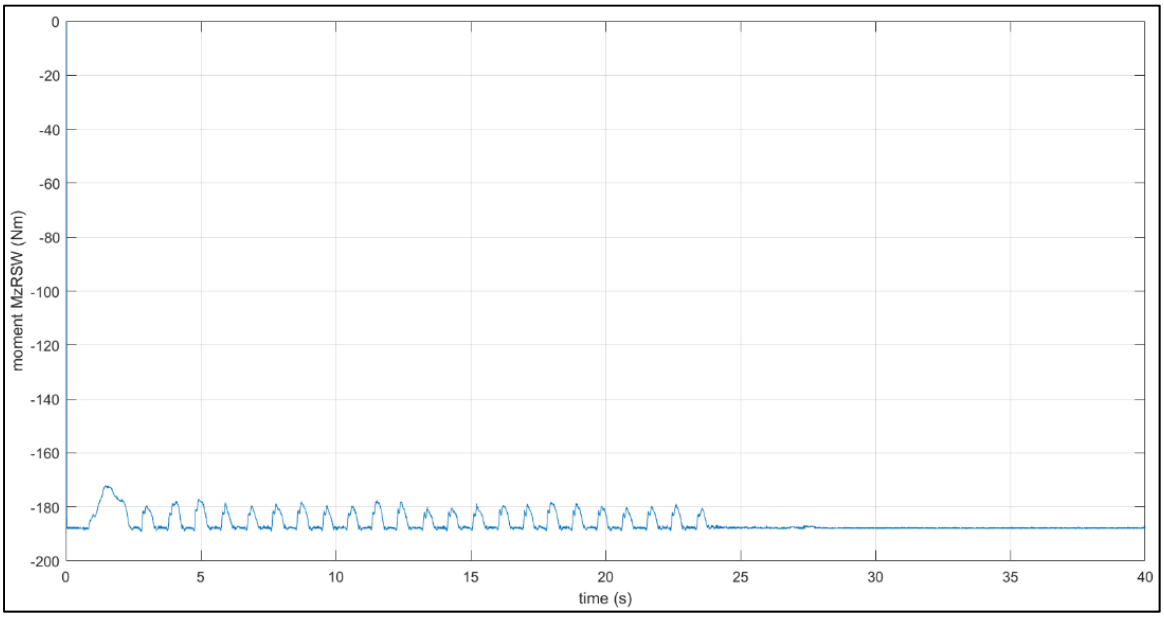

Figure 1.14 Moment $M_{zR,SW}$ read by the Smartwheel before offset correction

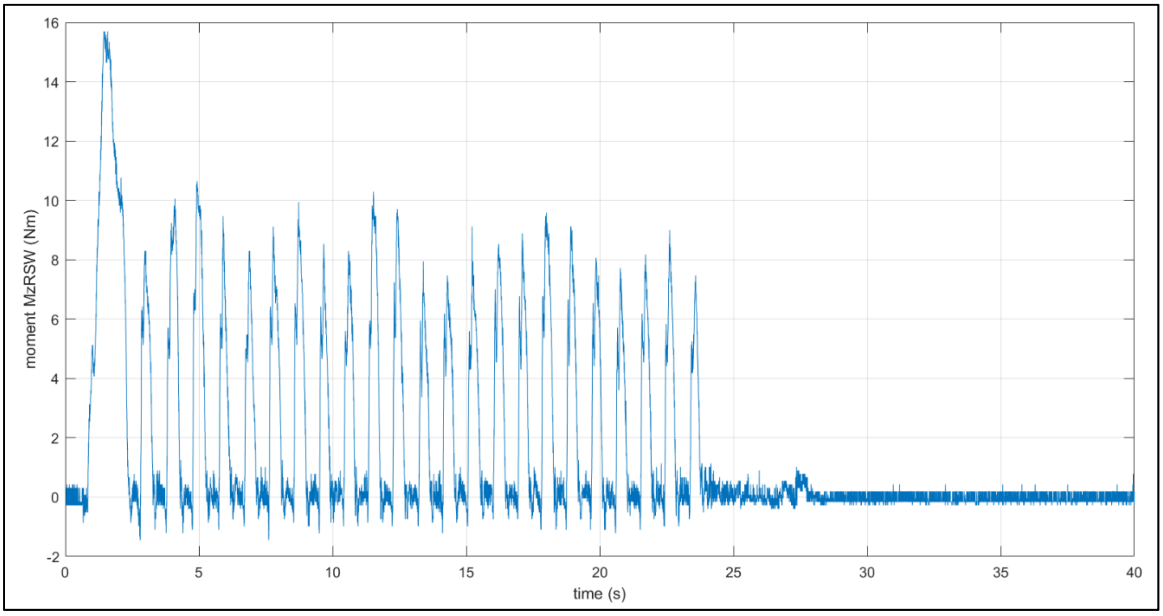

Figure 1.15 Moment $M_{zR,SW}$ read by the Smartwheel after offset correction

1.4.2 Treadmills

1.4.2.1 Aspects of manual wheelchair propulsion on treadmills

Treadmills are belted devices where a flat surface is moved continuously in a straight line by motors. They can usually be set to various speeds and slopes. Figure 1.16 shows an example of a treadmill being used to measure applied and reaction forces during manual wheelchair propulsion (Gagnon et al., 2016).

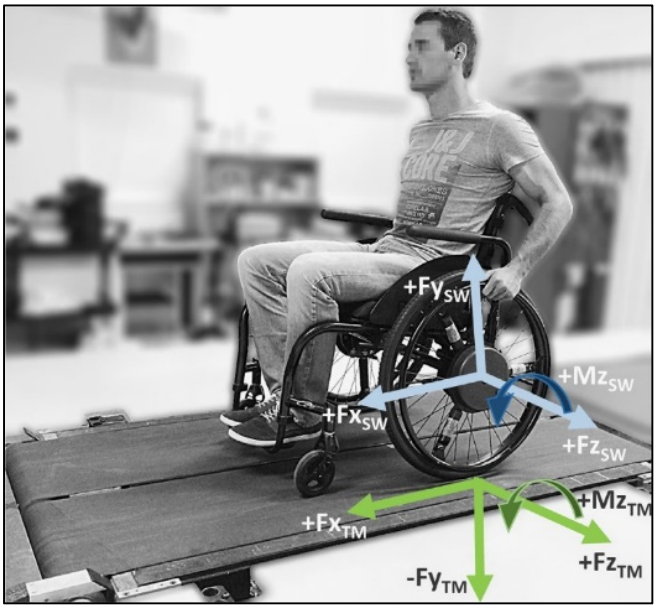

Figure 1.16 Treadmill being used as a wheelchair ergometer (Gagnon et al., 2016)

Researchers have used treadmills to perform experiments on wheelchair propulsion biomechanics with different kinds of equipment:

- video-motion capture systems (Stephens & Engsberg, 2010)
- instrumented wheels (Kwarciak et al., 2011)
- an instrumented treadmill (force platforms). The reaction forces on the treadmill can be used to calculate propulsive moments, push phase duration and recovery phase duration (Gagnon et al., 2016)

In order to ensure the safety of the participant during an experiment on a treadmill, several devices have been used to stabilize the wheelchair: center slider and backstop (Lakomy et al., 1987), rubber bands (Gauthier et al., 2017), linear bearing bars (Chénier et al., 2018) (Figure 1.17), sidebars (Mason et al., 2014) (Figure 1.18).

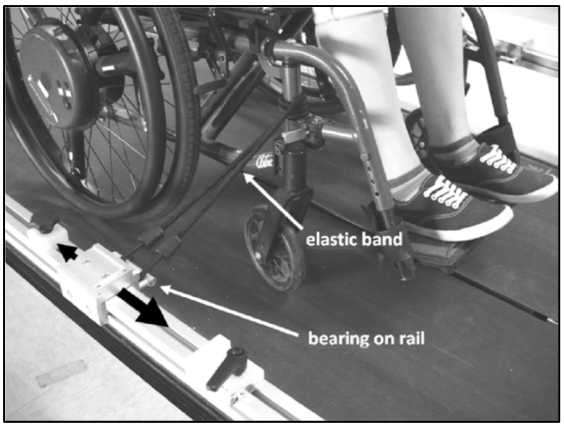

Figure 1.17 Safety system used on a treadmill ergometer (Chénier et al., 2018)

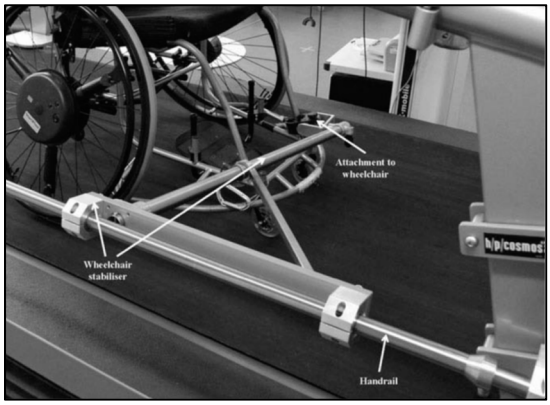

Figure 1.18 Treadmill attachment to the wheelchair (Mason et al., 2014)

1.4.2.2 Realism of treadmill ergometers

In Table 1.1, we look at how treadmill ergometers meet the design requirements for high realism enunciated in section 1.3.

Table 1.1 Treadmills: requirements for realism

req.	yes / no	explanation	references
ROD1	yes	Treadmills provide mechanically accurate simulation of straight-line regular wheelchair wheeling. However, tasks are mostly limited to steady state. Acceleration tasks cannot be easily conducted because the safety system could interfere with the performance of such tasks	Kwarciak et al., 2011 de Klerk et al., 2019
ROD2	yes	Trunk oscillations and shifts in center of gravity contribute towards wheelchair speed	Mason et al., 2014
ROD3	yes	Rolling resistance is realistic on treadmills. For example, trunk oscillations that drive wheels forward results in a forwards shift of the center of gravity towards the smaller caster wheels, which increases the rolling resistance compared with when the center of gravity is positioned above the larger rear wheels. However, the simulated rolling resistance is limited to that of a wheel-on-rubber interface.	van der Woude et al., 2001
ROD4	no	Air drag is not simulated in treadmill propulsion (only an issue at speeds higher than 2 m/s).	Chénier et al., 2018
ROD5	yes	Ascending slopes can be simulated on a treadmill, as the grade can be varied	Chénier et al., 2018
ROD6	yes	Descending slopes can be simulated on a treadmill, as the grade can be varied	Chénier et al., 2018
ROD7	no	Cross-slopes cannot be simulated on a treadmill because this setting is usually not available.	
ROD8	yes	Treadmills simulate 1D motion. When biomechanical parameters were compared between treadmill and overground wheelchair propulsion, the differences were not significant	Kwarciak et al., 2011
ROD9	no	Due to the stabilizing safety elements and the fact that turning would create a crash, steering is not possible, only straight-line propulsion is performed. The load on the participant may be decreased if the safety system applies any force to maintain the wheelchair in place. Therefore, curvilinear paths are not simulated	de Klerk et al., 2019
ROD10	no	Out-of-plane paths are not simulated.	

Table 1.1 Treadmills: requirements for realism (continued)

req	yes / no	explanation	references
RSF1	yes	Treadmills have the advantage that the user's wheelchair can be used	de Klerk et al., 2019
RSF2	yes	Haptic feedback is provided at the wheels for rolling resistance, and ascending and descending slopes	Mason et al., 2014
RSF3	yes	Proprioceptive feedback can be provided for ascending and descending slopes by modifying the grade of the belt	Mason et al., 2014
RSF4	no	No study was found that coupled a treadmill ergometer to visual feedback of a scene	
RSF5	no	No study was found that coupled a treadmill ergometer to auditory feedback of a scene	
req	**yes / no**	**explanation**	**references**
RCR1	yes	It's possible to measure propulsion forces and torques if the wheelchair is equipped with instrumented wheels	Gagnon et al., 2016
RCR2		workload can be calculated through drag tests manipulated using a pulley system by altering the speed or gradient	Van der Woude et al., 1986, Veeger et al., 1989, Mason et al., 2014
RCR3	no	No study was found that measured the reaction forces on the seat or backrest.	
RCR4	yes	Studies have measured physiological parameters	Lakomy et al., 1987
RCR5	yes	It's possible to accommodate different wheelchair configurations, such as different cambers in sports wheelchairs or positions of the axle in regular wheelchairs	Rice et al., 2020 Veeger et al., 1989

Having established the level of realism with respect to criteria, we turn next to the results of studies that have compared treadmill to overground propulsion, using a variety of parameters.

1.4.2.3 Comparison of propulsion on a treadmill and overground propulsion

Several studies have been performed comparing manual propulsion overground to that on a treadmill. On the one hand, Vanlandewijck et al. (2001) performed a study whereby they concluded that treadmills were a valid measurement device. Kwarciak (2011) compared several biomechanical variables (contact angle, peak force, average force) and found no statistical difference between overground and treadmill propulsion. It should be noted that the researchers raised the grade of the treadmill until power output was the same as overground.

On the other hand, a study by van der Woude (2001) concluded that validity of treadmills for research and training may be reduced because that modality may have an effect on propulsion kinematics. Moreover, usually, studies on wheelchair biomechanics performed on treadmills keep the belt speed constant. This does not simulate real life conditions, where the speed of the wheelchair depends upon the force applied by the user (Abel & Frank, 1992).

Stephens and Engberg's study (2010) performed a quantitative comparison of hand trajectories for overground and treadmill propulsion and concluded that they were significantly different. They cautioned that results obtained from research or training on treadmills should not automatically be viewed as valid for overground propulsion. Chénier et al. (2018) performed a study to investigate speed perception of propelling overground compared to that on a treadmill. The authors found that subjects' self-selected speed on a treadmill was always lower than self-selected speed overground. They recommended both speeds be matched when conducting training on manual wheelchair propulsion on a treadmill.

Mason (2014) concluded that a 0% treadmill gradient and a single-roller ergometer are not suitable for accurately replicating the physiological demand or biomechanics of overground wheelchair propulsion specific to wheelchair sports. He suggested that resistive forces (rolling resistance, internal friction, air resistance) demonstrated different responses with regards to speed in a laboratory environment to what was elicited in the field.

Notwithstanding, it is worth noting, that with regards to walking, studies that have compared overground and treadmill walking by measuring kinematic and kinetic parameters have shown differences (Alton et al., 1998; Riley et al., 2007). It could perhaps be possible to maintain the validity of measurements by compensating for the differences observed. Mason (2014)

matched oxygen uptake between overground conditions and on a treadmill by modifying the inclination angle of the treadmill.

To overcome challenges of using treadmills, researchers have tried building devices specifically for manual wheelchair research. The integrated ergometer is such a device and is described in the next section.

1.4.3 Integrated ergometers

An integrated manual wheelchair ergometer is a stationary wheelchair-like device, in which the rear wheels and front casters are above ground (Figure 1.19). They are elaborate electromechanical machines, comprising of a large number of sensors, actuators, control systems, all inter-connected with the goal of simulating overground wheelchair propulsion with a high degree of realism. Integrated ergometers are usually very flexible, being able to adjust several parameters over a wide range. They can also add power to, or subtract power from, that generated by the human user. We will detail integrated ergometers found in the literature in the past thirty years, then establish how they measure up against requirements for high realism.

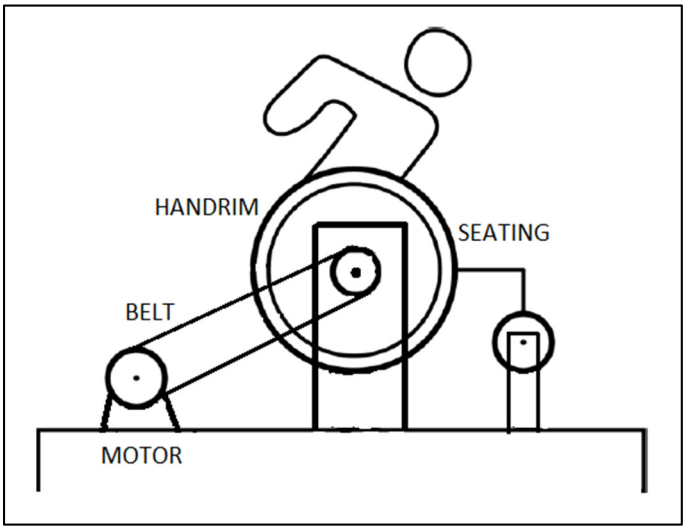

Figure 1.19 Diagram of an integrated ergometer

1.4.3.1 Integrated ergometers in the literature

The integrated ergometer built by Niesing et al. (1990) is shown on Figure 1.20. It is a complex electromechanical machine built to conduct experiments studying the physiology and biomechanics of wheelchair propulsion. The translational inertia of the wheelchair-use system is simulated by a computer program. It is very well instrumented allowing for the measurement of a large number of parameters. Between the handrims and the wheelchair-axis, torque transducers are mounted to measure the real torque that causes propulsion. It has a seat and backrest consisting of two stiff frames, connected by three two-dimensional force transducers, for frontal and vertical force measurement.

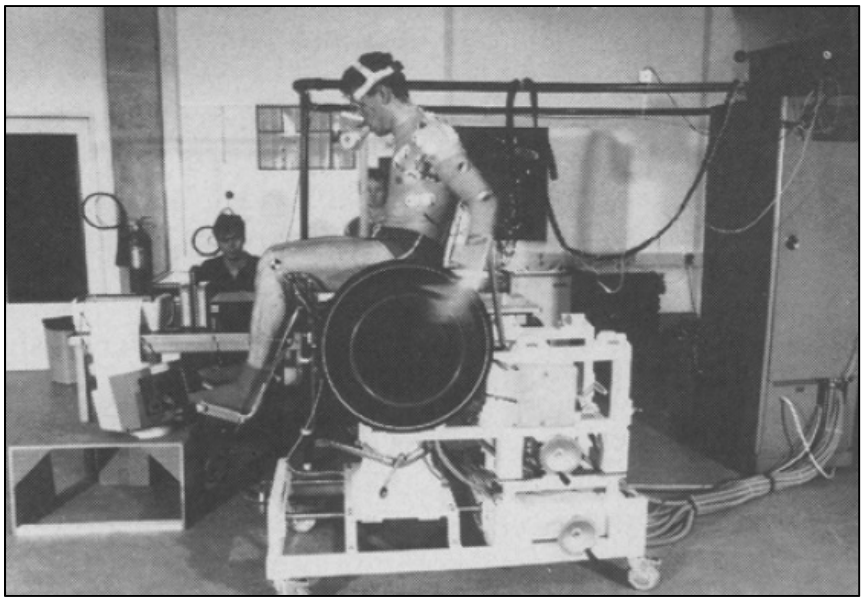

Figure 1.20 Integrated wheelchair ergometer by Niesing et al. (1990)

The Gifu Simulator is an integrated ergometer located in the Human Support Systems Laboratory at Gifu University in Gifu, Japan. It is shown on Figure 1.21. It is a Virtual Reality System built to simulate the displacement of a wheelchair inside a building to evaluate its accessibility (Bando et al., 2004). It was built in response to the need of building designers to ensure full accessibility of buildings as required by the laws enacted in the year 2000 in Japan establishing formally disabled individuals' rights in society.

Figure 1.21 Gifu Simulator
(Bando et al., 2004)

The integrated ergometer built at the University of Toronto is shown on Figure 1.22. It is located inside the Challenging Environment Assessment Laboratory (CEAL) (Figure 1.23) housed at the Toronto Rehabilitation Institute. The ergometer uses adapted seating and not a real wheelchair. The motors drive the wheels directly, and are attached to them at their side, thus impeding free natural circular movement of the arm during the recovery phase.

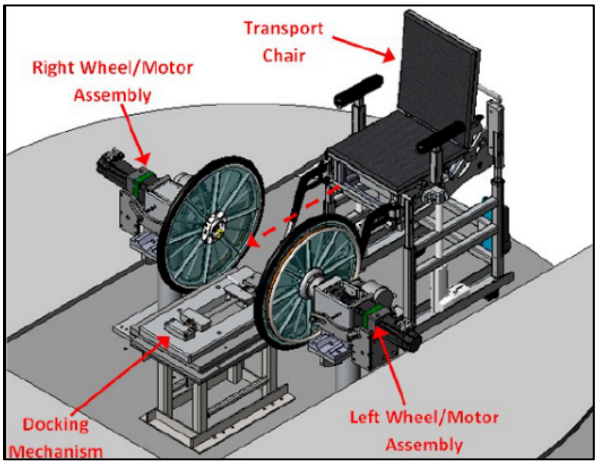

Figure 1.22 Integrated ergometer housed at
the University of Toronto (Crichlow, 2011)

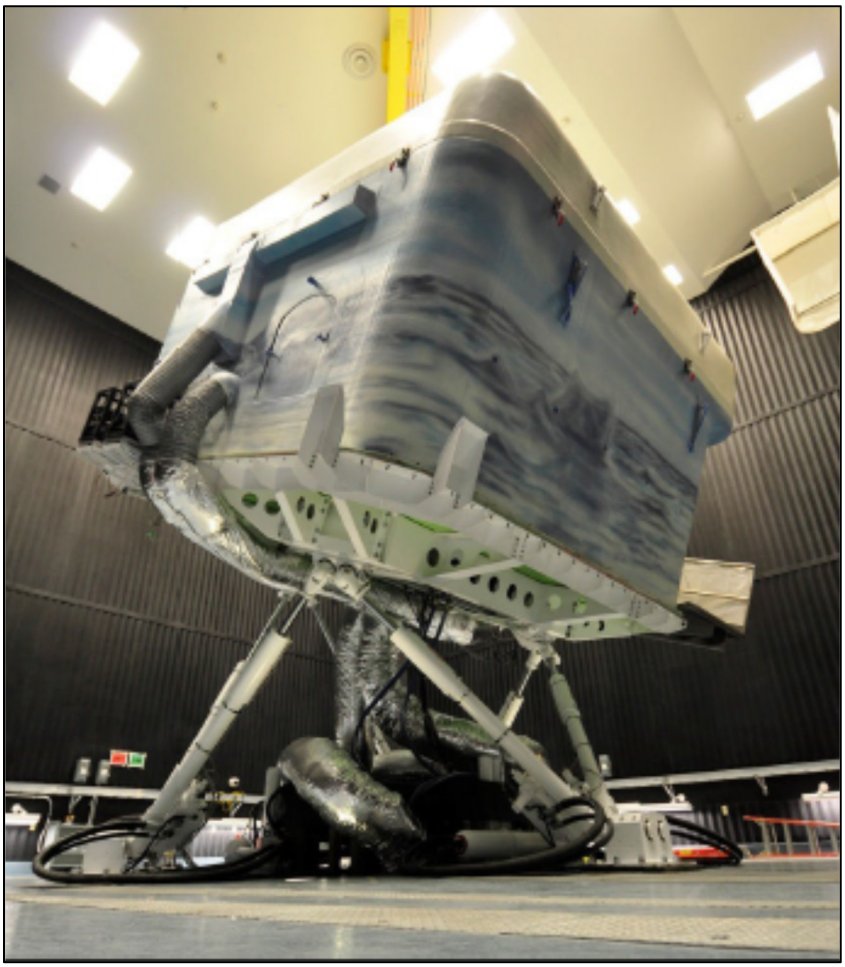

Figure 1.23 The CEAL at the Toronto Rehabilitation Institute (Crichlow, 2011)

1.4.3.2 Realism of integrated ergometers

Table 1.2 below shows how each of the three integrated ergometers described in this section measures up against the requirements for realism listed in section 1.3.

Table 1.2 Integrated ergometers : requirements for realism

		Rotterdam	**Gifu**	**Toronto**
		Niesing (1990)	**Bando (2004)**	**Crichlow (2011)**
no.	**requirements for realism: overground dynamics ROD**			
1	realistic simulation of the linear inertia of the weelchair user system (m(tot).a)	simulated in a computer program	simulated in a computer program written in C	simulated in a computer program
2	simulation of horizontal force due to movement of subject + trunk	not measured	not measured	motion capture equipment
3	adequate simulation of friction due to rolling resistance (mu.N = mu.m(tot).g.cos(alpha))	different rolling resistances can be simulated	not taken into account	yes (+ detection of user's shifting center of gravity)
4	adequate simulation of friction due to air resistance (above 2 m/s) $0.5.rho.(Vwc-Vair)^2.A.Cd$	different wind forces can be simulated	not taken into account	not taken into account
5	simulation of ascending slopes	yes	yes	yes
6	simulation of descending slopes	yes	yes	yes
7	simulation of cross slopes	yes, wheels controlled separately	no	yes
8	linear paths (1D model of wheelchair propulsion)	1D model	1D model	1D model
9	curvilinear paths (2D model of WC propulsion)	no	2D model	2D model
10	out-of-plane paths (3D model of WC propulsion)	no	no	3D model

Table 1.2 Integrated ergometers: requirements for realism (continued)

		Rotterdam	**Gifu**	**Toronto**
no.	**requirements for realism: sensory feedback RSF**			
1	respect ergonomic properties of the wheelchair-user interface (user's wheelchair, seat height, camber)	cannot use user's wheelchair	cannot use user's wheelchair	cannot use user's wheelchair
2	provide haptic feedback to the user (at the wheels)			
	rolling resistance	yes	yes	yes
	ascending, descending, cross slopes	yes	yes	yes
	collisions with objects	no	yes	no
3	provide proprioceptive feedback to user (platform under wheelchair)			
	ascending, descending, cross lopes	no	yes (Stewart platform)	yes (Stewart platform)
	vibrations due to uneven ground	no	yes	yes
4	provide visual feedback to user			
	screen	no	no	yes
	head-mounted display	no	yes	no
5	provide auditory feedback to the user	no	no	yes
no.	**requirements for measurement: ergometer RCR**			
1	measurement of forces and moments applied by the user on the handrims			
	tangential, radial, medio-lateral	yes	no	no
	torque	yes	yes	yes
2	can measure biomechanical parameters (power output, angle per push, cycle times)	yes	yes	yes
3	can measure reactions forces (on the seat, in the backrest)	yes	no	no
4	can measure physiological parameters (VO2 max, power output, heart rate)	yes	no	yes
5	can accomodate different wheelchair configurations (seat height, rear wheel camber, axle position)	yes	no	yes

1.4.4 Roller ergometers

1.4.4.1 Introduction

An ergometer is considered to be a roller ergometer if there is at least one roller on which a real wheelchair is placed. Just like integrated ergometers, roller ergometers provide a constrained wheelchair testing environment. The wheelchair is securely fastened to the platform, and each wheel is placed on top of a roller or two, allowing the wheelchair to remain stationary at all times. No steering is required to keep the wheelchair on the ergometer.
We will restrict our definition of roller ergometer to a device which does not have a force measurement device, motors, or incorporates a control system.
In the next few pages, we will present several of the roller ergometers built in past few years that have been reported in the scientific literature.

1.4.4.2 Roller ergometers in the literature

Ferguson-Pell and his student Wu (2013) developed a roller ergometer at the University of Calgary, presented on Figure 1.24. Their primary goal was to compare wheelchair propulsion overground and on an ergometer, in an attempt to justify the use of stationary devices for the study of manual wheelchair propulsion. A secondary goal was to quantify the propulsion during the transition from one surface to another, in this case synthetic grass to carpet.

Vanlandewijck et al. (2011) ran a study at the Université Catholique de Louvain, in Belgium related to the classification of wheelchair athletes. They wanted to evaluate the effect that reduced trunk muscle power had on wheelchair racing performance. Part of their study was conducted on a roller ergometer (Figure 1.25), in which the roller was coupled to a flywheel.

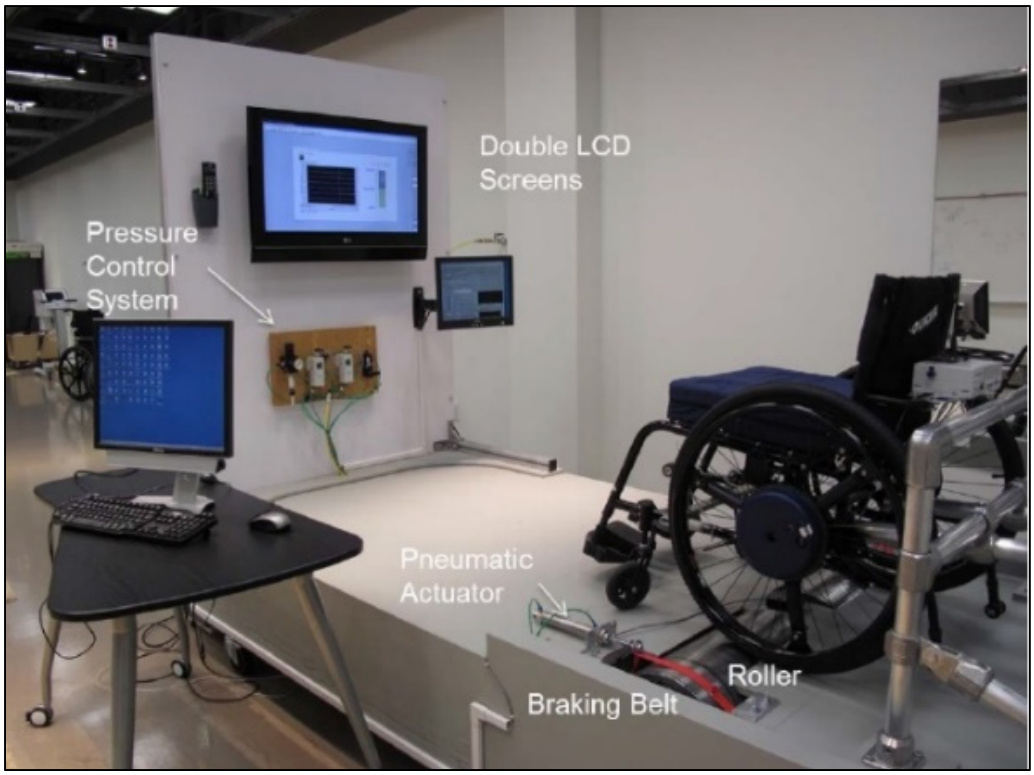

Figure 1.24 Roller ergometer at the University of Calgary (Wu, 2013)

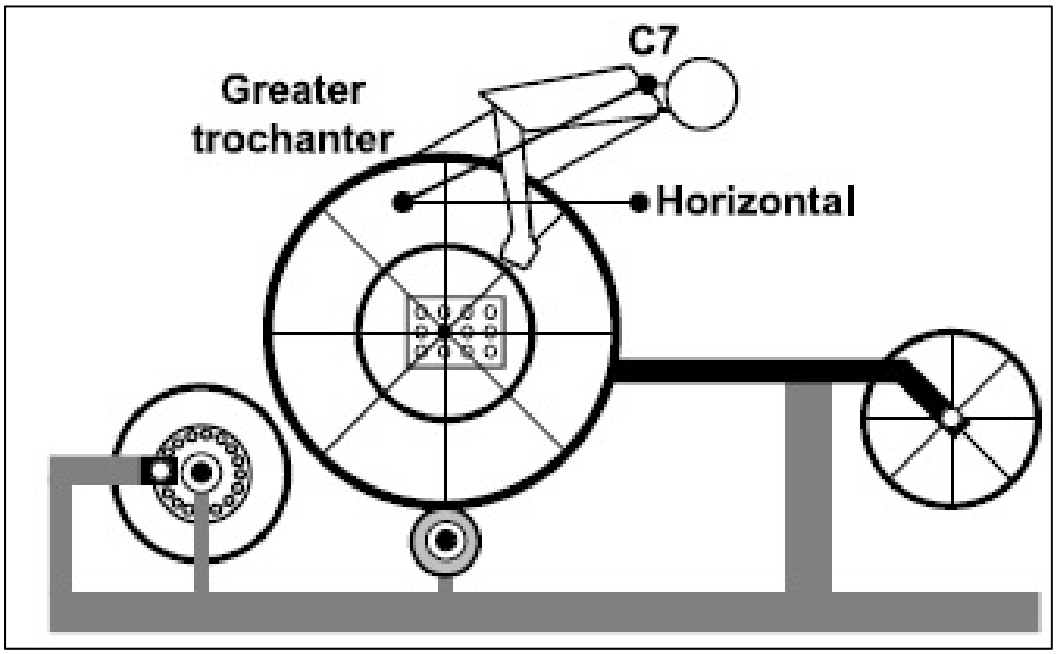

Figure 1.25 Sketch of the flywheel/roller ergometer system at the Université Catholique de Louvain (Y. C. Vanlandewijck et al., 2011)

Hwang (2012) and his colleagues at Yonsei University in Korea built a roller ergometer, shown in Figure 1.26. Their goal was to perform fundamental research on manual wheelchair propulsion in an effort to reduce the physical strain and pain in the daily life of manual wheelchair users. They used their ergometer to measure torque and power output of wheelchair propulsion. They wanted to compare those values between experienced and novice users under different propulsion conditions.

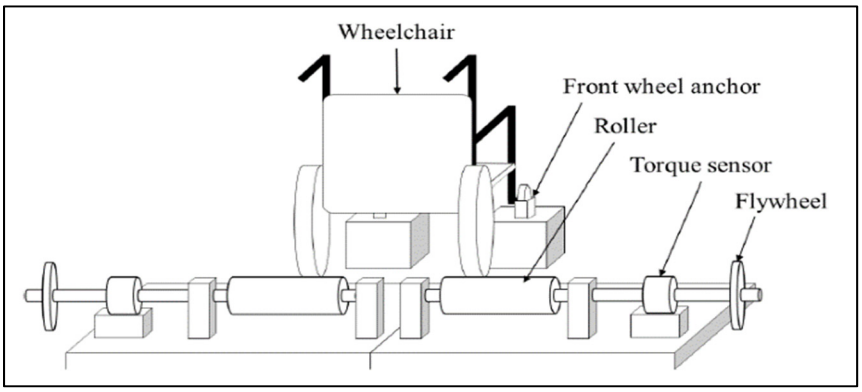

Figure 1.26 Ergometer at Yonsei University (Hwang et al., 2012)

Kurt (2008) built a dual roller ergometer at Marmara University, in Turkey. It is shown in Figure 1.27. It a device built to train manual wheelchair users at different level of resistance. The variable resistance is achieved by modifying the strength of the magnetic brake.

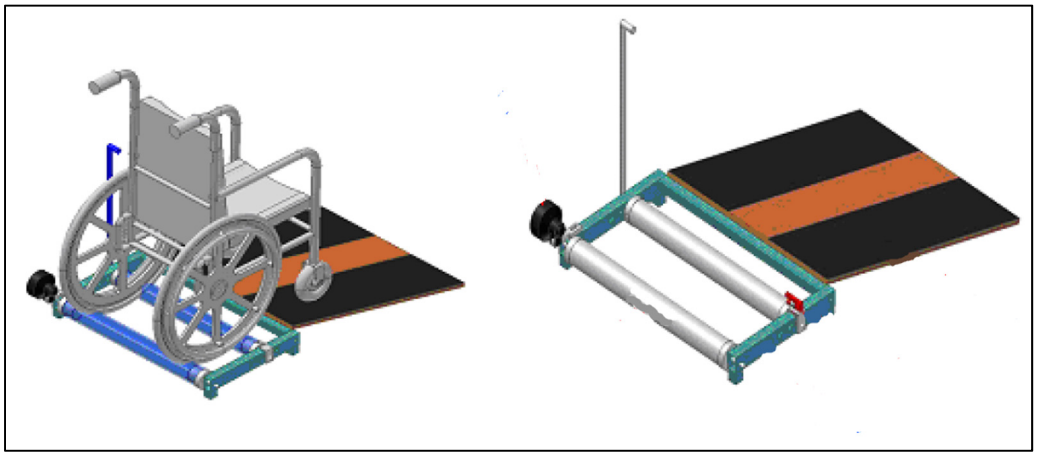

Figure 1.27 Dual roller ergometer at Marmara University (Kurt et al., 2008)

The ergometer built by Harrison et al. (2004) incorporates an encoder. The latter measures the incremental angular displacement of either wheel on the motion platform. This is used to calculate wheelchair displacement and the motion of the visual field can be calibrated in relation to actual displacement. Feedback from the graphics system determines whether the brakes, clutch, or motors should be actuated to provide a physical level of feedback to the user. Control of the entire wheelchair platform is therefore accomplished at the physical level on the basis of events occurring in the virtual world. Their simulator is located at the University of Strathclide, in England. The part of the ergometer which comprises the motor, clutch, encoder, roller and wheel is shown on Figure 1.28.

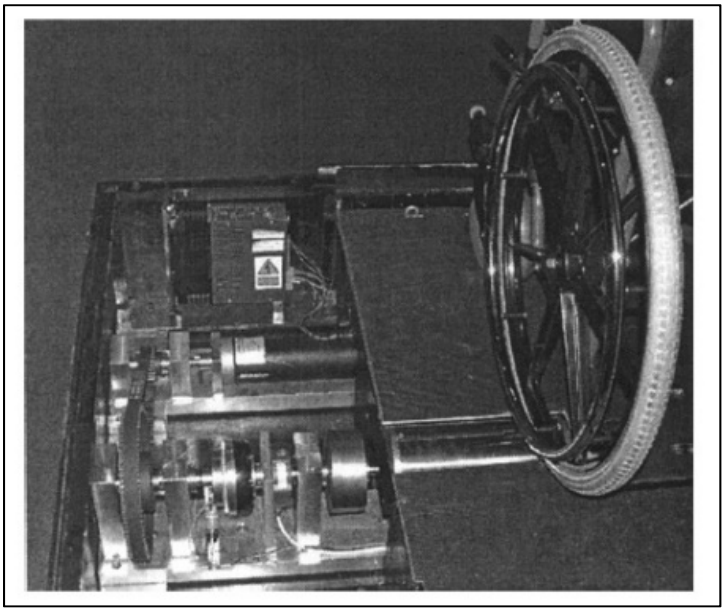

Figure 1.28 Motion platform roller assembly at the University of Strathclyde (Harrison et al., 2004)

1.4.4.3 Realism of roller ergometers

Table 1.3**Erreur ! Source du renvoi introuvable.** evaluates the realism of the five roller ergometers presented in this section according to the criteria given in section 1.3.

Table 1.3 Roller ergometers: requirements for realism

no	**requirements for realism: overground dynamics ROD**	**Alberta Wu (2013)**	**UCL Valandewijck (2011)**	**Yonsei Hwang (2012)**	**Marmara Kurt (2008)**	**Strathclyde Harrison (2004)**
1	realistic simulation of the linear inertia o the weelchair user system (m(tot).a)	yes (fixed mass rollers)	yes (flywheel with adjustable ratios)	yes (variable mass rollers)	no (roller mass not matched)	yes (variable mass rollers)
2	simulation of horizontal force due to movement of subject + trunk	measured with IMU	yes (markers)	yes (markers)	no	no
3	adequate simulation of friction due to rolling resistance mu.N = mu.m(tot).g.cos(alpha)	yes (brakes, pneumatic actuators	yes (brake through a belt over the pulley)	yes (passive)	yes, brake (magnetic)	yes, mechanical brake
4	adequate simulation of friction due to air resistance 0.5.rho.(Vwc-Vair)^2.A.Cd	not taken into account	not taken into account	not taken into account	not taken into account	not taken into account
5	simulation of ascending slopes	not taken into account	not taken into account	not taken into account	not taken into account	yes (motors)
6	simulation of descending slopes	not taken into account	not taken into account	not taken into account	not taken into account	yes (motors)
7	simulation of cross slopes	not taken into account	not taken into account	not taken into account	not taken into account	no
8	linear paths (1D model of WC propulsion)	1D model	1D model	1D model	1D model	1D model
9	curvilinear paths (2D model of WC propulsion)	no	no	no	no	2D model
10	out-of-plane paths (3D model of WC propulsion)	no	no	no	no	no

Table 1.3 Roller ergometers: requirements for realism (continued)

no	**requirements for realism: RSF**	**Alberta**	**UCL**	**Yonsei**	**Marmara**	**Strathclyde**
1	respect ergonomic properties of the wheelchair-user interface (user's wheelchair, seat height)	yes	yes	yes, including camber	yes	yes
2	provide haptic feedback to the user at the wheels					
	rolling resistance	yes	yes	yes	yes	yes
	ascending, descending, cross slopes	no	no	no	no	yes
	collisions with objects	no	no	no	no	yes
3	provide proprioceptive feedback to user					
	ascending, descending, cross slopes	no	no	no	no	no
	vibrations due to uneven ground	no	no	no	no	no
4	provide visual feedback (scene)					
	screen	yes	no	no	no	yes
	head-mounted display	no	no	no	no	no
5	provide auditory feedback to the user	yes	no	no	no	yes
no	**requirements for measurement: RCR**	**Alberta**	**UCL**	**Yonsei**	**Marmara**	**Strathclyde**
1	measurement of forces applied on the handrims					
	tangential, radial, medio-lateral	yes	no	yes	no	no
	torque	yes	no	yes	no	no
2	can measure biomechanical parameters (power output, angle per push, cycle times)	yes	no	yes	no	yes (motion of rollers)
3	can measure reactions forces (seat, backrest)	no	no	no	no	no
4	can measure physiological parameters (VO2 max, aerobic power, heart rate)	no	no	no	no	no
5	can accomodate different wheelchair configurations (seat height, rear wheel camber,	yes, but not camber	yes, but not camber	yes, including camber	yes, but not camber	yes, but not camber

1.4.4.4 Aspects and physics of manual wheelchair propulsion on roller ergometers

As for treadmills, roller ergometers have the advantage that they can be used with the user's own wheelchair. In a roller ergometer, the change in velocity of the wheelchair wheel is dictated by the torque applied by the user, inertia of the rollers, frictional torque in the bearings of the ergometer and wheelchair and the contact friction of the wheel on the roller. Roller types in these devices range from fully passive rollers (Kurt et al., 2008) to highly-advanced computer-controlled systems with electronic brakes (Harrison et al., 2004). Roller ergometers with electronic brakes or an electronic control system offer more flexibility to mechanically emulate wheelchair propulsion, but they still have to adjust for system friction. Some roller ergometers use a motor to simulate overground propulsion, which can generate braking and assistive torques. However, they require more advanced calibration methods (DiGiovine, 2001).

Wheelchairs on rollers need proper compensation for the inertial properties of the wheelchair/user system. The translational inertia of wheelchair propulsion on a roller ergometer have been simulated either of two ways: mechanical (the roller's mechanical inertia matches with the translational inertia of the wheelchair) or electronic (using an electronically-controlled motor or brake).

Friction is simulated by a standard friction belt or other braking system. This setup can only simulate a constant friction which is the least complicated way of simulating rolling resistance. However, this strays away from reality because friction depends on the proportion of weight on the casters and rear wheels as mentioned in Eq. (1.11) (Bascou et al., 2013; Kurt et al., 2008; Sauret et al., 2012). In overground propulsion, moving the trunk and upper body forward shifts the weight toward the castor wheels, which, by their smaller diameter, temporarily increases the rolling resistance (Sauret et al., 2013). On roller ergometers, the opposite happens: since the castor wheels do not turn, shifting the trunk forward only decreases the weight on the rear wheels, which reduces the total rolling resistance. Moreover, a friction belt

or constant braking system is also usually not sufficient to simulate velocity-dependent friction such as air drag, which is not important for simulation of everyday wheelchair wheeling, but would be important for simulation of wheelchair racing (Forte et al., 2016).

In roller ergometers, acceleration tasks can be performed safely compared to treadmills, where the ground is always moving (and the user must take the treadmill's speed into account). Thus, roller ergometers can use the user's own wheelchair (a benefit of treadmills but a disadvantage of integrated ergometers) and can also simulate turns (a benefit of integrated ergometers but a disadvantage of treadmills). Simulating curvilinear propulsion is possible if the mathematical model of the wheelchair is at least two-dimensional and takes into account the vertical moment of inertia of the wheelchair (Chénier et al., 2014). As such, we can describe the dynamics of one rear wheel of a wheelchair roller ergometer using Newton's Second Law of Motion for rotating systems. Chénier gives such a description if his Ph.D. thesis (2012):

$$\sum M_O = I_O \ddot{\theta} \tag{1.12}$$

Where O is the center of the wheel, M_O are the moments applied around its axis and $\ddot{\theta}$ is its acceleration. Expanding:

$$M_{app,i} - sgn(\dot{\theta}_{R,i}) M_{F,i} = I_O \ddot{\theta}_{R,i} \tag{1.13}$$

where $M_{app,i}$ is the moment of the applied force F_{prop} at the handrim by the user:

$$M_{app,i} = F_{app,i} r_R \tag{1.14}$$

where r_R is the radius of the handrim, $M_{F,i}$ is the moment of the rolling resistance $M_{F,i} = F_{roll} \cdot r_R$, $I_O = \frac{mr_R^2}{2}$, and $\ddot{\theta}_{R,i}$ and $\dot{\theta}_{R,i}$, are the angular acceleration and velocity of the wheelchair rear wheel.

Therefore, the simulation of the straight line propulsion model, as implemented on a two-roller ergometer, is given by:

$$\dot{\theta}_{R,i} = \int \left(\frac{2M_{app,i}}{mr_R^2} - \frac{sgn(\dot{\theta}_{R,i}) F_{roll}}{mr_R} \right) dt \tag{1.15}$$

1.4.5 Manual wheelchair simulators

1.4.5.1 Haptic control loop

To overcome the adjustments needed to calibrate motorized simulators (matching the inertia and resistance), wheelchair roller ergometers equipped with the latest technology use haptic control loops to reproduce simulated conditions, which means that the inertia and resistance of the simulator can be changed on the fly using software. We will classify this special group of roller ergometers as wheelchair simulators, which now become a subset of haptic robots. A theoretical model of the admittance control loop of a wheelchair simulator designed as a haptic robot is shown on Figure 1.29.

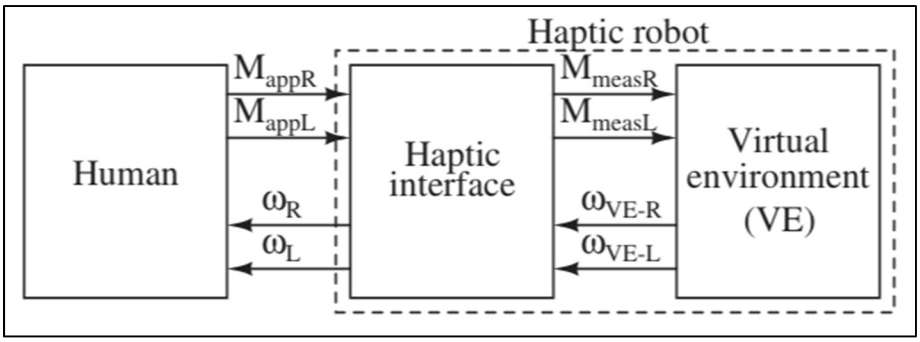

Figure 1.29 Theoretical model of the admittance control of a wheelchair simulator designed as a haptic robot (Chénier et al., 2014)

The haptic interface is comprised of the instrumentation portion (the force sensor and the encoders which allow for the estimation of the motor speeds), the actuation portion (the motors and drives), and the control system in software which allows the roller speed to be matched to that provided by the mathematical model.

The virtual environment is a simulation of the space in which the wheelchair operates, e.g., on level ground, on ascending and descending slopes, inside a building, in a room, in an apartment or house, in an office, in the street.

The haptic interface and the virtual environment together make up the haptic robot, which interacts with the human user.

1.4.5.2 Manual wheelchair simulators in the literature

Currently existing manual wheelchair simulators will be featured in the next few pages.

Washington University in St. Louis, located in the city of St. Louis, Missouri, United States houses a manual wheelchair simulator (named the WheelMill System or WMS) where each rear wheel sits on two rollers (Klaesner et al., 2014). The torque at the rollers is measured and is input to a software control system that determines the speed of wheels and can simulate different surfaces and slopes. The platform is highly adjustable, with rollers large enough to accommodate a wide range of wheelchair widths and cambers, and also being physically able to simulate ascending, descending and cross slopes. Figure 1.30 shows this ergometer. The main goal for the researchers is to release their device for independent use in research institutions, fitness centers and rehabilitation facilities. Clinicians could place users on the WMS on different slopes to help determine optimal axle placement. In a public gym, athletes with disabilities could enhance their physical conditioning.

Figure 1.30 Manual wheelchair simulator housed at
Washington University in St. Louis (Klaesner et al., 2014)

Bentaleb et al. (2019) built a manual wheelchair simulator (shown on Figure 1.31) in their laboratory located at the Hauts-de-France Polytechnic University, in France. It has a 3D visual and sound restitution system composed of six full HD screens (180º horizontal field of view) and a multi-channel audio system. It is mounted on a Stewart platform allowing it to simulate ascending, descending and cross slopes, as well as vibrations due to rough terrain.

Figure 1.31 Manual Wheelchair Simulator at the Hauts-de-France Polytechnic University, Valenciennes, France (Bentaleb et al., 2019)

De Klerk et al. (2020) worked in collaboration with the company Lode BV to build a manual wheelchair simulator, shown on Figure 1.32. It is housed at the Center for Human Movement Sciences at the University of Groningen in The Netherlands. It comprises motorized rollers and a haptic interface that uses two force cells (one on each side) to measure the forces applied at the handrims. It was built to facilitate capacity assessment, training and skill acquisition in rehabilitation and adapted sports.

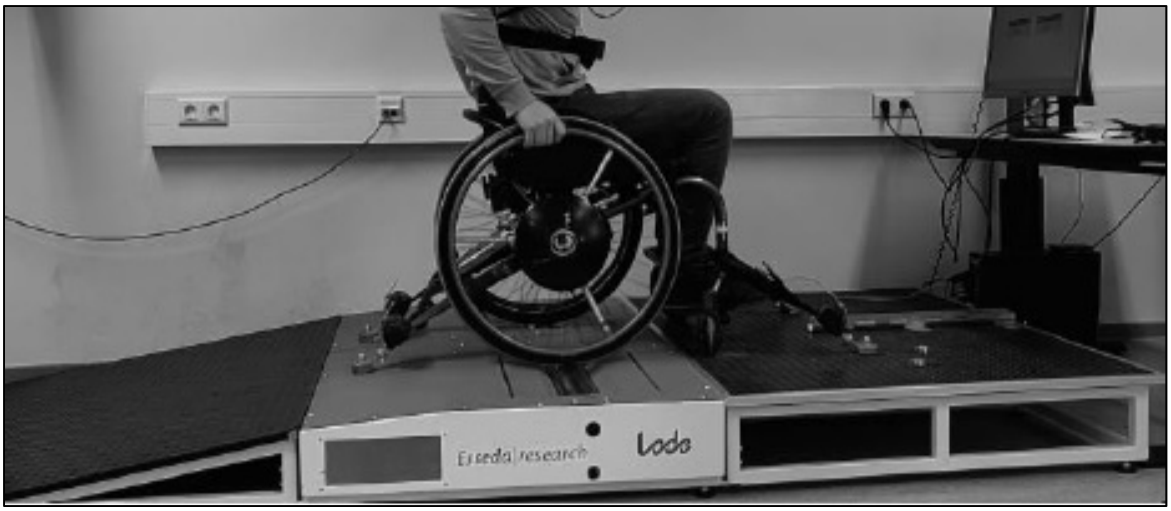

Figure 1.32 Manual wheelchair simulator at the University of Groningen, Netherlands (de Klerk, Vegter, Veeger, et al., 2020)

1.4.5.3 Realism of manual wheelchair simulators

Table 1.4 shows how each of the three wheelchair simulators meets the requirements for realism which were enunciated in section 1.3.

The mathematical models in the virtual environment of these manual wheelchair simulators are one-dimensional. Therefore, they cannot simulate curvilinear paths. In contrast, the LIO simulator does incorporate a two-dimensional model, which includes the moment of inertia around the vertical axis, allowing it to simulate turns. The model also takes into account the orientation of the front casters in determining the angular speed of the wheels (Chénier et al., 2014). As this is the simulator that the work presented in this thesis is built upon, we will discuss it shortly in detail. This way, we will be able to understand its inner workings and its advantages.

Table 1.4 Manual wheelchair simulators: requirements for realism

		Washington	**Hauts-de-France**	**Groningen**
		Klaesner (2014)	**Bentaleb (2019)**	**DeKlerk (2020)**
no	**requirements for realism: overground dynamics ROD**			
1	realistic simulation of the linear inertia of the weelchair user system (m(tot).a)	yes	yes	yes
2	simulation of horizontal force due to movement of subject + trunk	no	no	no
3	adequate simulation of friction due to rolling resistance mu.N = mu.m(tot).g.cos(alpha)	yes	yes	yes
4	adequate simulation of friction due to air resistance (above 2 m/s) 0.5.rho.(Vwc-Vair).A.Cd	not taken into account	not taken into account	not taken into account
5	simulation of ascending slopes	yes	yes	yes
6	simulation of descending slopes	yes	yes	yes
7	simulation of cross slopes	yes	no	no
8	linear paths (1D model of wheelchair propulsion)	1D model	1D model	1D model
9	curvilinear paths (2D model of WC propulsion)	no	no	no
10	out-of-plane paths (3D model of WC propulsion)	no	no	no

Table 1.4 Manual wheelchair simulators: requirements for realism (continued)

		Washington	Hauts-de-France	Groningen
no.	**requirements for realism: sensory feedback RSF**			
1	respect ergonomic properties of the wheelchair-user interface (user's wheelchair, seat height, camber)	yes, including camber	yes, but not camber	yes, but not camber
2	provide haptic feedback to the user at the wheels			
	rolling resistance	yes	yes	yes
	ascending, descending, cross slopes	yes	yes	yes
	collisions with objects	no	no	no
3	provide proprioceptive feedback to user (platform under wheelchair)			
	ascending, descending, cross slopes	yes	yes	no
	vibrations due to uneven ground	no	yes	no
4	provide visual feedback to user			
	screen	no	yes	no
	head-mounted display	no	no	no
5	provide auditory feedback to the user	no	yes	no
no.	**requirements for measurement: ergometer RCR**			
1	measurement of forces applied by the user on the handrims			
	tangential, radial, medio-lateral	no	no	yes
	torque	yes	yes	no
2	can measure biomechanical parameters (power output, angle per push, cycle times)	yes	yes	yes
3	can measure reactions forces (on the seat, in the backrest)	no	no	no
4	can measure physiological parameters (VO2 max, aerobic power, heart rate)	yes	no	no
5	can accomodate different wheelchair configurations (seat height, rear wheel camber, axle position)	yes, including camber	yes, but not camber	yes, but not camber

1.5 The LIO Simulator

The team at the LIO built a motorized rollers ergometer with haptic feedback. The main goal of the research program was to develop a tool for investigation into, and training of, propulsion techniques of manual wheelchair users (Chénier, 2012). The complete laboratory setup is shown on Figure 1.33. This picture includes the platform containing the motors, rollers and real wheelchair; the drives and power supplies in the corner; on the left, the screen for the Simulink real-time computer (running the control system and the mathematical model); and on the right the screens for the MATLAB computer (interface with, e.g. the clinician).

Figure 1.33 The LIO manual wheelchair simulator

The simulator was built with motorized rollers because by incorporating them, the simulator can adjust to a specific inertia and rolling resistance on the fly, it can use the user's wheelchair, it can use a curvilinear model of wheelchair propulsion, and it can provide biofeedback. We will begin by describing the retention system of the current LIO Simulator, which fixes the wheelchair to the platform. This will be a major part of the hardware remodeling during the implementation of the new force transducer.

1.5.1 Retention system

The wheelchair is placed on the rollers and is free to move if it is not retained. The retention system has two parts, which prevent translation in the horizontal plane and along the vertical axis, and prevents rotation about the roll, pitch and yaw axes. The wheelchair thus remains stationary on the platform as the human user propels it.

The first part is made up of two u-shaped supports whose height is adjustable. Its detail is shown on Figure 1.34. It retains the transversal axis of the wheelchair (one should note that not all wheelchair configurations have such a transversal axis) and prevents the wheelchair from rotating around the vertical axis.

Figure 1.34 LIO Simulator retention system:
transversal axle U-shaped supports

The second part retains the two casters and prevents the wheelchair from rotating about the transversal axis (pitch axis) and falling backwards, and prevents rotation about the yaw and roll axes. It is shown on Figure 1.35.

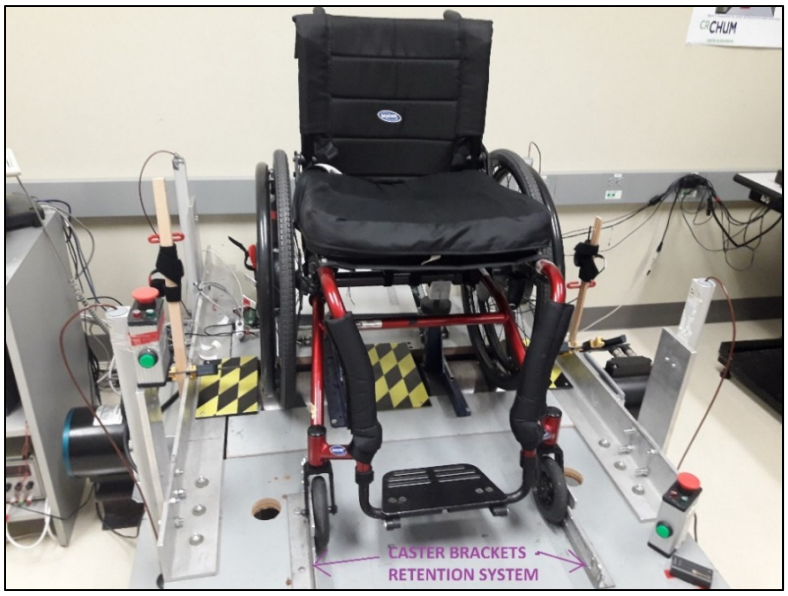

Figure 1.35 LIO Simulator retention system: Caster brackets

1.5.2 LIO Simulator as a haptic robot

Figure 1.36 shows the structure of the LIO Simulator concept as a haptic robot. We can decompose it into the real-world portion, the sensors/actuator portion and the real-time computer portion.

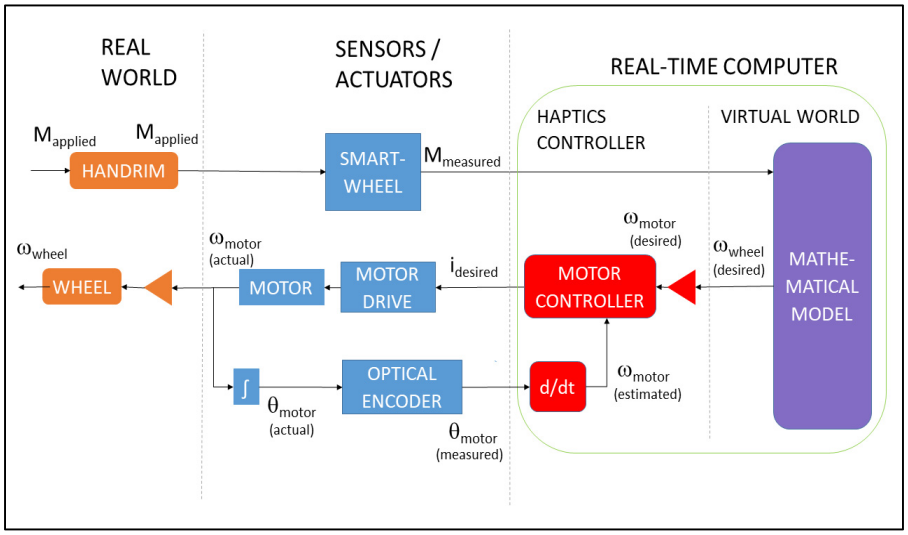

Figure 1.36 LIO Simulator concept as a haptic robot

1.5.3 Real world

The real world is comprised of the hardware elements that directly affect the user's interaction with the device. The user applies a moment $M_{applied}$ on the handrim. On the other side, the wheelchair wheel turns at a speed ω_{wheel} due to a control input.

1.5.4 Sensors/Actuators

1.5.4.1 Smartwheels

Smartwheels were described in section 1.4.1. Their function in Figure 1.36 are to measure the propulsion moments applied by the user on the wheels.

1.5.4.2 Motor drives

The motors are driven by two AKD-B00606 120 V 1-phase drives manufactured by the Kollmorgen company. They are controlled by a current loop integrated in the drive and they receive an input from the control system implemented on Matlab/Simulink Real-Time.

1.5.4.3 Optical encoders

An optical encoder is embedded within the motor casing and measures the angular position of the motor. This position can be filtered and differentiated in software in order to estimate the angular speed of the motor. This information is sent to the haptics controller.

1.5.5 Real-Time Computer

1.5.5.1 Haptics controller

The control system is focused on the wheelchair wheel-roller-motor assembly, shown on Figure 1.37.

Our ultimate goal is to control the angular speed of wheelchair wheels. However, for purposes of control, the plant in the wheelchair simulator is the motor. The motor and roller turn at the same speed because they are locked together by nut and bolt. We assume that there is sufficient friction between the wheelchair wheel and roller so that there is no slip between them. The angular speed of the wheel is related to the speed of the roller by a factor equal of the ratio of the two radii.

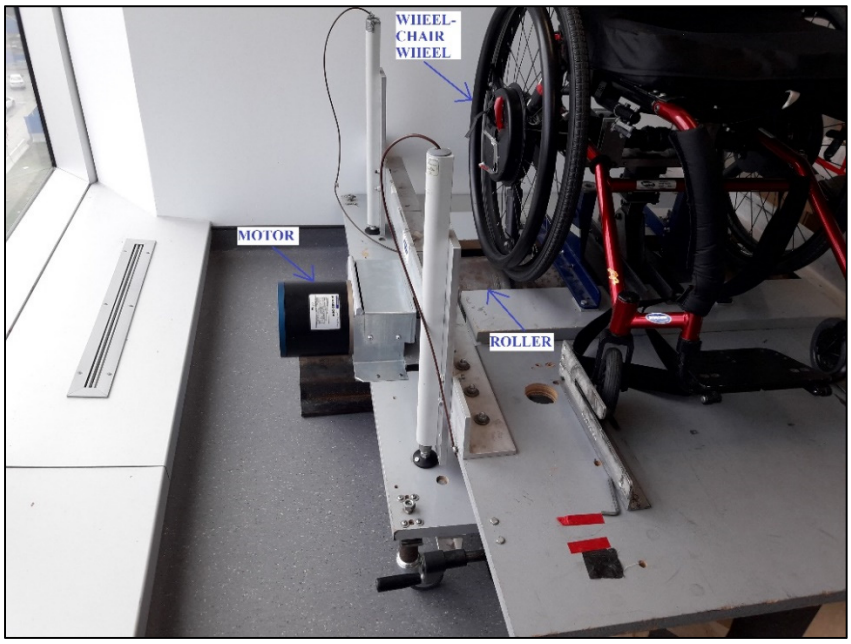

Figure 1.37 Wheelchair wheel-roller-motor assembly

The control system is a Proportional-Integrator (PI) controller. A block schematic of this controller is shown on Figure 1.38, and the variables are described in Table 1.5, both taken from Chénier et al. (2014).

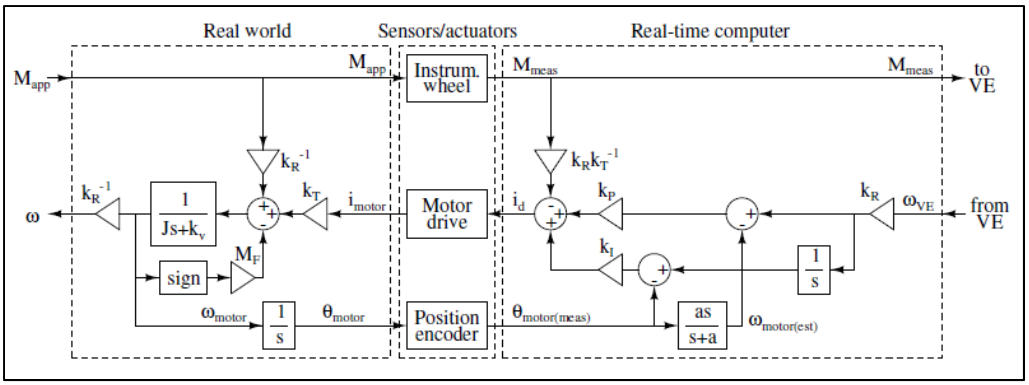

Figure 1.38 Block schematic of the LIO Simulator Haptic controller (Chénier et al., 2014)

Table 1.5 Variables in the block schematic of the Haptic Controller (Chénier et al., 2014)

symbol	**description**	**unit**
M_{app}	moment applied by the user	Nm
M_{meas}	measured moment M_{app}	Nm
ω_{VE}	velocity of the virtual wheel	rad/s
ω_{motor}	velocity of the motor	rad/s
θ_{motor}	position of the motor	rad
$\omega_{motor(est)}$	estimated velocity of the motor	rad/s
$\theta_{motor(meas)}$	measured position of the motor	rad
ω	velocity of the wheelchair's wheel	rad/s
i_d	current reference of the motor	A
i_{motor}	current in the motor	A
k_R	ratio of radii between the wheelchair's wheels and the rollers. On our prototype, $k_R = 2.21$	
k_T	torque gain of the motor = 4.406 for the D063M motors	Nm/A
J	total moment of inertia of the wheel (reported about around the motor's rotation axis) (unknown parameter)	$kg \cdot m^2$
k_v	viscous moment of friction of the roller (reported about around the motor's rotation axis) (unknown parameter)	Nm·s
M_F	dry moment of friction of the motor (reported about around the motor's rotation axis) (unknown parameter)	Nm
k_P	proportional gain of the compensator (set experimentally)	
k_I	integral gain of the compensator (set experimentally)	

The Simulink model for one wheel of the LIO Simulator is shown on Figure 1.39. The control system for the other wheel looks exactly same.

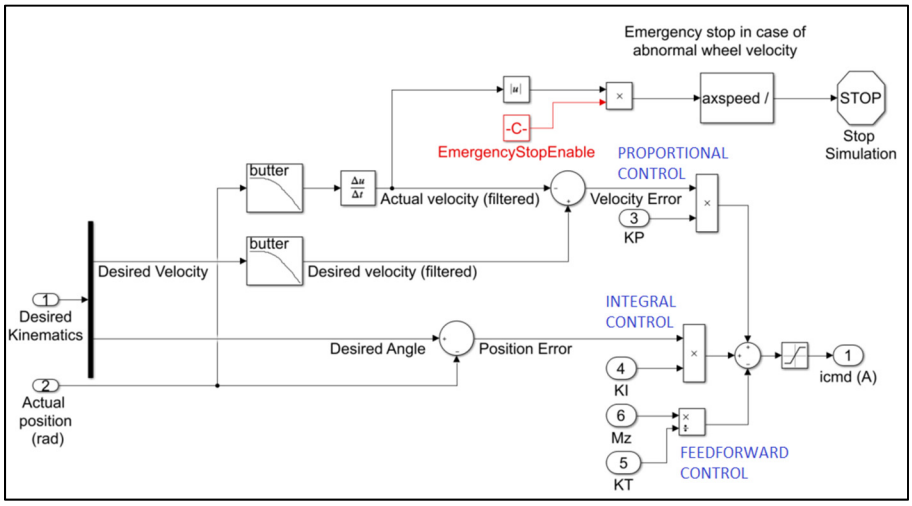

Figure 1.39 Simulink model of the control system for one wheel of the LIO Simulator (Chénier, 2012)

The reference signal is the desired velocity, located on the left-hand side of the figure. It is the output of the mathematical model. The handrim is subject to a disturbance which is the torque applied by the user. This disturbance is measured by the Smartwheels and is incorporated as a feedforward term in the control system.

1.5.5.2 Virtual world

The Virtual Environment (VE), also called the virtual world, is a mathematical description of the movement of a wheelchair on a level ground path (Chénier et al., 2015). The dynamic input to the VE is the measured torques on the handrims. The mathematical model used estimates of the orientation of the casters based on the velocity of the rear wheels and the wheelchair geometry. This estimate of the orientation is used in a 2D dynamic model of the wheelchair. The model is 2D because it incorporates the vertical moment of inertia of the wheelchair-user system. The model estimates the rear wheel speeds based on the moments generated by the user. These speeds are the dynamic output of the VE to the motor controller.

1.5.6 State of realism of the LIO Simulator

In this section, we look at how the LIO Simulator meets the requirements for a high realism manual wheelchair simulator (Chénier, 2012).

Table 1.6 LIO Simulator: requirements for realism

no.	**requirements for realism: overground dynamics ROD**	**explanation**
1	realistic simulation of the linear inertia of the weelchair user system (m(tot).a)	yes
2	measure horizontal force applied by user + trunk movement	not taken into account
3	adequate simulation of friction due to rolling resistance mu.N = mu.m(tot).g.cos(alpha)	modeled as a constant
4	adequate simulation of friction due to air resistance (above 2 m/s) 0.5.rho.(Vwc-Vair)^2.A.Cd	no
5	simulation of ascending slopes	yes
6	simulation of descending slopes	yes
7	simulation of cross slopes	no
8	linear paths (1D model of wheelchair propulsion)	1D model
9	curvilinear paths (2D model of WC propulsion)	2D model
10	out-of-plane paths (3D model of WC propulsion)	no
no.	**requirements for realism: sensory feedback RSF**	**explanation**
1	respect ergonomic properties of the wheelchair-user interface (user's wheelchair, seat height, camber)	yes, but wheels replaced by instrumented wheels
2	provide haptic feed to the user at the wheels (rolling resistance, slopes, collisions with objects)	provided for rolling resistance, ascending and descending slopes
3	provide proprioceptive feedback to user (platform underneath the wheelchair)	platform statically placed at a given angle for ascending and descending slopes
4	provide visual feedback to user	a screen and a head-mounted display are available
5	provide auditory feedback to the user	no

Table 1.6 LIO Simulator: requirements for realism (continued)

no.	**requirements for measurement: ergometer RCR**	**explanation**
1	measurement of forces applied by the user on the handrims (tangential, radial, medio-lateral, torque)	yes
2	can measure biomechanical parameters (power output, angle per push, cycle times, propulsion	measured or calculated
3	can measure reactions forces (on the seat, in the backrest)	no
4	can measure physiological parameters (VO2 max, aerobic power output, heart rate, etc.)	no
5	able to accomodate different wheelchair configurations (seat height, seat tilt angle, rear wheel camber, axle position)	limited in its ability to accommodate different kinds of wheelchair configurations, especially when it comes to axle positions and camber

The LIO Simulator is one of the more advanced manual wheelchair simulators in the world. It addresses many requirements of a high-realism simulator listed in section 1.3. However, several aspects of its realism could still be improved. For example, a main assumption of the mathematical model of the LIO Simulator is that trunk movement does not influence the motion of the wheelchair, which constitutes a limitation. Moreover, the simulator can use the user's wheelchair, but the wheelchair must be modified by substituting the wheels for Smartwheels.

In this thesis, we have addressed these two points by seeking to use force transducers to control the simulator instead of the Smartwheels. Those points lead to research questions, that we lay in the next chapter.

1.6 Conclusion of the literature review

In this literature review, we started by mathematically describing propulsion of a wheelchair overground, which is what we would like to simulate in a stationary environment. We presented two one-dimensional models, one that considered the user and the wheelchair as one body, the second that considered the user's trunk and the wheelchair as separate bodies to take

into account forces related to the back and forth movement of the trunk. We listed design requirements for realism of stationary devices aimed at the evaluation of manual wheelchair propulsion. We reviewed those devices, including treadmills, integrated ergometers, roller ergometers and wheelchair simulators, and evaluated their level of realism. We described in detail the LIO Simulator, which is the basis for the work presented in this thesis, including the drawbacks that we attempted to address.

CHAPTER 2

RESEARCH QUESTIONS

2.1 Problem Statement

The force and moment sensors currently used in the LIO Simulator are two Smartwheels. These sensors replace the wheelchair's original wheels, thereby changing their geometry and rigidity. In a rehabilitation center, this extra step reduces the time patients spend with their therapists. Moreover, during the simulation, Smartwheels do not measure completely the dynamics occurring during the push cycle which are due to the back and forth movement of the trunk. These shortfalls may have a great effect on the realism of the simulator. If the simulation is not realistic, conclusions from research studies may not be reliable, and wheelchair skills learnt on the simulator may not be transferable to real life.

2.2 Objectives

The main objective is to replace the Smartwheels as the force and moment measuring instrument by a force transducer which remedies the two drawbacks mentioned in the previous section. This will improve the realism of the manual wheelchair simulation. We will then build and validate a control loop using this force transducer. The control loop to be developed will be based on the most appropriate control algorithm for a manual wheelchair simulator, which will be investigated.

2.3 Approach

We designed and chose a force transducer that measures pertinent forces and moments. We built a mechanical bracket to support the force transducer and also to retain the wheelchair. We then designed and developed a control loop on MATLAB/Simulink. We validated it with one able-bodied subject.

2.4 Research hypotheses

The work that we set out to perform leads us to two research hypotheses:

H1 We can build a stable haptic control loop using a force transducer that measures the forces applied by the user at the handrim and also the forces due to the movement of the user's trunk, to control the velocity of the wheelchair wheels of the LIO Simulator.

H2 This control loop can replicate the moment-velocity interaction of a manual wheelchair on the ground, with an improvement over the realism provided by Smartwheels.

CHAPTER 3

EXPERIMENTAL METHODOLOGY

3.1 Introduction

In this chapter, we describe the steps taken to design the implementation of a force transducer, expound how we choose it from available force transducers (based on the objectives defined) and detail the tests run to validate the measurements of the force transducer. We then design the associated control loop based on control loops that have been used in the past for manual wheelchair simulators, and for other haptic interfaces. Then, we detail the procedure used to evaluate the realism of the simulator with this new control loop.

3.2 Design and experimental methodology for the force transducer

3.2.1 Forces to be measured

As we saw in the literature review, there is a relationship between, on the one hand, the forces the user applies at the handrims and those related to his movement, and on the other hand, the motion of the wheelchair observed. This relationship can be described by a mathematical model that takes into account parameters such as mass, rolling resistance and center of mass, amongst others. This is true of straight-line propulsion, and of non-linear paths, such as curvilinear propulsion, pure turning, amongst others. In our case, we will concentrate on straight-line propulsion.

The wheelchair simulator is a stationary device. The mathematical model of Eq. (1.7), run in a computer in real time, is used to determine the speed of each wheel of the wheelchair on the simulator, based on the input forces. In order to calculate the output speed, it is necessary to use a measurement device that can measure the forces that have an impact on the dynamics of the wheelchair.

The forces that govern the horizontal movement of the wheelchair are the reaction forces from the ground onto the wheels at the ground-tire interface and the forces from the human onto the

wheelchair due to movement of the human's trunk. Figure 3.1 shows those forces in a top-view free-body diagram of the wheelchair when it is placed on the ergometer.

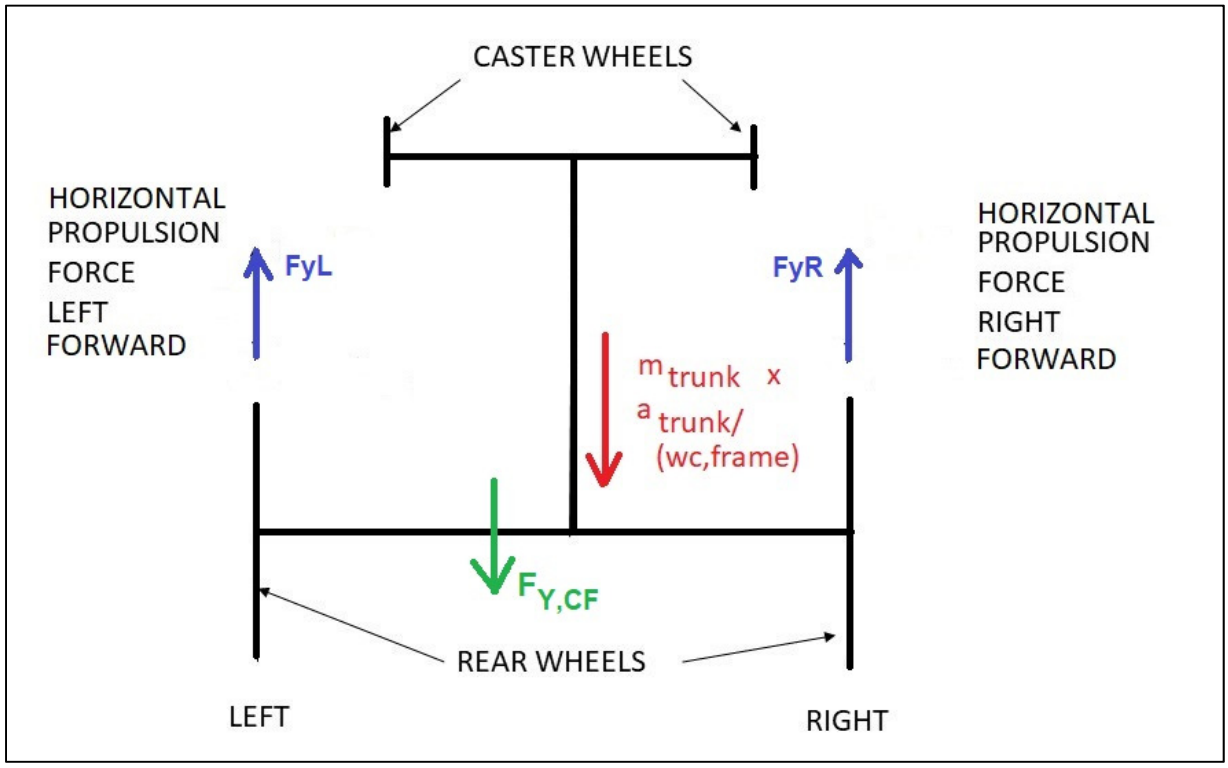

Figure 3.1 On the LIO simulator: dynamic forces due to a human user, to be measured during wheelchair propulsion

Since both wheels are independent, the force transducer must also allow us to determine the value of the forces applied at the handrim, separately on the left and right sides.

3.2.2 Force sensors

Three types of force sensors have been used in manual wheelchair ergometers to control the moment-velocity interaction at the wheelchair wheels: instrumented wheels, torque transducers and force cells.

3.2.2.1 Instrumented wheels

The Smartwheel is the first instrumented wheel that was built for manual wheelchair propulsion research (Cooper, 2009). It replaces the original wheels of the wheelchair. It was described previously in section 1.4.1.

The Optipush Feedback System is also a set of instrumented wheels that replaces the original wheels of the wheelchair. One such wheel is shown on Figure 3.2. A modular instrumentation design allows the system to incorporate different-sized wheels (20", 22", 24", 25" and 26" diameter). The wheel measures handrim loads using a commercially available 6 degree-of-freedom load cell. This load cell can measure up to 770 N for forces in the plane of the wheel, 2310 N for forces perpendicular to the plane of the wheel and 70 Nm for torques about all three axes. The wheel transfers its data wirelessly through a Bluetooth protocol and provides biofeedback for 11 propulsion variables (Guo et al., 2011).

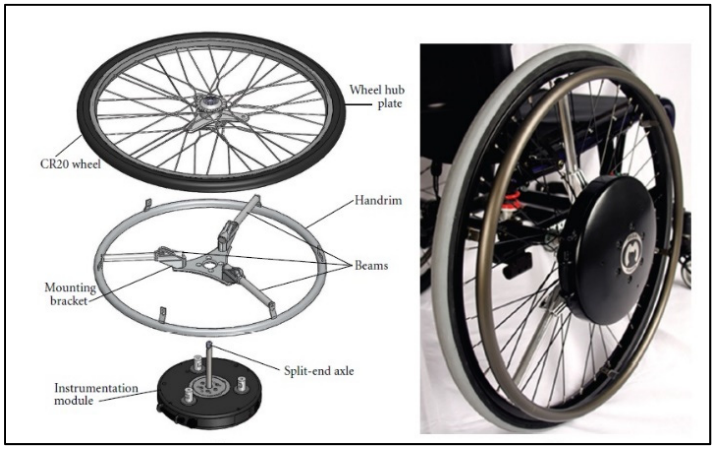

Figure 3.2 Optipush wheel (on the left: components, on the right: assembly) (Guo et al., 2011)

The Sensewheel is a lightweight instrumented wheel which incorporates load cells that replace the three pillars. Load cells are pre-calibrated for tangential, radial and axial force, with raw data telemetered by ultra-high frequency radio. The Sensewheel is shown on Figure 3.3 (Symonds et al., 2016).

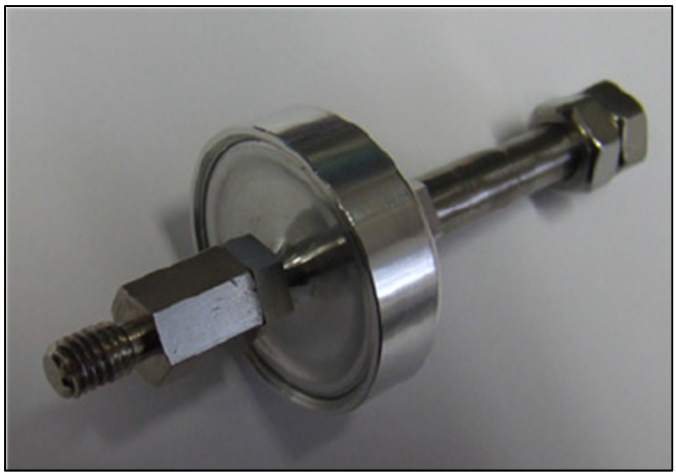

Figure 3.3 Sensewheel force sensor
(Symonds et al., 2016)

3.2.2.2 Torque transducers

Torque transducers have been used as the force/moment measurement device in integrated ergometers (Niesing et al., 1990; Yamada & Muto, 2004). They measure the torque applied on the motor. The torque transducer used in the manual wheelchair simulator located in the Human Support System Laboratory at Gifu University in Gifu, Japan is shown on Figure 3.4.

Figure 3.4 Torque transducer in the Gifu Simulator at the
Human Support Systems Laboratory at Gifu University,
Gifu, Japan (Bando et al., 2004)

3.2.2.3 Generic force cell

Generic force cells have been used in the development of a commercial wheelchair ergometer (de Klerk, Vegter, Veeger, et al., 2020). The force cell used in this ergometer is shown on Figure 3.5. This ergometer was described in section 1.4.5.

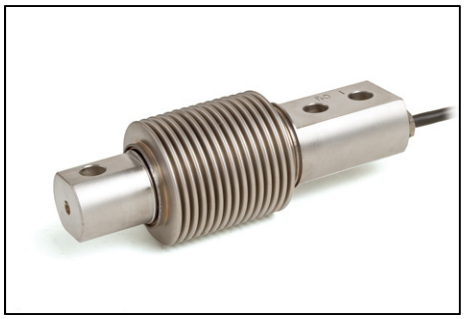

Figure 3.5 The Utilcell Model 300
(de Klerk, Vegter, Veeger, et al., 2020)

AMTI force cells are another example of a generic force cell that is used to measure forces and moments and is usually installed statically.

3.2.2.4 Choice of type of force transducer, sensor specifications and choice of sensor

Instrumented wheels directly measure torques applied by the user. These torques can be translated into propulsion forces applied on the wheelchair. However, they cannot measure the force applied on the wheelchair related to the movement of the user's trunk. Instrumented wheels will therefore not be used in the new control system.

Torque transducers measures the torques applied on the motors, so they indirectly measure the propulsion torques applied by the user. Nonetheless, they cannot measure the force related to the user's trunk. Torque transducers will therefore not be chosen as part of the new control system.

A force cell, if affixed between the simulator and wheelchair, can measure the forward propulsion forces and incorporate the forces due to the movement of the user's trunk. Based

on the objectives for force measurement and the types of force transducer available for our purpose, we select the force cell to control the force-moment interaction of the LIO Simulator.

We calculate the maximum force that the candidate force cell must be able to measure. We base the calculation on a worst-case scenario:

- We assume that the wheelchair-user system is heavy and weighs 150kg
- The user must go up a ramp of 45 degrees

This free-body-diagram (FBD) for condition is shown in Figure 3.6.

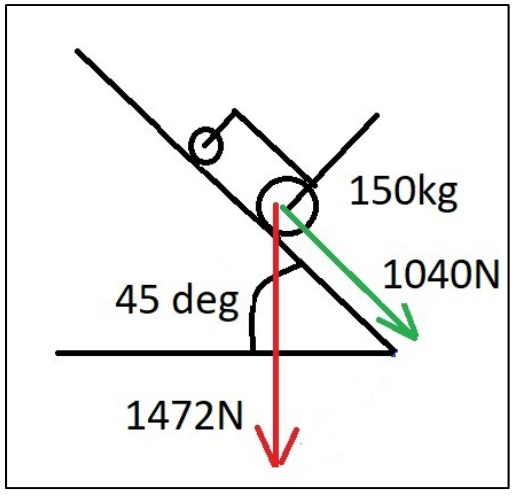

Figure 3.6 Worst case scenario FBD

Under these conditions, the force that the user must generate to hold the wheelchair stationary is calculated by:

$$F_{spec} = mg.\cos(45°) \tag{3.1}$$

$$F_{spec} = 150kg.\left(9.81\frac{m}{s^2}\right).\frac{\sqrt{2}}{2} \tag{3.2}$$

$$F_{spec} = 1040N \tag{3.3}$$

The force cell that we will use as the measurement device must therefore have a maximum of more than 1040N in the plane of movement. The AMTI suite of force cells were strong candidates for our application. Their specifications are shown in Table 3.1.

Table 3.1 MC3A force cell specifications

MC3A Series Specifications	100	250	500	1000
Fz Capacity, lb (N)	100 (445)	250 (1112)	500 (2224)	1000 (4448)
Fx, Fy Capacity, lb (N)	50 (222)	125 (566)	250 (1112)	500 (2224)
Mz Capacity in*lb (Nm)	50 (5.6)	125 (14)	250 (28)	500 (56)
Mx, My Capacity in*lb (Nm)	100 (11)	250 (28)	500 (56)	1000 (113)

The 500 version of the AMTI MC3A can measure up to 1112 N. This would be sufficient for our application. However, we decided to increase our margin of safety for this application and for future applications (as a pre-emptive measure, in case the design of the simulator changes in the future, requiring the measurement of larger loads). We chose the 1000 version of the MC3A, which can measure linear forces up to 2224 N and moments around the vertical axis of up to 56 Nm. The force cells' front side (with the signal interface) is shown on Figure 3.7.

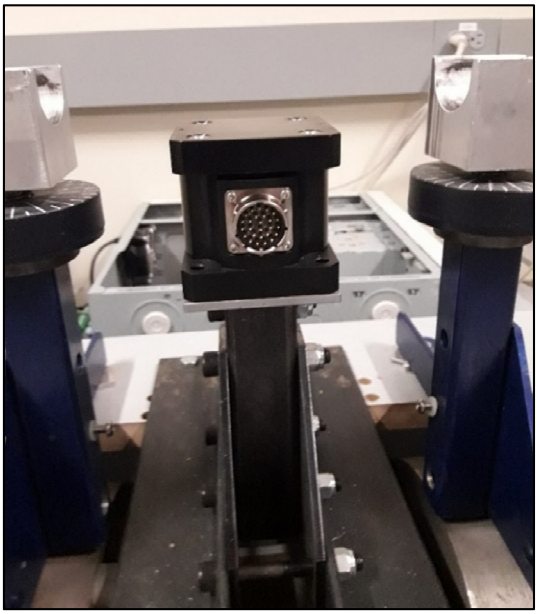

Figure 3.7 Force cell (front side)

3.2.3 Physics of an ergometer with a force cell

A sketch of the manual wheelchair simulator with motorized rollers and a force cell is shown on Figure 3.8. We also draw an FBD of the wheelchair frame, shown on Figure 3.9.

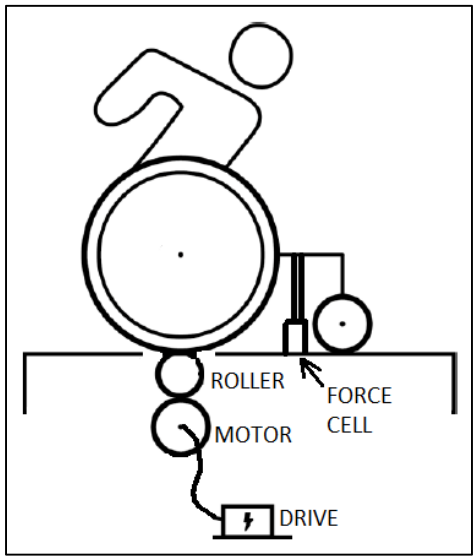

Figure 3.8 Sketch of the MWC simulator with motorized rollers and instrumented with a force cell

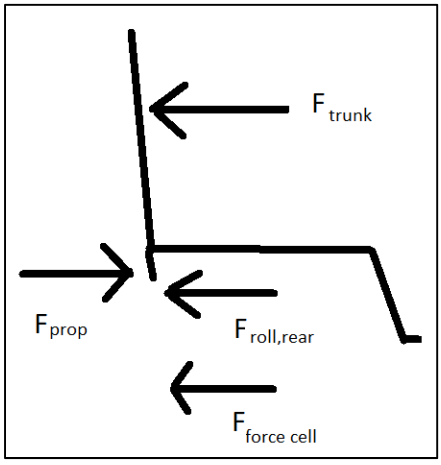

Figure 3.9 FBD of the frame of a wheelchair sitting on a roller

We derive the equation of motion for a wheelchair placed on rollers, based on the free body diagram of Figure 3.9. Applying Newton's Second Law of Motion, we obtain:

$$F_{prop} - F_{roll,rear} - F_{trunk} - F_{force\ cell} = m_{(wc\ frame)} . a_{(wc\ frame)} \quad (3.4)$$

The right-hand side is zero because the wheelchair frame has zero linear acceleration.
Eq. (3.4) reduces to:

$$F_{prop} - F_{trunk} - F_{roll,rear} - F_{force\ cell} = 0 \quad (3.5)$$

3.2.4 Force cell placement in the LIO simulator frame

Figure 3.10 shows a picture of the wheelchair on top of the rollers on the wooden platform. In order for the force cell to measure the propulsive forces, it must hold the wheelchair in place as it tries to move when the user applies forces on the handrims. The force cell must be rigidly attached to a stationary part of the laboratory (such as the walls or the wooden platform) and at the same time must be fixed to some part of the wheelchair (such as the backrest or some part of the frame) so that the latter does not move. It must therefore be part of the retention system of the wheelchair. The current retention system was described in section 1.5.1. We will design a mechanical support that holds the force cell and links it both to the wheelchair and to a stationary part of the laboratory.

We attached the force cell to the simulator platform, underneath the wheelchair, in the center of the two wheels. The simulator platform is heavy enough so that it will not move when subjected to the propulsive forces applied by the user. The force cell is approximately equidistant from the two wheels so that the measured moment of the horizontal components of the two forces applied by user at the handrims is almost zero when propelling on a straight line. The wooden platform and the location of the center of the two wheels are shown on Figure 3.11.

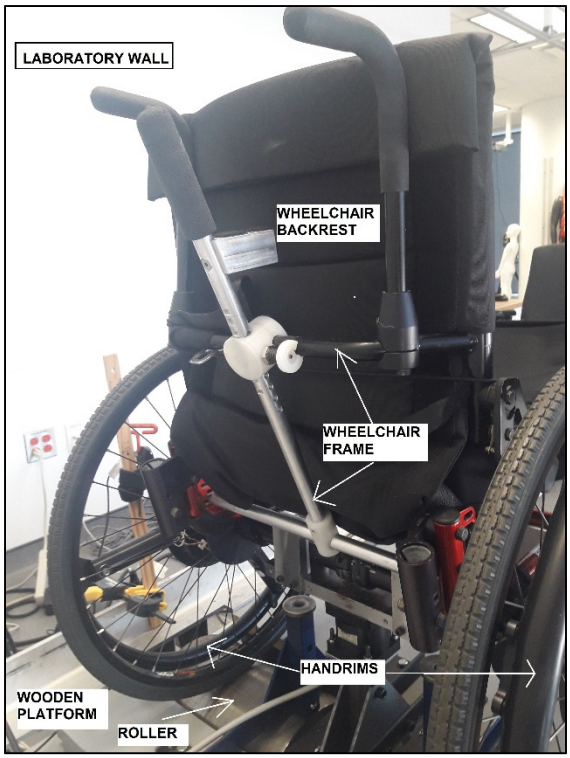

Figure 3.10 Laboratory setup at the LIO

Figure 3.11 Force cell placement
on the simulator platform

3.2.5 Construction of a mechanical bracket for the force cell

The mechanical bracket (support) used to install the force cell is shown on Figure 3.12 in front of the LIO Simulator. The computer-aided-design (CAD) drawings and manufacturing drawings of the bracket are shown in **Erreur ! Source du renvoi introuvable.**.

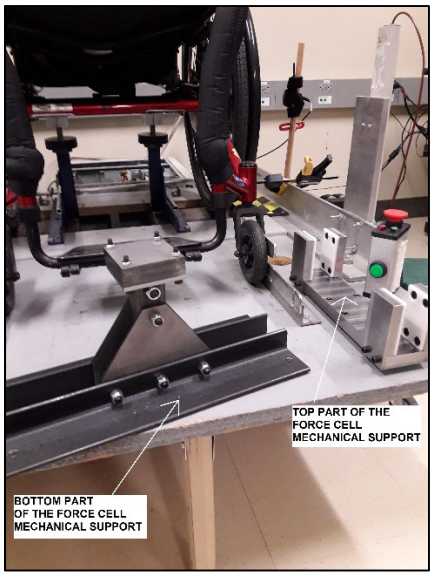

Figure 3.12 Force cell support
before installation

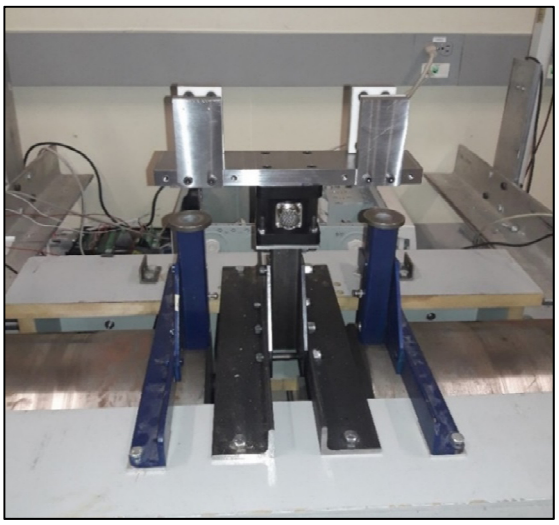

Figure 3.13 Force cell support installed

Figure 3.13 shows the lower part of the mechanical bracket bolted into the LIO Simulator platform, the force cell bolted to it, and the upper part of the mechanical bracket bolted into the force cell.

Figure 3.14 shows a wheelchair placed on the mechanical support. The purple wheel axle is placed in the upper part of the support. The red bar is part of the wheelchair frame.

Figure 3.14 Wheelchair, force cell and support installed on the LIO Simulator Platform

3.2.6 Force cell measurements

3.2.6.1 Force cell multiplication factors

A coordinate system is attached to the force cell and is shown on Figure 3.15 below, taken from the AMTI specifications sheets. The view above is a top view, while the view below is a front view.

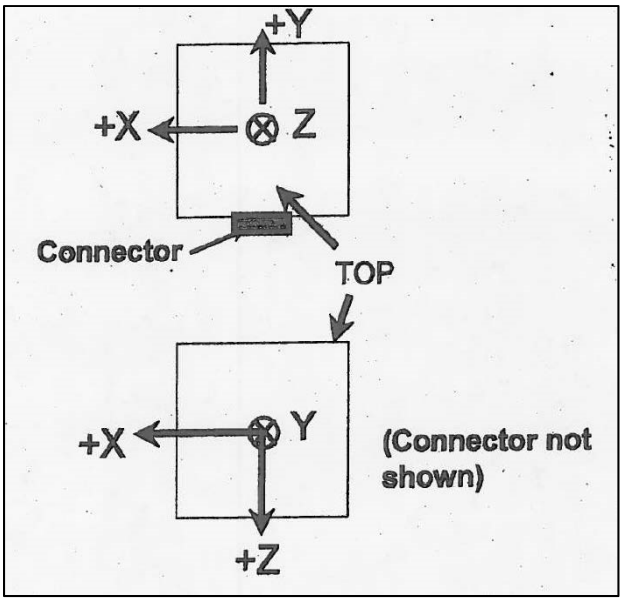

Figure 3.15 Force cell coordinate system, top view (above) and front view (below) (AMTI)

Two methods can be used to calculate the value in Newtons measured by each channel of the force cell, which we will call the accurate method and the approximate (simplified) method.

First, we describe the accurate method. To ensure the greatest degree of accuracy, we use the concept of sensitivity matrix and its inverse, the Cross-Talk matrix. The force along the x-direction is given by Equation **Erreur ! Source du renvoi introuvable.**.

$$F_x = V_{fx}.\frac{1}{S_{11}}.\frac{1}{CF_{fx}} + V_{fy}.\frac{1}{S_{12}}.\frac{1}{CF_{fy}} + V_{fz}.\frac{1}{S_{13}}.\frac{1}{CF_{fz}} + V_{Mx}.\frac{1}{S_{14}}.\frac{1}{CF_{Mx}} + V_{My}.\frac{1}{S_{15}}.\frac{1}{CF_{My}} + V_{Mz}.\frac{1}{S_{16}}.\frac{1}{CF_{Mz}} \quad (3.6)$$

The terms V_{fx}, V_{fy}, V_{fz}, V_{Mx}, V_{My}, V_{Mz} are voltages output by each channel of the force cell, which represent a value proportional to the force and moments measured.

The values of the terms in the equation are as follows:

$CF_{fx} = CF_{fy} = CF_{fz} = CF_{Mx} = CF_{My} = CF_{Mz} = G_f . V_{fexec}.10^{-6}$

$G_f = 1000$ in all directions (amplifier gain)

$V_{fexec} = 10$ in all directions (excitation voltage)

The terms S(i,j) make up was is called the Sensitivity Matrix, shown in Table 3.2 **Erreur ! Source du renvoi introuvable.** (given in Appendix B of the force cell's user manual)

Table 3.2 Sensitivity Matrix for the AMTI MC3A-1000 used in the LIO Simulator

Sensitivity matrix S(I,j)

0.68855	-0.00333	0.00007	-0.12078	0.38812	0.03293
0.01086	0.69108	-0.00035	-0.39402	0.01702	-0.18399
-0.00303	-0.00244	0.15803	-0.02106	-0.01263	-0.00188
0.00512	0.00588	-0.00376	38.26625	-0.09752	0.22307
0.00585	-0.00040	-0.00937	0.71665	38.07962	-1.32376
0.00130	0.00417	0.00061	0.06375	0.11209	27.92851

Substituting the numerical values of all terms in Eq. (3.6), we obtain Eq. (3.7), as follows:

$$F_x = V_{fx}.\frac{1}{0.68955}.\frac{1}{10^{-2}} + V_{fy}.\frac{1}{-0.00333}.\frac{1}{10^{-2}} + V_{fz}.\frac{1}{0.00007}.\frac{1}{10^{-2}} + V_{Mx}.\frac{1}{-0.12078}.\frac{1}{10^{-2}} + V_{My}.\frac{1}{0.38812}.\frac{1}{10^{-2}} + V_{Mz}.\frac{1}{0.03293}.\frac{1}{10^{-2}} \quad (3.7)$$

After simplification, we obtain:

$$F_x = V_{fx}.\frac{1}{0.0068955} + V_{fy}.\frac{1}{-0.0000333} + V_{fz}.\frac{1}{0.0000007} + V_{Mx}.\frac{1}{-0.0012078} + V_{My}.\frac{1}{0.0038812} + V_{Mz}.\frac{1}{0.003293} \quad (3.8)$$

Finally, we obtain:

$$F_x = V_{fx}.145.0221 + V_{fy}.(-30303) + V_{fz}.1428571 + V_{Mx}.(-827) + V_{My}.257 + V_{Mz}.3036 \quad (3.9)$$

The other terms, Fy, Fz, Mx, My, Mz are obtained is a similar manner.

$$F_y = V_{fx}.9208 + V_{fy}.(144.701048) + V_{fz}.(-285714) + V_{Mx}.(-254) + V_{My}.5875 + V_{Mz}.(-543) \quad (3.10)$$

$$F_z = V_{fx}.(-33003) + V_{fy}.(-40984) + V_{fz}.(632.791242) + V_{Mx}.(-4748) + V_{My}.(-7917) + V_{Mz}.(-53191) \quad (3.11)$$

$$M_x = V_{fx}.19531 + V_{fy}.(17006) + V_{fz}.(-26596) + V_{Mx}.(2.613269) + V_{My}.(-1025) + V_{Mz}.448 \quad (3.12)$$

$$M_y = V_{fx}.17094 + V_{fy}.(-25000) + V_{fz}.(-10672) + V_{Mx}.(140) + V_{My}.2.626077 + V_{Mz}.(-76) \quad (3.13)$$

$$M_z = V_{fx}.76923 + V_{fy}.(23981) + V_{fz}.(163934) + V_{Mx}.(1568) + V_{My}.892 + V_{Mz}.3.580571 \quad (3.14)$$

We will now describe the Simplified method. In this method, we assume there is no cross talk between channels. In general, this is a good assumption. These new equations are usually sufficient to predict forces in the direction of load to errors of less than 1 percent of full load and less than 2% of cross talk.

A governing equation relates the force cell's output voltage (V_{fout}) on one hand and the actual load $F_{f(Load)}$ (in Newtons or Newton-meters) on the other. The multiplication factors relating the two variables are calibrated gain sensitivity (S_f or S_m), amplifier gain (G_f), and excitation voltage (V_{fexec}). The equation is presented below:

$$F_{f(load)} = V_{fout}.\frac{1}{(S_f.V_{fexec}.G_f.10^{-6})} \quad (3.15)$$

The values of the terms in the equation are as follows:

V_{fexec} = 10 in all directions

G_f = 1000 in all directions

S_{fx} = 0.68955

S_{fy} = 0.69108

S_{fz} = 0.15803

S_{mx} = 38.26625

S_{my} = 38.07962

S_{mz} = 27.92851

The S terms are the diagonal terms in the Sensitivity matrix.

The simplified formulas are as follows:

$$F_x = V_{fxout}.145.022116 \quad (3.16)$$

$$F_y = V_{fyout}.144.701048 \quad (3.17)$$

$$F_z = V_{fzout}.632.791242 \quad (3.18)$$

$$M_x = V_{mxout}.2.613269 \quad (3.19)$$

$$M_y = V_{myout}.2.626077 \quad (3.20)$$

$$M_z = V_{mzout}.3.580571 \quad (3.21)$$

We will use Equations (3.16) to (3.21) in the simulator's MATLAB model.

3.2.6.2 Calculation of horizontal components of applied forces ($F_{yR,FC}$ and $F_{yL,FC}$) using the vertical moment ($M_{z,FC}$)

Experiments conducted as part of the research in this thesis looks at straight-line propulsion only, but with both rear wheels being independent. Therefore, the mathematical model which will be implemented in MATLAB divides the wheelchair into two identical halves. In order to use the 1-D mass-inertia model with the force cell setup, it is important to distinguish between the forces applied by the user on the wheelchair frame on the left and right sides ($F_{yL,FC}$ and $F_{yR,FC}$) separately.

The force cell measures the antero-posterior force $F_{Y,FC}$ applied by the user onto the simulator platform. This includes the two forces applied on the handrims and the force due to the relative acceleration of the trunk. The force cell also measures the moment $M_{Z,FC}$ about the z-axis (vertical). The forces are shown on Figure 3.16.

Forces $F_{yL,FC}$ and $F_{yR,FC}$ are calculated as follows:

$$F_{yR,FC} + F_{yL,FC} = F_{y,FC} \quad (3.22)$$

$$F_{yL,FC}.arm_L - F_{yR,FC}.arm_R = M_{Z,FC} \quad (3.23)$$

Rearranging (3.22)

$$F_{yR,FC} = F_{y,FC} - F_{yL,FC} \tag{3.24}$$

Inserting (3.24) into (3.23):

$$F_{yL,FC}.arm_L - \left(F_{y,FC} - F_{yL,FC}\right).arm_R = M_{Z,FC} \tag{3.25}$$

$$F_{yL,FC}.arm_L - F_{y,FC}.arm_R + F_{yL,FC}.arm_R = M_{Z,FC} \tag{3.26}$$

$$F_{yL,FC}.arm_L + F_{yL,FC}.arm_R = M_{Z,FC} + F_{y,FC}.arm_R \tag{3.27}$$

$$F_{yL,FC}.(arm_L + arm_R) = M_{Z,FC} + F_{y,FC}.arm_R \tag{3.28}$$

We obtain:

$$F_{yL,FC} = \frac{M_{Z,FC} + F_{y,FC}.arm_R}{arm_L + arm_R} \tag{3.29}$$

$$F_{yR,FC} = F_{y,FC} - F_{yL,FC} \tag{3.30}$$

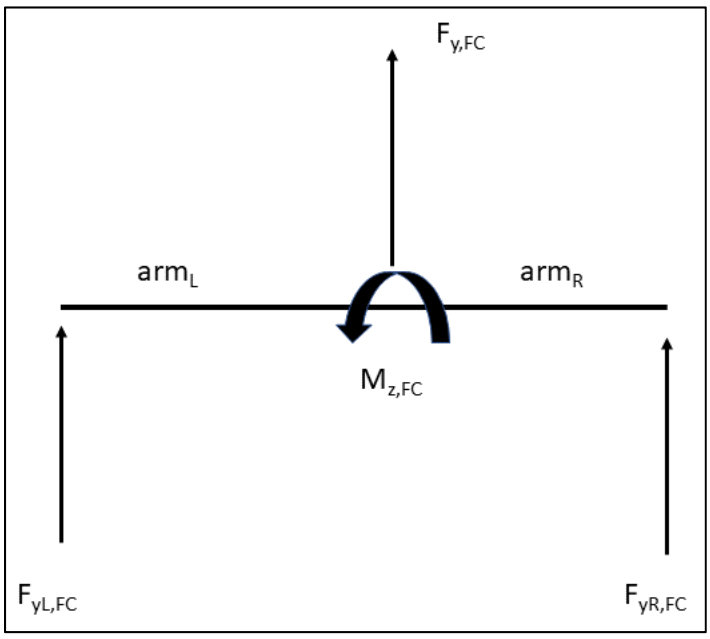

Figure 3.16 Measured force $F_{Y,FC}$ and moment $M_{Z,FC}$ and equivalent forces $F_{yL,FC}$ and $F_{yR,FC}$

3.2.6.3 Determination of the moment arms

In order to use Eqs. (3.29) and (3.30), we need to know the values of the moment arms arm_L and arm_R, which are constant. We proceeded to determine them experimentally. First, with a meter, we measured the distance between center of the mechanical bracket and the centers of the left and right parts of the upper brackets, where the force will be concentrated. Then, we confirmed the values of the moment arms with the following procedure. A person pulled on one end of the upper part of the force cell mechanical bracket (that part which holds the wheelchair axle in place). The force cell measures the moment $M_{Z,FC}$ around the z-axis (vertical) and the force $F_{Y,FC}$. We plotted the variables $M_{Z,FC}$ and ($F_{Y,FC}$. arm_i) on the same graph, and changed the moment arm arm_i until we notice that both curves overlap.

3.2.7 Conclusion of the methodology for the force cell

The steps in section 3.2.6 are intermediate validation steps for the simulator. The results will be given in APPENDIX III.

3.3 Design and experimental methodology for the control loops

3.3.1 Introduction

Two identical haptic control loops (one on the left side, one on the right side) determine the moment-velocity interaction of the wheels on the LIO Simulator. The word haptic is used because it involves the human being's sense of touch.

There are two types of control systems for haptic interfaces: admittance control and impedance control. Impedance control is well suited to systems will low inertia. However, a manual wheelchair-user system has high inertia (Chénier, 2012). This is why control systems for manual wheelchair simulators in the past have used admittance control. The LIO Simulator's haptic control loop (described in section Haptics controller) incorporating the Smartwheels is an admittance control loop with a feedforward component.

The haptic control loops we will design for the LIO Simulator will incorporate a new sensor (the force cell we have chosen as the measuring instrument for the forces and moments applied by the user at the handrims and for the reaction force that allows the movement of the trunk).

3.3.2 Control loops for MWC simulators and haptic devices

3.3.2.1 Control loops used in manual wheelchair simulators

In order to choose the most appropriate type of control loop for the LIO Simulator, we will review control loops used in the three manual wheelchair simulators that were described in section 1.4.5.

The wheelchair simulator built by Klaesner et al. (2014) at Washington University in St. Louis is highly adjustable. The authors did not give much information regarding the control system used by the simulator. They did mention that the software control system took inputs from the torques measured on the rollers and output the required wheel speed. An optical sensor measured the roller speed.

The wheelchair simulator built by Bentaleb et al. (2019) at Hauts-de-France Polytechnic University in Valenciennes, France uses an admittance control loop which incorporates instrumented wheels as the force transducer. The control strategy had two objectives: first, to generate force feedback during the push phase, and second, to assist control to make the wheelchair movement more realistic in the virtual environment during the recovery phase. Handrim rotation torques are measured by torquemeters and the wheel speed is measured by encoders. The hardware and software systems are driven using Matlab/Simulink software. The simulator incorporates a PI controller with anti-windup, for which the PI gains were obtained via trial-and-error techniques. The control includes a feedforward controller, for which the control input is calculated by multiplying the measured torque by a factor. The error corrector is based on admittance control, i.e. on the speed of the wheels.

The wheelchair simulator built by De Klerk (2020) at the University of Groningen in The Netherlands uses closed-source software written in the C programming language. Therefore, very few details are given. However, the authors do mention that the simulator uses an admittance control loop which takes force data as input, calculates a new control speed and sends the new control speed to the motor controller at 100 Hz.

3.3.2.2 Haptic control loops used for other haptic interfaces

In order to have a broader understanding of which type of control loop is appropriate for different kinds of applications, it is very useful to review control systems that have been used for haptic interfaces on systems other than manual wheelchair simulators.

Ellis et al. (1996) describe a haptic interface as a device that can sense a human operator's hand motion and actuate the operator with forces or torques, without significantly impeding the hand motion. The researchers' planar haptic interface device is shown on Figure 3.17. The authors developed an accurate force-control strategy (impedance control), using proportional control.

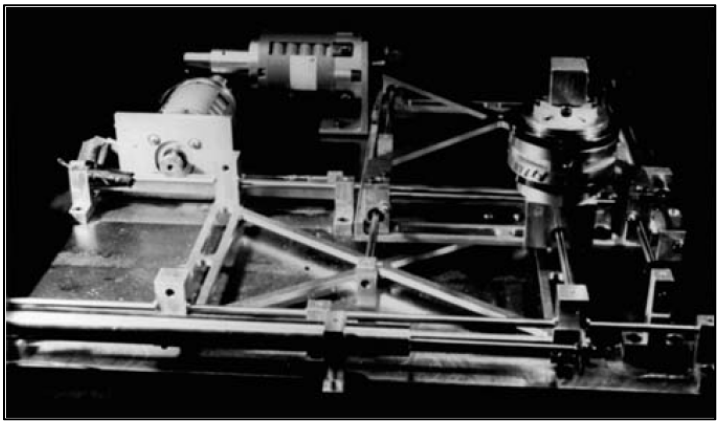

Figure 3.17 Planar haptic interface (Ellis et al., 1996)

Faulring et al. (2016) designed a Cobotic (collaborative robot) Hand Controller using admittance control. A CAD rendering of the cobot is shown on Figure 3.18. They used several control systems. For the joint motion control block, they used a PID feedback controller with

a feedforward component. The robot had a steering system that used a PI controller in its control system.

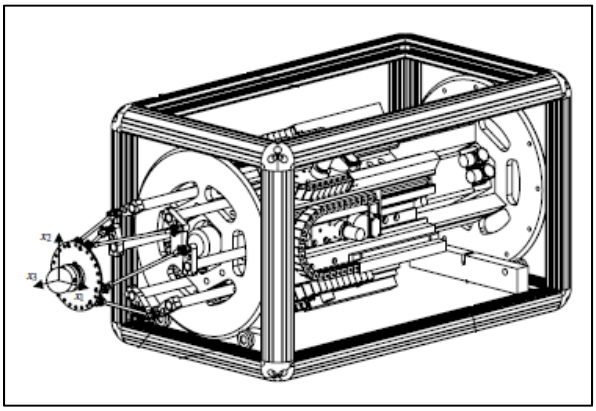

Figure 3.18 CAD rendering of the cobot (Faulring et al., 2016)

Peer and Buss (2008) built an admittance-type haptic interface for bimanual manipulations. Their robot is shown on Figure 3.19. They used PD controllers in their control schemes, independent joint controller and computed torque schemes.

Figure 3.19 Bimanual manipulator with haptic interface (Peer & Buss, 2008)

Virtual environment simulators have become increasingly refined. As a result, whereas haptic systems used to run a single algorithm for dynamics simulation and control, they have now turned to separating them into two independent processes. Admittance-type robots are mostly characterized by their high inertia, low back drivability and are usually controlled with admittance-type controllers. Abdossalami & Sirouspour (2008) describe in a research paper controllers that deal with admittance-type and impedance-type virtual environments. Their experiments with admittance-type virtual environments produced very good results and they concluded that they were suitable for high performance haptics applications. Experiments with impedance-type virtual environments suffered from stability problems.

3.3.3 Experimental methodology to address H1: stability of the control loop of the simulator controlled by the force cell

3.3.3.1 Choice of type of control system: admittance haptic control loop

Based on control systems that have been successful in previous research efforts on the development of manual wheelchair simulators, we have decided to implement an admittance haptic control loop to control the moment-velocity interaction of the wheelchair wheels, while using the force cell as the force sensor. Two identical control loops are applied separately to each of the left and right sides. The control loop for one wheel is shown on Figure 3.20 as a block diagram, which shows how the hardware and the software interact. The force cell provides the propulsive force to the mathematical model, and the latter outputs the desired wheel speed. The design of Figure 3.20 will be implemented in MATLAB/Simulink.

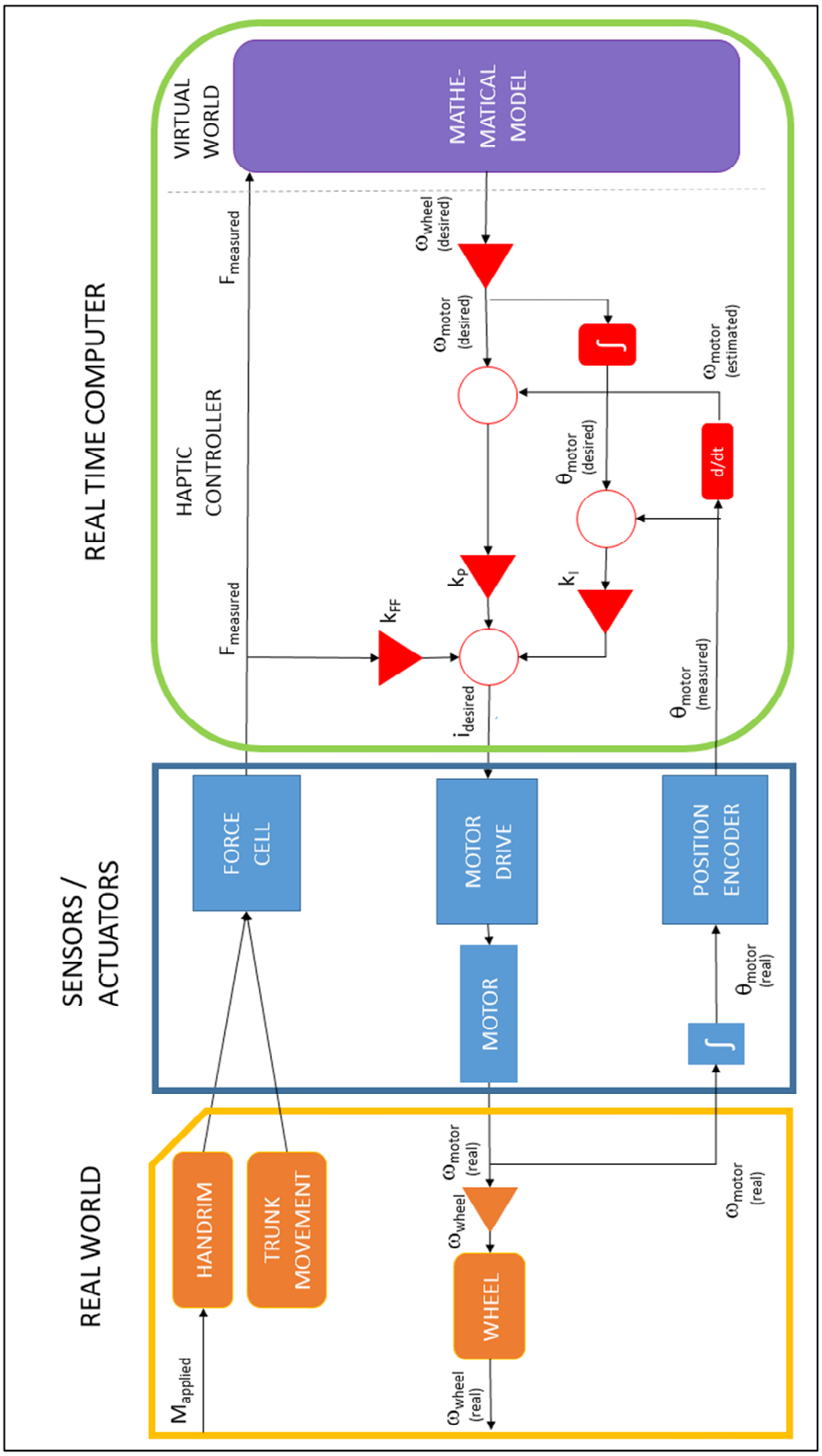

Figure 3.20 Admittance control block diagram

3.3.3.2 Determination of the control gains and stability of the control loop

We will implement Proportional-Integral (PI) control with a feedforward controller. Each portion of the controller will have a gain: k_P is the proportional gain, k_I is the integral gain and k_{FF} is the feedforward gain.

Once the Simulink model has been created and has no errors, the next step is to tune the three controls gains: k_P, k_I and k_{FF}. This will be done by trial and error. First, we will determine k_P, k_I and we will set $k_{FF} = 0$.

The goal for this first step is to have a stable control loop without the feedforward portion of the control system. The starting point for the values of k_P, k_I will be those of the LIO Simulator with its full 2D model where the Smartwheels were used as force transducers. We conduct the following experiment: we run the simulator for about 20 seconds while a subject propels bilaterally, keeping both wheels at the same speed, at about 1 m/s. We verify the stability of the control loop by visual inspection, looking to see if the value of the measured wheel speeds oscillate around the desired speeds. We then proceed to change the gains k_P, k_I to specific values and re-run the experiment. We attempt to find the gains where the difference between the two speeds is minimized. Once that has been achieved, we lock the gains.

We now proceed to determine k_{FF}. We set k_{FF} to a specific value, and once again run the same experiment as before: a subject propels bilaterally for about 20 seconds, keeping both wheels at the same speed, at about 1 m/s. We plot the graph of desired vs. actual wheel speeds, and make a visual inspection. For this experiment, we are looking to see if the value of the measured wheel speeds oscillate with a maximum amplitude to 10% away from the desired speeds. Once the two values are within 10% of each other, we lock the gain k_{FF}.

3.3.3.3 Control loop in the LIO simulator with Smartwheels as the force measurement device

The admittance control loop developed in this thesis incorporated the force cell as the force measurement device. However, as part of the validation of the newly implemented control

loop, we will compare the degree of realism afforded by the force cell versus the original control loop that used the Smartwheels.

In order to do so, the MATLAB model incorporated a switch to run the same control loop developed in the previous section, but with the Smartwheel outputs $M_{zL,SW}$ and $M_{zR,SW}$, in real-time. When the simulator is run based on the Smartwheels' output, the input to the mathematical model is the tangential force F_{TAN} applied to the wheelchair because this is the force that propels the wheelchair. This is obtained by dividing the moments $M_{zL,SW}$ and $M_{zR,SW}$ by the radius r_H of the handrim.

The optimal stable values for three gains k_P, k_I and k_{FF} are those obtained by Chénier in his Ph.D. thesis (2012), since his 2D mathematical model simplifies to a 1D model when propelling in a straight line. To double check this, we ran a few trials where the values of the gain were modified slightly from the values obtained by Chénier. Then we plotted the graphs of measured angular speed and desired speed, and visually inspected how close they were to each other.

3.3.4 Experimental methodology to address H2: quantification of the degree of realism of the simulator controlled by the force cell

3.3.4.1 Overview

In order to evaluate the degree of realism of the simulator with the new control loop, we ran experiments comparing 1) manual wheelchair propulsion on the ground to 2) propulsion on the original simulator controlled by the Smartwheels and to 3) propulsion on the simulator controlled by the new force cell. One able-bodied participant propelled in the three conditions. In the next few sections, we will describe the experiments that were run to obtain raw data, which were measured by the Smartwheels in all 3 conditions. Second, we will describe the data processing that was used to obtain variables used for comparison of wheelchair propulsion. Third, we will describe the visual and qualitative analysis that was used to compare results of the three conditions.

3.3.4.2 Experiments with the wheelchair on the ground (equipped with Smartwheels)

A manual wheelchair was fitted with two Smartwheels in order to record kinetic (forces and moments) and kinematic (angular position and linear speed) parameters during ground propulsion. The wheelchair is shown on Figure 3.21.

Figure 3.21 Wheelchair equipped with Smartwheels

The subject familiarized himself with overground wheelchair propulsion. He found his comfortable speed (which was about 1 m/s). We marked the corridor outside our laboratory with two lines of tape marking a distance of 20 meters (Figure 3.22). The participant propelled the wheelchair several times until he propelled at a regular speed of 1 m/s.
When the participant was ready, we ran three trials (to ensure we had good data) and recorded F_X, F_Y, F_Z, M_X, M_Y, M_Z, the angle and the linear speed bilaterally using the SmartWheels.

3.3.4.3 Experiments on the simulator with Smartwheels input control

For these sets of experiments, the simulator used the Smartwheels as force input. The participant sat on the wheelchair simulator and familiarized himself with propulsion on it. He propelled on the simulator until he was able to maintain a speed of 1 m/s for at least 20 seconds.

Then, three trials were conducted to make sure the data was recorded, transferred, and saved correctly. F_X, F_Y, F_Z, M_X, M_Y, M_Z and the angular position were measured and recorded bilaterally by the Smartwheels for further processing.

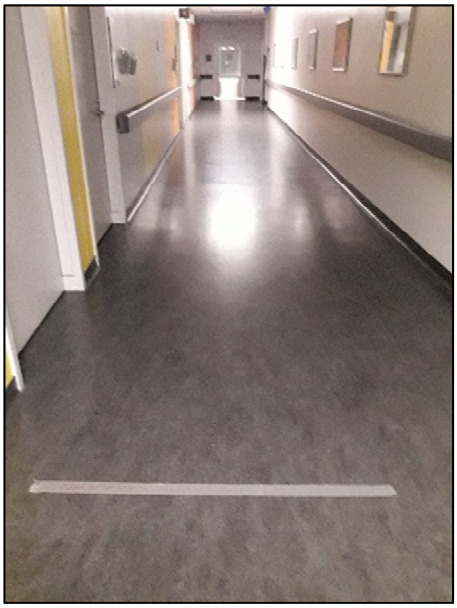

Figure 3.22 The corridor with tape marking the starting point

3.3.4.4 Experiments on the simulator with force cell input control

The same protocol as in 3.3.4.3 was used, with the simulator using the force cell as force input.

3.3.4.5 Data processing using the Kinesiology ToolKit (KTK)

Data obtained during the three conditions were run through the Kinesiology Toolkit (a MATLAB library), developed by Prof. Chénier in his Mobility and Adaptive Sports Research Laboratory located at the Université du Québec à Montréal.

The first operation performed by the library proceeded to remove the offsets. Offsets are sinusoidal for F_X, F_Y, M_X, M_Y, and constant for F_Z and M_Z. This is shown on Figure 3.23 and Figure 3.24.

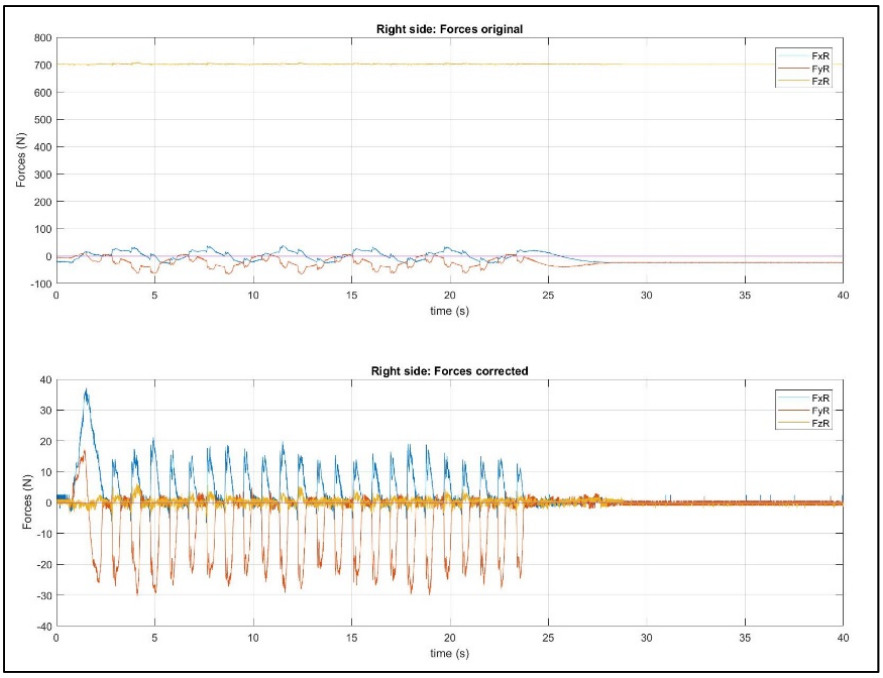

Figure 3.23 Forces on right wheel F_xR, F_yR, F_zR original (with offset, above) and corrected (with offset removed, below)

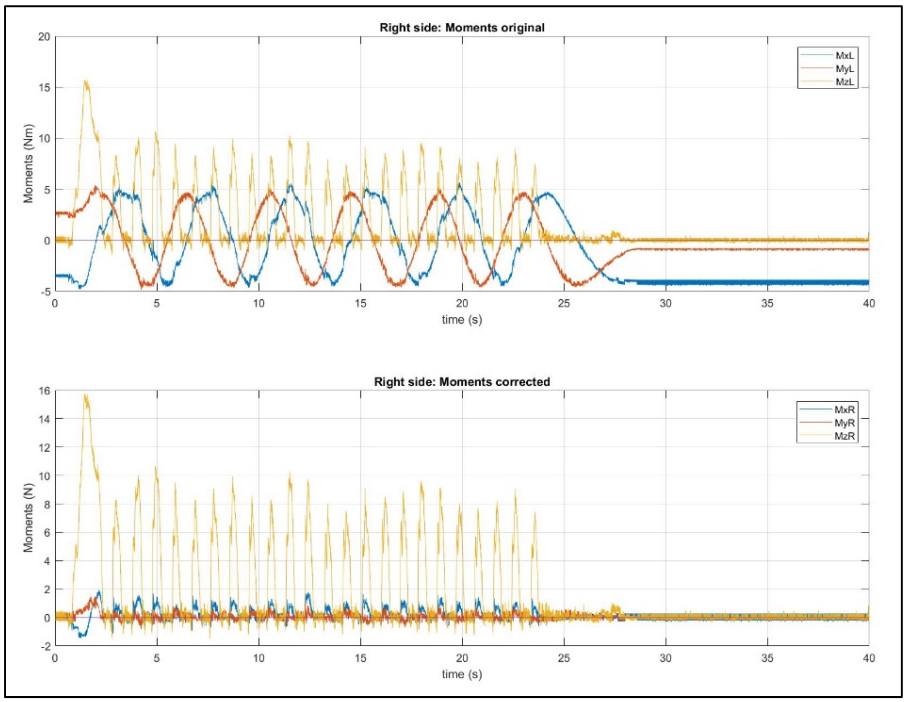

Figure 3.24 Moments on right wheel M_xR, M_yR, M_zR original (with offset, above) and corrected (with offset removed, below)

After this step, the library separated the cycles into push phase and recovery phase. This is done using the data for the variable F_{TOT} (vectorial sum of the three force components). When the value goes above 5N, the start of the push phase is detected. When the value goes below 2N, the start of the recovery phase is detected. This is shown on Figure 3.25.

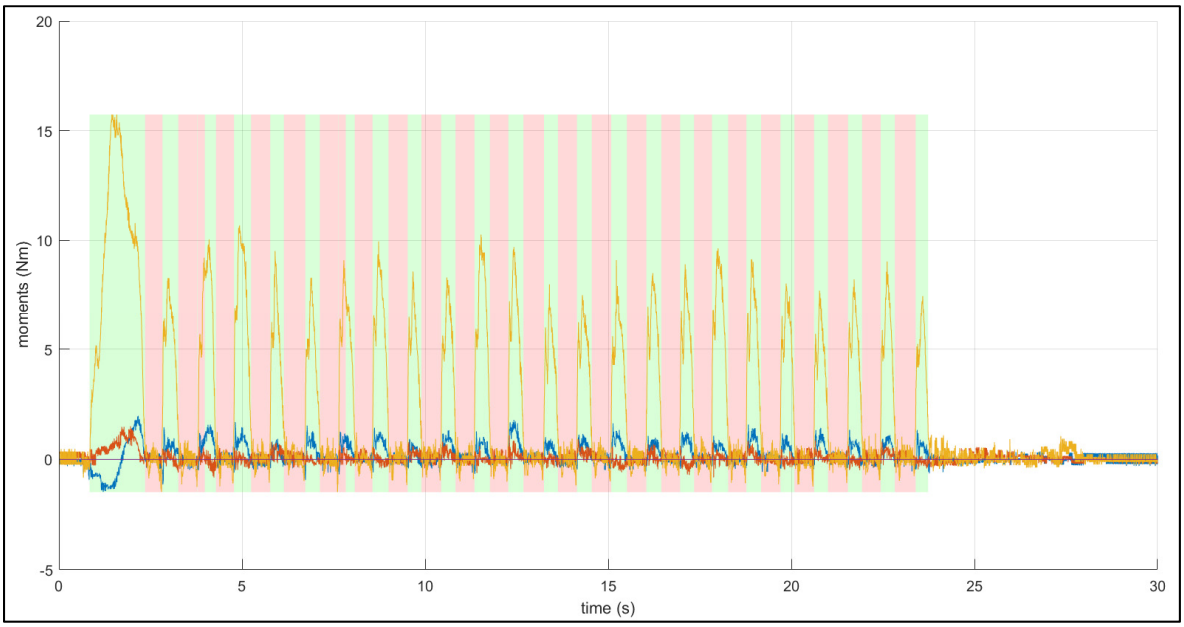

Figure 3.25 Moments Mz: push phases (green) and recovery phases (pink)

The next operation is to select the ten pushes whose data will be used to calculate the biomechanical parameters used for comparison. This is shown on Figure 3.26. The first four and the last four pushes are not chosen because the wheelchair was not in steady state propulsion. Starting at the fifth push, pushes were selected consecutively, unless there was a glitch in the recording which didn't allow for a clean identification of a push.

The operations that used the KTK library ended here, and the data the for ten pushes were placed in vectors.

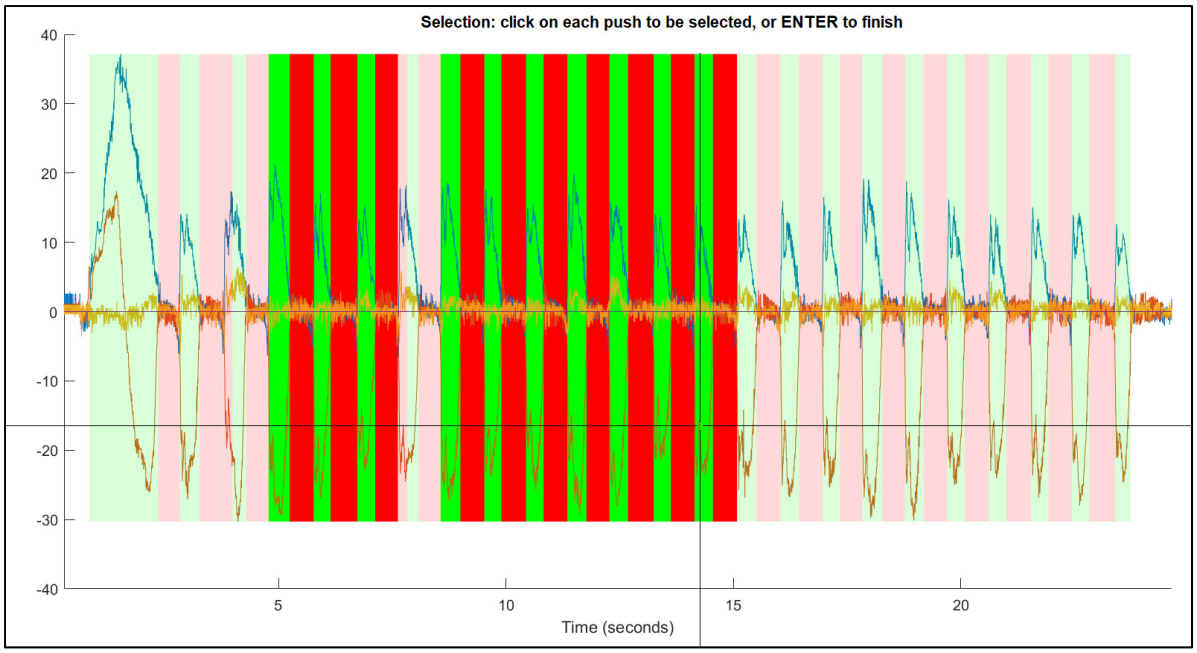

Figure 3.26 Selecting ten pushes for the calculation of biomechanical parameters

Next, a MATLAB script was written that took the vectors output by KTK and calculated the biomechanical parameters that were used to compare manual wheelchair propulsion between the three conditions. These parameters were: maximum propulsion moment M_{zmax} (Nm), maximum applied force $F_{TOT,max}$ (N), push time (s), recovery time (s).
We copied these values to an excel sheet to present the results as a table and graphics.

3.3.4.6 Visual inspection of results

Through data acquisition and processing using KTK and the MATLAB script, we were able to calculate the variables which would be subject to inspection for the qualitative evaluation of realism, allowing us to make a visual judgement on **H2**. We are comparing overground propulsion (OG), propulsion on the simulator with Smartwheels (SW) and propulsion on the simulator with the force cell (FC).

CHAPTER 4

RESULTS

4.1 Results for the evaluation of H1: stability of the haptic control loop of the simulator controlled by a force cell

4.1.1 Implementation of the Admittance Control System

The MATLAB model that implements the admittance control system block diagram from Figure 3.20 in section 3.3.3.1 is shown on Figure 4.1. The full model is too large to be seen clearly on one page, so we will zoom in on different parts of the model and explain each part separately.

The model starts with the force measurements taken by the force cell, shown on Figure 4.2. The two variables used in the MATLAB model are the antero-posterior force $F_{Y,FC}$ and the moment around the vertical axis $M_{Z,FC}$. These values are output by the data acquisition block as voltage. They are multiplied by their corresponding factors to obtain values in Newtons and Newton-meters. The raw measurements are noisy and are filtered by a 1^{st}-order Butterworth filter with a cutoff frequency of 5 Hz. These next step is to input those parameters to a block called "Force cell forces" which applies Equations (3.29)**Erreur ! Source du renvoi introuvable.** and (3.30)**Erreur ! Source du renvoi introuvable.** and calculates $F_{yR,FC}$ and $F_{yL,FC}$.

We will now look at the model of the right side of wheelchair. We have a switch called "FappR for admittance math model." The switch allows us to use either the output from the Force cell or the Smartwheels when running the simulator. F_{appR} is the force that propels the wheelchair forward. When the force cells' output is in use, $F_{appR} = F_{yRFC}$.
The value of $F_{yR,FC}$ is the input to the one-dimensional (linear) mathematical model, contained in the block called "Admittance Function Math Model Right" and shown on Figure 4.3. It is a MATLAB function, whose details are shown on Figure 4.4.

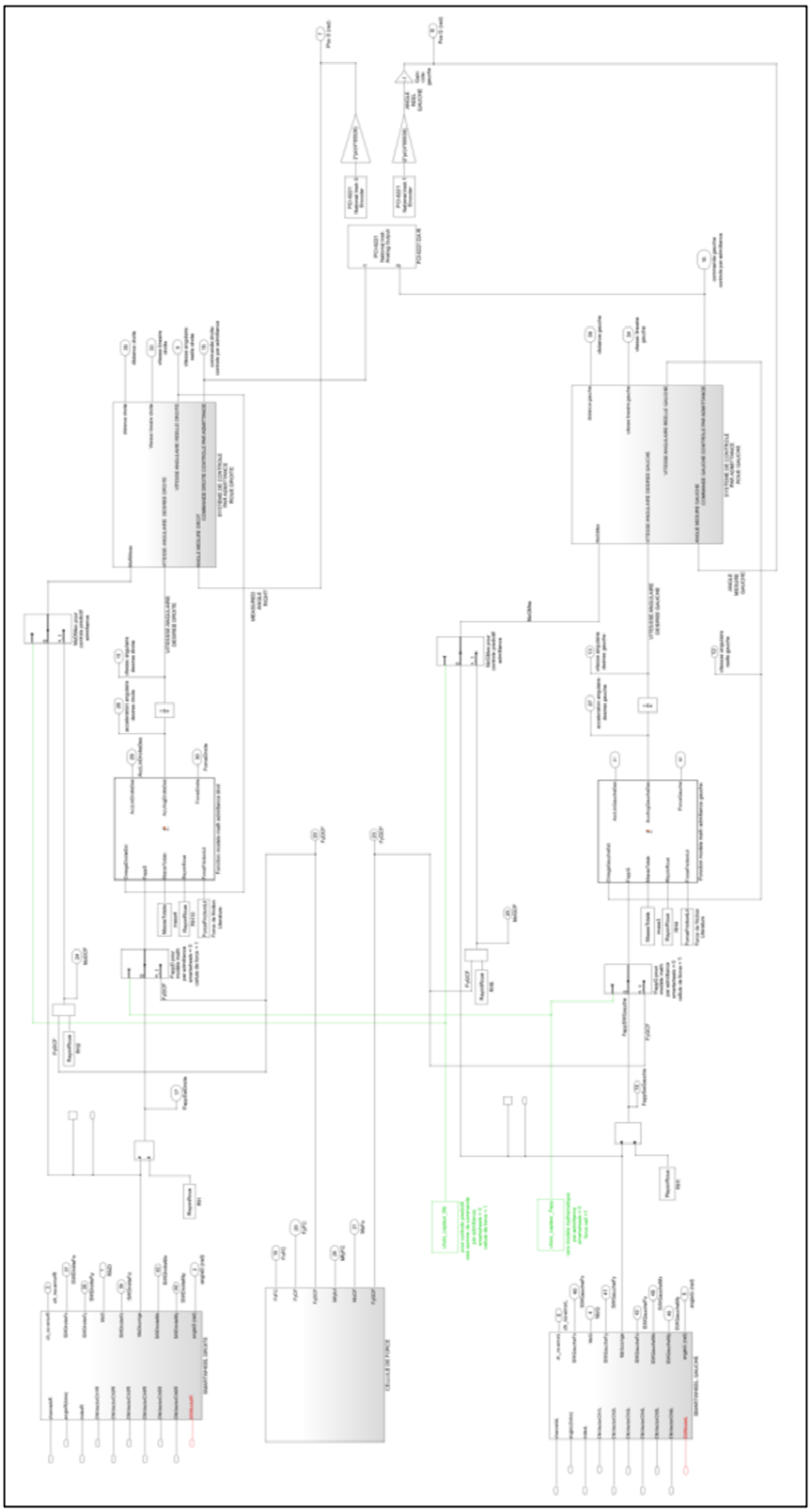

Figure 4.1 Admittance control system implementation: MATLAB model

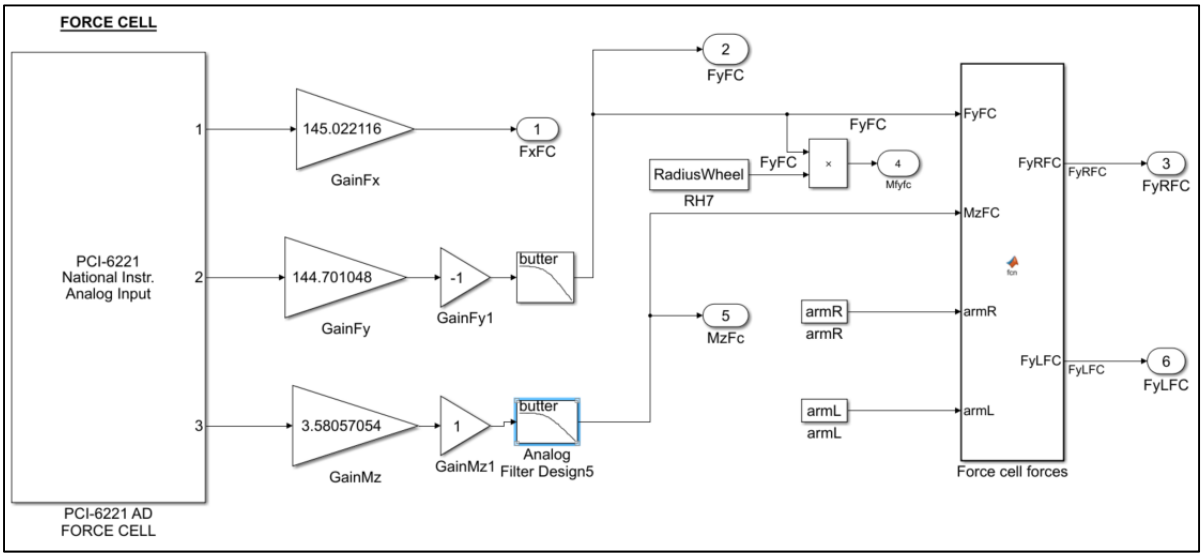

Figure 4.2 Force cell measurements, gains

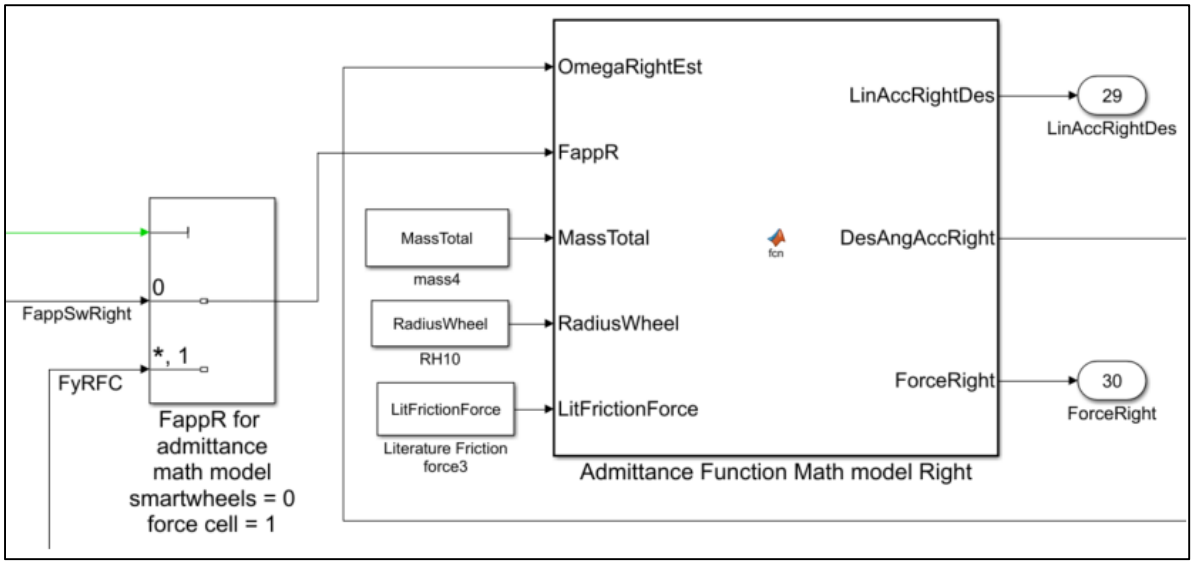

Figure 4.3 1-D mathematical model of the wheelchair

```
function [LinAccRightDes,DesAngAccRight,ForceRight]=
fcn(OmegaRightEst,FappR,MassTotal,RadiusWheel,LitFrictionForce)

if OmegaRightEst > 0
    FR = FappR - LitFrictionForce;
elseif OmegaRightEst < 0
    FR = FappR + LitFrictionForce;
elseif OmegaRightEst == 0
    if FappR > LitFrictionForce
            FR = FappR - LitFrictionForce;
    elseif FappR < -LitFrictionForce
            FR = FappR + LitFrictionForce;
    else
            FR = 0;
    end
else
    FR = 0;
end

LinAccRightDes = FR/MassTotal;
DesAngAccRight = LinAccRightDes/RadiusWheel;
ForceRight = FR;
```

Figure 4.4 1-D math model (function)

The other inputs to the MATLAB math model function are constants: half of the total mass of the wheelchair-user system, the radius of the wheelchair wheel and the rolling resistance force. The output of the mathematical model is the desired angular velocity. This is passed to the controller, which is detailed next.

The control system is a Proportional-Integral controller, shown as a block on Figure 4.5. We can see the control system has three main inputs: the measured applied moment used for the feedforward control, the measured angle, and the desired angular velocity. It has one main output, called admittance control input right (located at the bottom right of the block).

Figure 4.6**Erreur ! Source du renvoi introuvable.** shows the detail of the control system. The PI controller has two gains to be tuned, k_P is the proportional gain and k_I is the integral

gain. The new control system uses the same wheels, motors and drives but the force cell is the new sensor, so the control gains might change. The starting point for the values of the gains were those obtained by Chénier (2012), which were $k_P = 2.0$ and $k_I = 6.0$.
After several trials conducted according to the methodology described previously, the final values used in the new control system remained unchanged at $k_P = 2.0$ and $k_I = 6.0$.
The control system also incorporates a feedforward portion. The control inputs on the right and right sides due to feedforward are evaluated as follows:

$$u_{FF,R} = M_{zR,FC}.k_{Mz} \tag{4.1}$$

$$u_{FF,L} = M_{zL,FC}.k_{Mz} \tag{4.2}$$

$M_{zR,FC}$ and $M_{zL,FC}$ (estimates of the moments applied by the user on the handrims) are perturbations on the control system which attempts to control the angular speed of the wheels according to the reference input.

$$M_{zR,FC} = F_{yR,FC}.r_H \tag{4.3}$$

$$M_{zL,FC} = F_{yL,FC}.r_H \tag{4.4}$$

$$k_{Mz} = \frac{1}{k_R k_T} k_{FF} \tag{4.5}$$

where:
- r_H is the radius of the wheel (24 inches = 60.96 cm = 0.6096 m)
- $k_R = 2.21$ (ratio of the radii of wheelchair wheels to rollers)
- $k_T = 4.406$ nM/A
- k_{FF} is the feedforward gain

By trial and error, we obtain $k_{Mz} = 0.0257$.

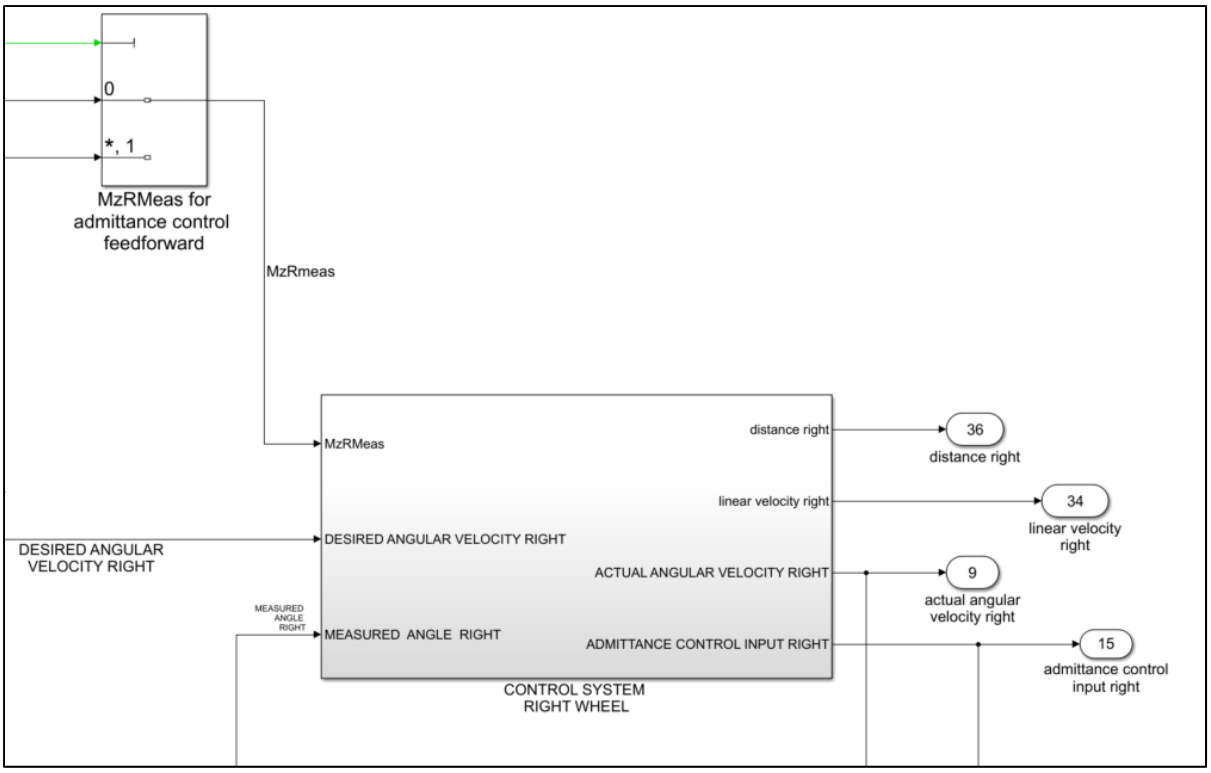

Figure 4.5 Right wheel, control system (block)

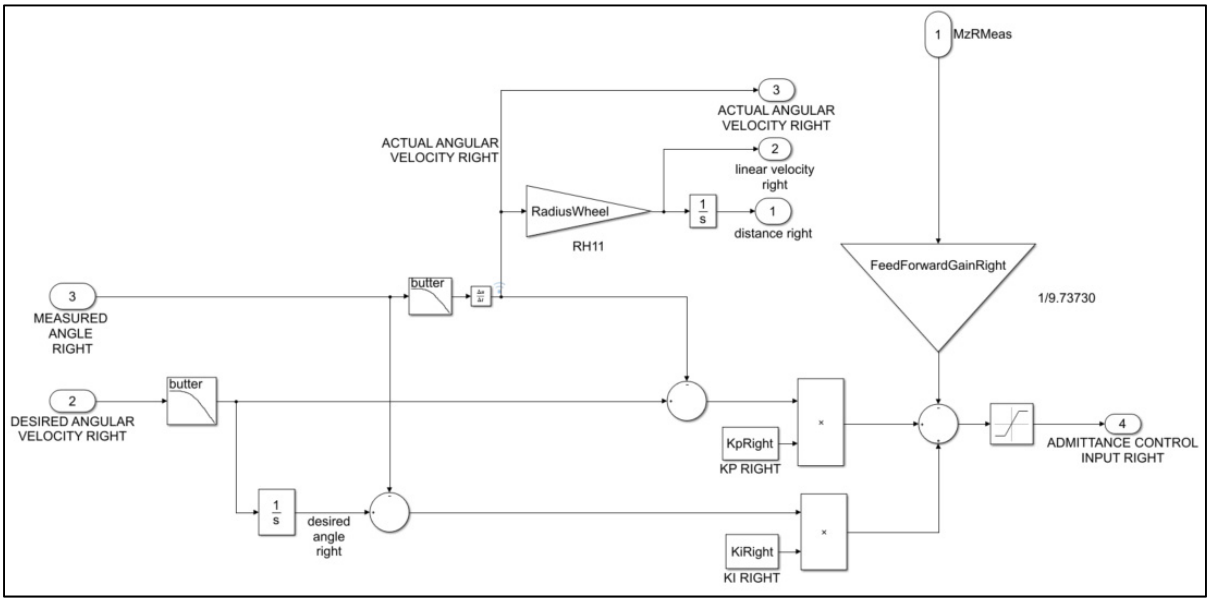

Figure 4.6 Right wheel, control system (detail)

4.1.2 Stability of the control loop using the force cell

In this section, we will show the results of the simulations of the LIO Simulator when the force cell's output is used. We recall here that we ran several simulations during which the subject propelled on the simulator for about 20 meters as he tried to maintain a linear speed of 1 m/s on both wheels. When using the gains, $k_P = 2.0$, $k_I = 6.0$, $k_{FF} = 0.25$, we obtained the graph of the desired wheel angular speed and the actual speed shown on Figure 4.7. By visual inspection, we determined the graphs on this figure to be the ones where both curves had the best overlap.

We note that even though the actual speed does follow the desired speed, some noise is present. To better appreciate it, we zoom into the graph between 2 and 4 m/s. This is shown on Figure 4.8.

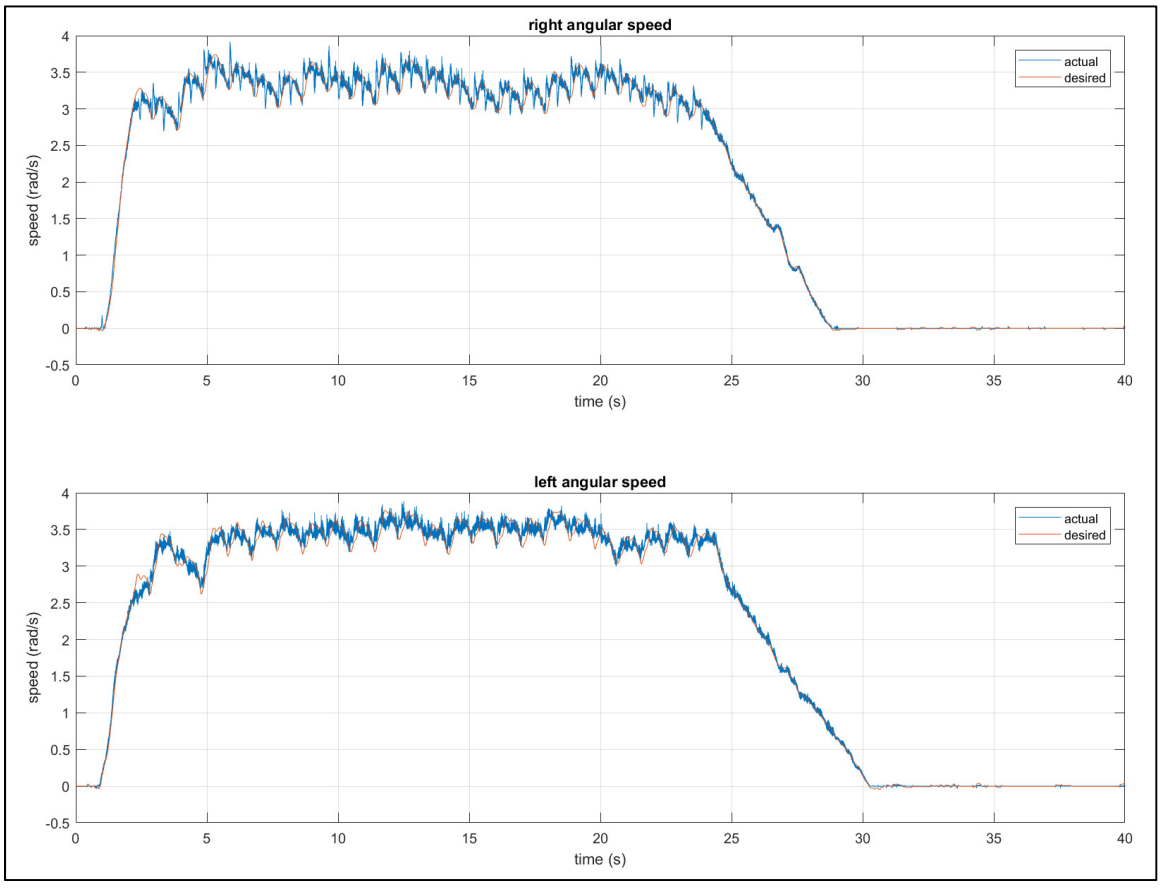

Figure 4.7 Desired and actual wheel angular speeds

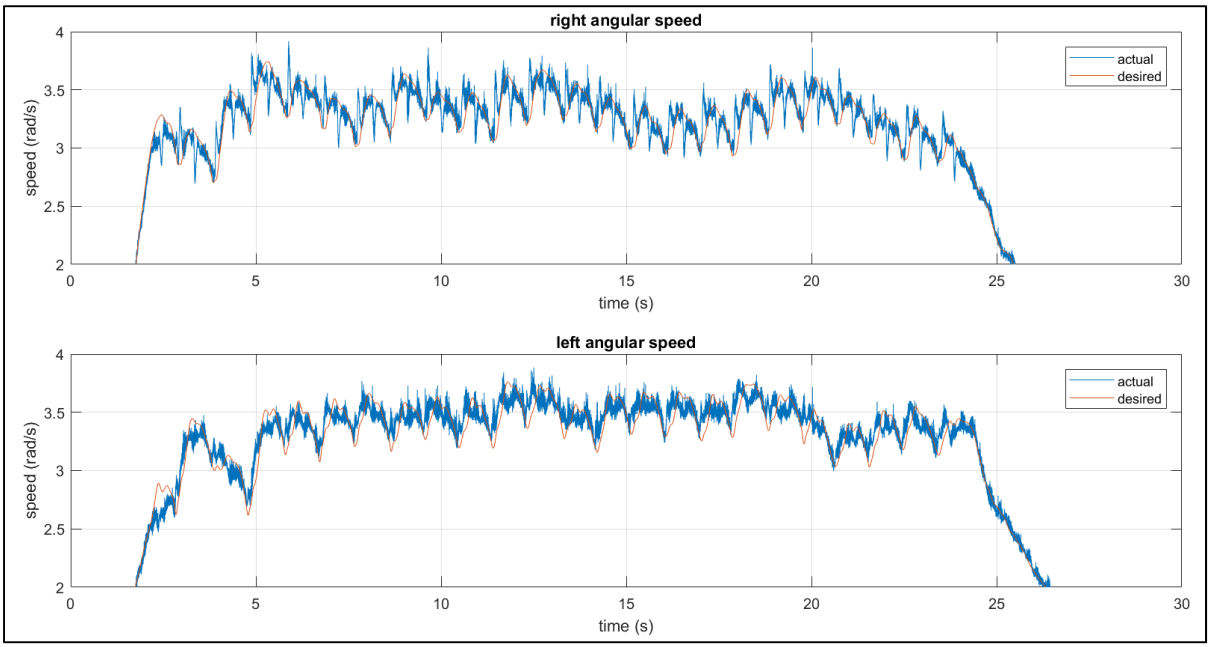

Figure 4.8 Desired and actual wheel angular speeds (zoomed in between 2 and 4 m/s)

4.1.3 Control loop in the LIO simulator with Smartwheels as the force measurement device

In this section we will show the results of the simulations of the LIO Simulator when the Smartwheels' output is used. We recall that the best stability of the control system, as determined by the superposition of the desired vs. measured wheel angular speed, was expected to be at the gains $k_P = 2.0$, $k_I = 6.0$, $k_{FF} = 1$. This was indeed the case. The plots are shown on Figure 4.9.

As in the previous section, we will zoom in on the area between 2 and 4 m/s. This is shown on Figure 4.10. We notice that there is less noise when using the Smartwheel than when using the force cell. This difference will be discussed in the next chapter.

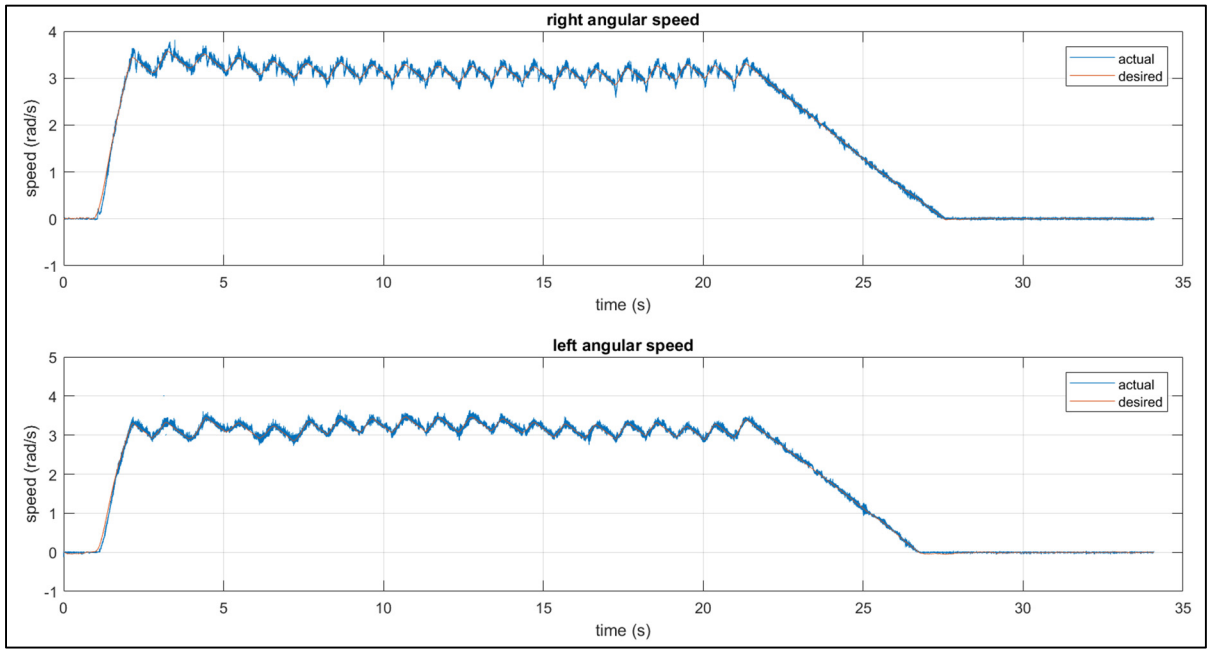

Figure 4.9 Smartwheel input: desired vs. actual angular speeds

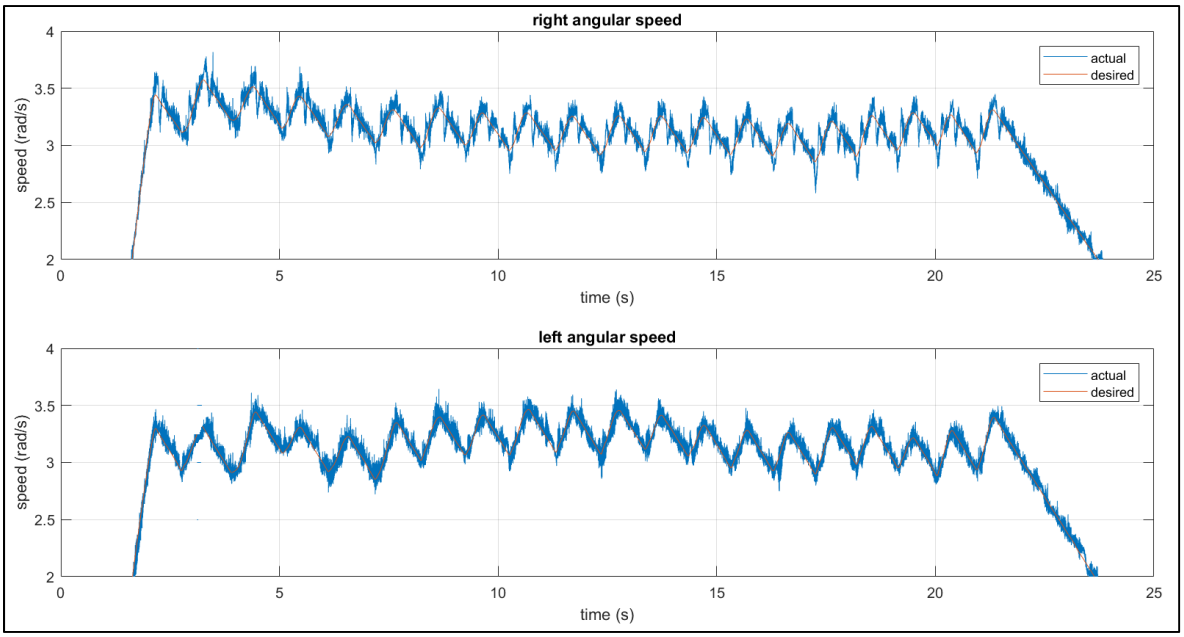

Figure 4.10 Smartwheel input: desired vs. actual angular speeds (zoomed in)

4.2 Results for the evaluation of H2: quantification of the degree of realism of the simulator controlled by the force cell

For the single subject, bilateral propulsion experiments were run for each of the following three conditions: overground (OG), on the simulator controlled by the Smartwheels (SW), on the simulator controlled by the force cell (FC).

The raw data was used to calculate the following biomechanical parameters:

- Maximum propulsion moment $M_{Z,MAX}$ (Nm)
- Maximum applied force $F_{TOT,MAX}$ (N)
- Push time (s)
- Recovery time (s)

The results of those calculations are shown on Table 4.1.

Table 4.1 Experimental results of manual wheelchair propulsion: Overground (OG) vs. Simulator with Smartwheels (Sim SW) vs. Simulator with force cell (Sim FC)

Variable	Side	OG	Sim SW	Sim FC	Sim SW - OG	Sim FC - OG
Mzmax (Nm)	Left	9.4 ± 2.0	7.3 ± 0.8	8.6 ± 1.4	-2.1 ± -1.2	-0.8 ± -0.6
	Right	8.7 ± 1.7	7.2 ± 0.4	9.2 ± 1.0	-1.4 ± -1.3	0.5 ± -0.7
Ftotmax (N)	Left	53.3 ± 9.1	29.5 ± 3.6	34.0 ± 3.2	-23.8 ± -5.5	-19.3 ± -5.9
	Right	51.2 ± 7.3	23.9 ± 1.3	30.7 ± 2.4	-27.3 ± -6.1	-20.5 ± -4.9
Push time (s)		0.32 ± 0.03	0.46 ± 0.04	0.41 ± 0.03	0.14 ± 0.01	0.09 ± 0.00
Recovery time (s)		0.55 ± 0.03	0.57 ± 0.03	0.53 ± 0.03	0.01 ± 0.00	-0.02 ± 0.00

We will now present the results in graphical form in Figures Figure 4.11, Figure 4.12, Figure 4.13, Figure 4.14.

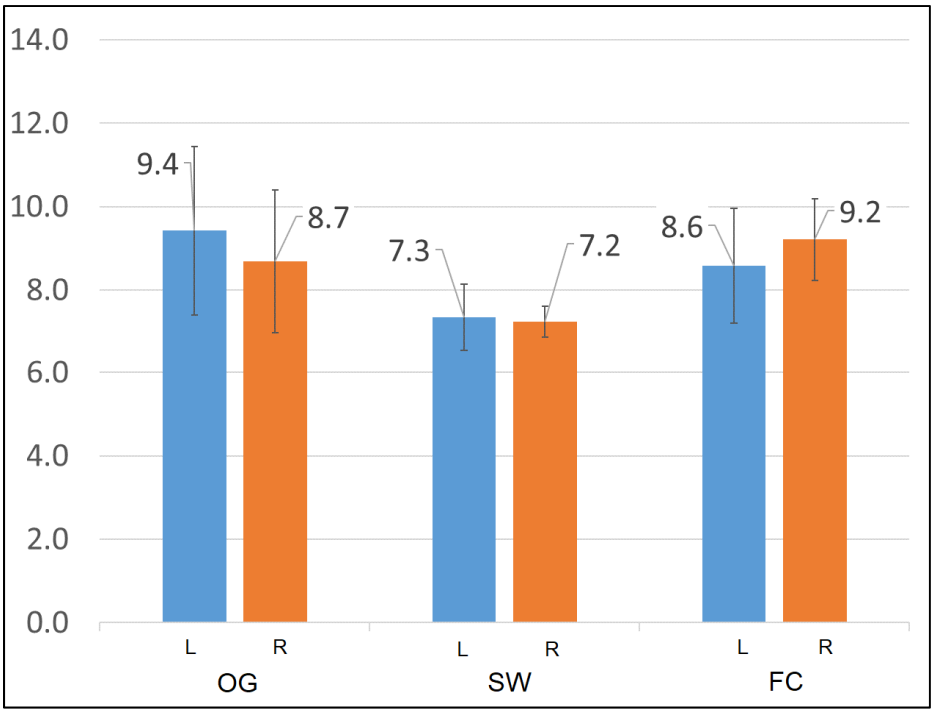

Figure 4.11 Mzmax (Nm): mean of maximum applied moment during 10 propulsion cycles for 1 able-bodied subject

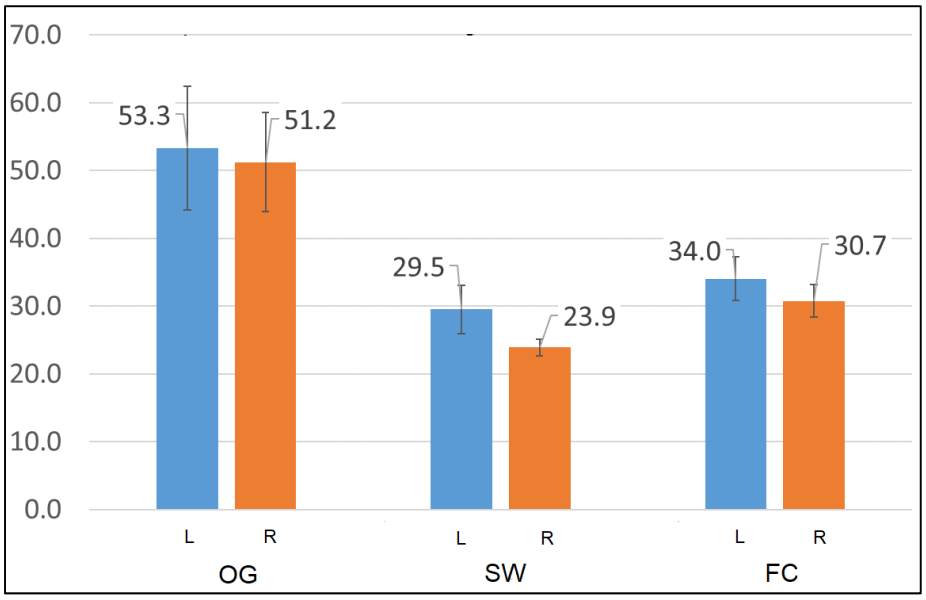

Figure 4.12 Ftotmax (N): mean of maximum applied force during 10 propulsion cycles for 1 able-bodied subject

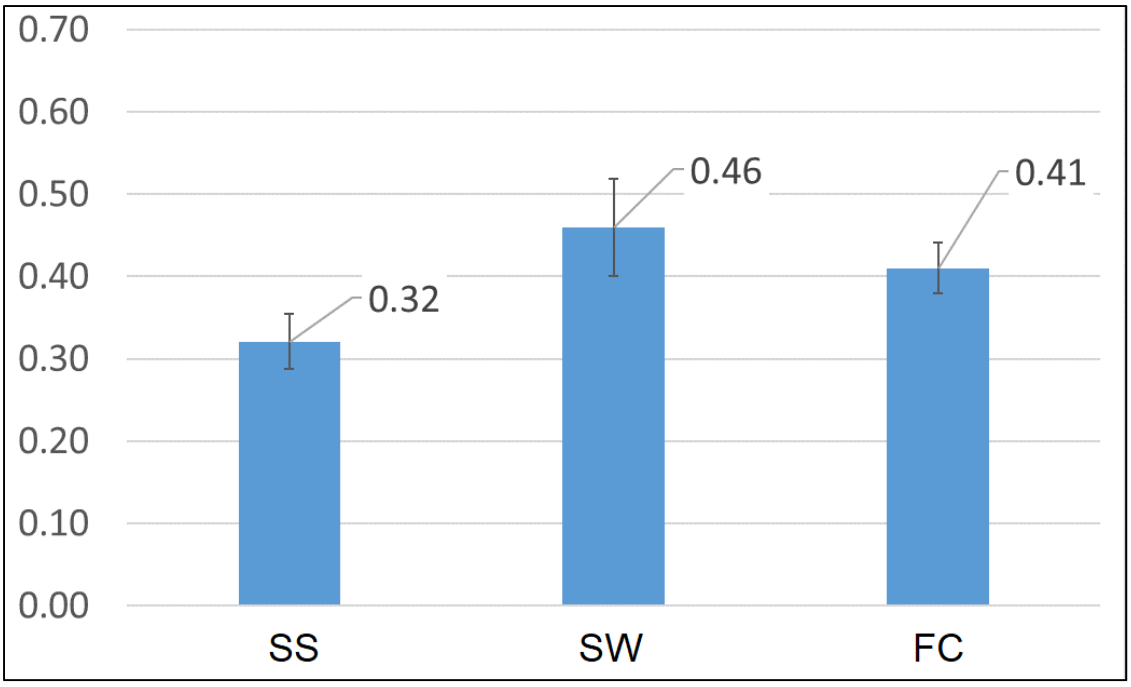

Figure 4.13 Push time (s): mean over 10 propulsion cycles for 1 able-bodied subject

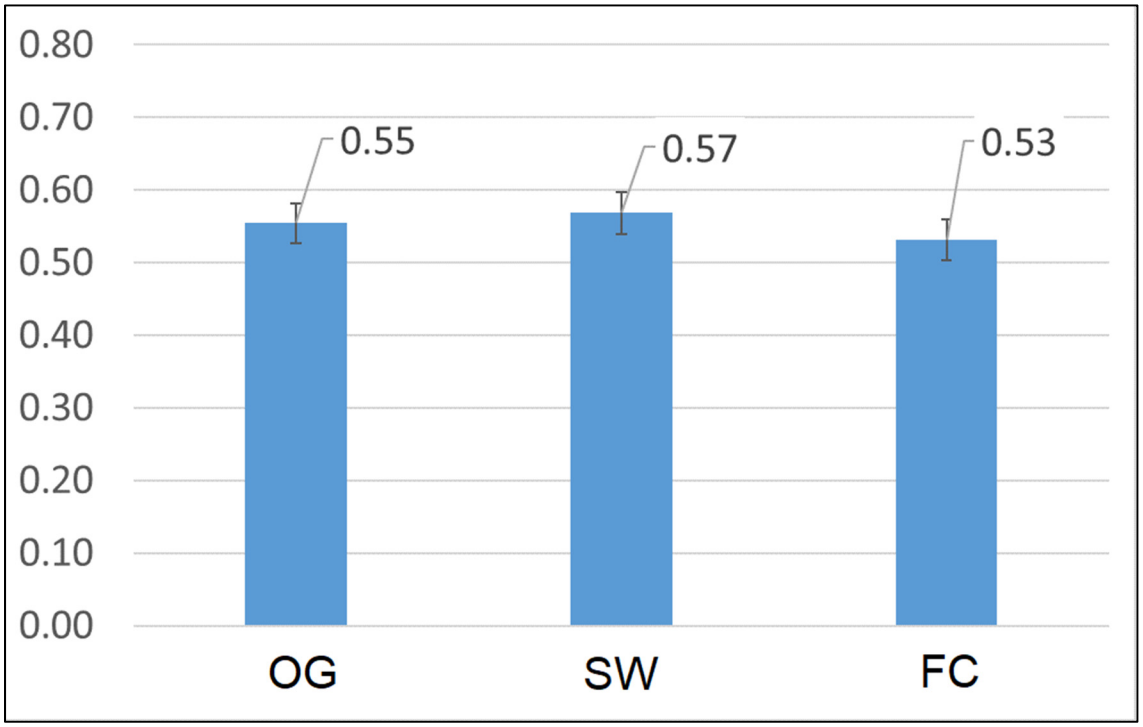

Figure 4.14 Recovery time (s): mean over 10 propulsion cycles for 1 able-bodied subject

We now proceed to reporting our findings based on the tabular results and the visual inspection of the previous four figures.

For MzLmax, the difference between Sim FC and OG (-0.8) was smaller than the difference between Sim SW and OG (-2.1). For MzRmax, the difference between Sim FC and OG (0.5) was also smaller than the difference between Sim SW and OG (-1.4).

For FtotLmax, the difference between Sim FC and OG was large (-19). The difference between Sim SW and OG was large as well (-23). For FtotRmax, the difference between Sim FC and OG was large (-20). The difference between Sim SW and OG was large as well (-27).

For push time, the difference between Sim FC and OG was large (0.09). The difference between Sim SW and OG was large as well (0.14).

For recovery time, the difference between Sim FC and OG was small (0.02). The difference between Sim SW and OG was also small (0.02).

CHAPTER 5

DISCUSSION

5.1 Discussion on the force cell

5.1.1 Comparison of the input signal between the force cell and the Smartwheels

The force cell measures the antero-posterior force $F_{Y,FC}$ applied by the user onto the rest of the simulator structure. This includes the components along the horizontal direction of the two forces applied on the handrims and the reaction force applied by the trunk on the wheelchair.
The Smartwheels measure the moment $M_{Z,SW}$ applied on the handrims. The applied force $F_{APP,SW}$ (which we also call the force F_{TAN} tangential to the handrim) that moves the wheelchair forward is calculated by: $F_{APP,SW}=M_{Z,SW}/r_H$, where r_H is the radius of the handrims.

We ran a 30 second simulation during which a subject propelled bilaterally with the same amount of force. First, we calculated the total force applied on handrims, as measured by the Smartwheels. On each side, the forces are $F_{APP,R,SW} = M_{ZR,SW}/r_H$ (right wheel) and $F_{APP,L,SW} = M_{ZL,SW}/r_H$ (left wheel). The total applied force is $F_{APP,SW} = F_{APP,R,SW} + F_{APP,L,SW} = M_{ZR,SW}/r_H + M_{ZL,SW}/r_H = (M_{ZR,SW} + M_{ZL,SW})/r_H$.
We plot and compare the following two variables on Figure 5.1.
- in red, the force $F_{APP,FC} = F_{Y,FC}$ as measured by the force cell
- in blue, the force $F_{APP,SW}$ as measured by the Smartwheels

There is a slight difference between the two curves. During the push phase, we notice the value of the force measured by the force cell is slightly higher than that measured by the Smartwheels. This difference is possibly due to the movement of the trunk. Just at the start of the recovery phase, the force $F_{Y,FC}$ goes up a little bit, then comes down, before going back up as the user pushes on the handrim. This difference in the value of the force probably corresponds to a change of linear momentum due to the movement of the user's trunk.

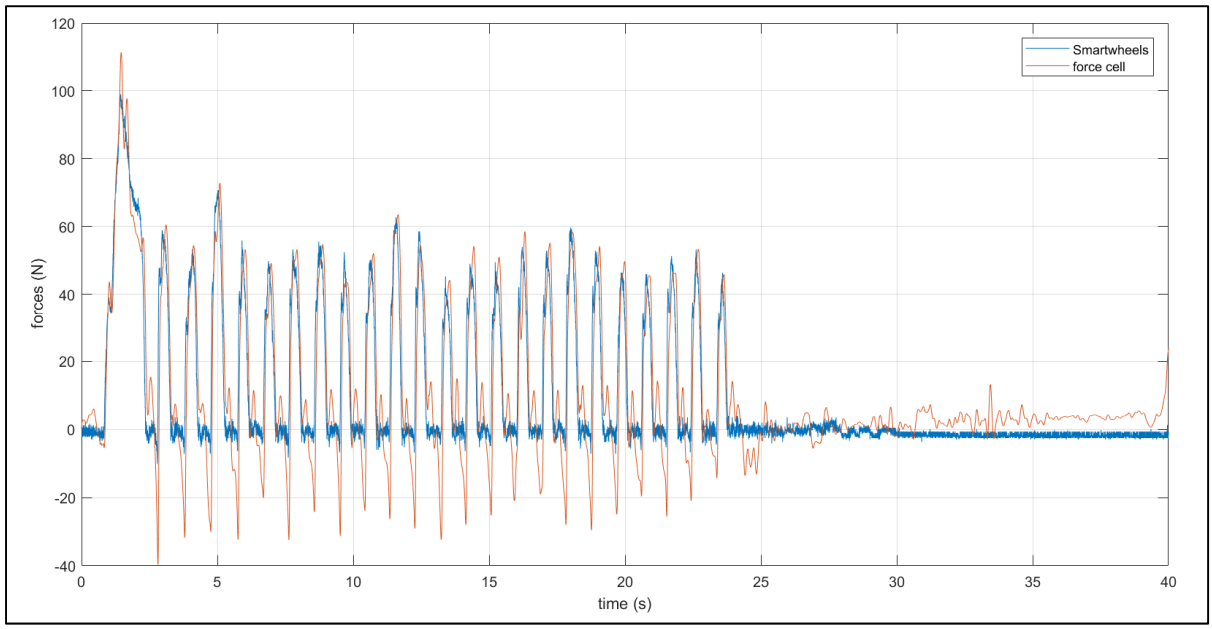

Figure 5.1 Force cell force $F_{Y,FC}$ and Smartwheels sum of calculated forces ($M_{zR,SW}/r_H$ + $M_{zL,SW}/r_H$)

5.1.2 Comparison of results to those obtained on the Manual Wheelchair Simulator located the University of Groningen in the Netherlands

De Klerk et al. (2020), in collaboration with the company Lode BV (Groningen, The Netherlands) have built a manual wheelchair simulator (a roller ergometer) which incorporates two force cells as the force measurement instruments. As part of the validation procedure of their simulator, they equipped the test wheelchair with Optipush instrumented wheels. This allowed the researchers to compare the torque measured by the force cells to those measured by the Optipush wheels, which are considered to be very reliable (Guo et al., 2011).

Upon visual inspection, we notice that their plot of torque vs. time resembles ours (Figure 5.2). The force cell records a slightly higher force during the push phase, and a slightly lower force during the recovery phase. This data appears to confirm that the measurements taken with the LIO Simulator are reliable.

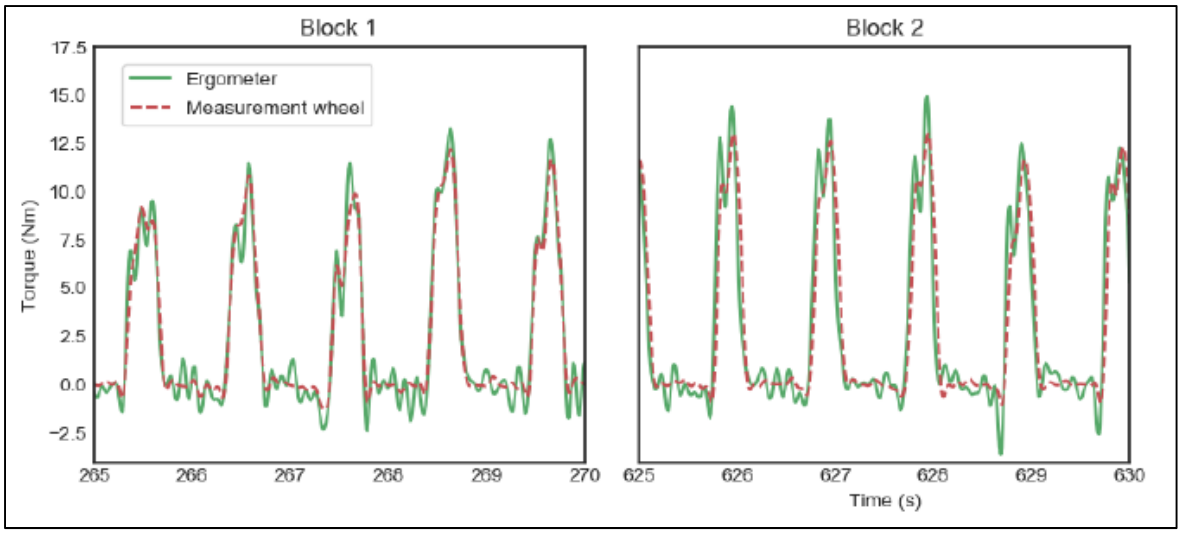

Figure 5.2 Comparison of torque measured by the Optipush instrumented wheel and by the manual wheelchair simulator at the University of Groningen (de Klerk, Vegter, Veeger, et al., 2020)

5.1.3 Advantages of using a force cell as the force measurement instrument

When using a force cell to control the simulator instead of the Smartwheels, the ergometer can be used with any wheelchair configuration (e.g., handrim types, axle type), without changing the wheelchair-user interface (in most measurement wheels the configuration is fixed). This allows for faster testing, which is especially important in a clinical environment.

It also makes the ergometer more suitable for measuring in a sports environment as measurement wheels are usually not built for sports wheelchairs and the high strains experienced during testing of athletes.

5.1.4 Location of the force cell

The test wheelchair used in the LIO Simulator has a transversal axis between the two wheels. Both the original retention system and the retention system built as part of this thesis to include the force cell were made for this design of wheelchair. Not all models of wheelchair include this kind of transversal axis so other ways of attaching the force cell could be explored. One

option to be investigated would be as follows: we would attach a sturdy bracket to the wall, we would attach another bracket to the tubes supporting the wheelchair's backrest, and finally, we would attach the force cell to both brackets, top and bottom. This is shown in Figure 5.3**Erreur ! Source du renvoi introuvable.** and **Erreur ! Source du renvoi introuvable.** Figure 5.4 below.

The question that arises with this new configuration is the following: if we change the location of the force cell, would we be able to use the control loop as is, as was determined for a force cell located under the wheelchair?

Figure 5.3 Bracket attached to the wall

5.1.5 Number of force cells

We could also investigate if it would be advantageous to place two force cells underneath the wheelchair, as was done by De Klerk et al. (2020) in their manual wheelchair simulator. They would be placed on either side of the central line. The measurements of the left and right forces would still contain some noise, but to a lesser extent than when they are calculated by using the measurement of vertical moment.

Figure 5.4 Bracket attached to the wheelchair

5.2 Discussion on the control loop

5.2.1 Discussion on H1: development of a stable haptic control loop using a force cell

We built an admittance control system that incorporates a PI controller, with feedforward control. We measured the anterior-posterior force applied on the simulator structure by using a force cell. We calculated the equivalent propelling forces applied on each wheel by using the moment of forces around the vertical axis, which is also measured by the force cell.

The control problem is that of regulation. The speed of the wheels, controlled by motors, was to follow the desired speed calculated by a mathematical model. This mathematical model of a wheelchair on the ground takes the equivalent propulsive forces as input.

Through a process of trial and error, we settled on values of the control gains as $k_P = 2$, $k_I = 6$, and $k_{FF} = 0.25$. By visual inspection, we confirmed that the measured angular speed will follow the desired angular speed, when using these gains. The actual speed oscillates around the desired speed with some noise.

We confirm Hypothesis **H1**, stating that a stable control loop using a force cell could be built to control this manual wheelchair simulator.

However, we don't know if under other conditions, such as when the user propels at 0.5, 0.8, 1.5, 2.0 m/s, the control loops remains stable. That remains to be checked.

We evaluated different graphs by making a visual inspection. In the future, however, we can quantify the spread between the desired and actual angular speeds by calculating the rms error between the curves.

The optimal values of the control gains were obtained by running through different values of parameters of k_P, k_I, k_{FF}. In the future, we could determine them using optimization algorithms already embedded in MATLAB, or using other algorithms to be found in the literature.

5.2.2 Discussion on H2: quantification of the degree of realism of the simulator controlled by the force cell (fidelity to overground propulsion)

We compared manual wheelchair propulsion in three conditions: 1) on the ground (OG), 2) on the simulator controlled by Smartwheels (SW), 3) on the simulator controlled by a force cell (FC). The parameters used for the comparison were the maximum applied moment $M_{Z,max}$ (Nm), the maximum total force applied $F_{TOT,max}$ (N), push time (s) and recovery time (s).

The analysis of the tabular and graphical data showed that realism seems to be slightly increased when the force cell is used as opposed to the Smartwheels. Differences of values for parameters M_{zRmax} and M_{zLmax} between conditions OG and FC were smaller than the differences between OG and SW. That means FC is closer to real propulsion OG than SW, for these parameters.

For $F_{TOT,MAX}$ and push time, the differences between OG and FC and between OG and SW were considered large, on both the left and right sides. We don't believe we can draw any conclusions from these results as both the FC and SW conditions tended to give similar results. For recovery time, the difference between OG and FC and between OG and SW were considered small, on both the left and right sides. We don't believe we can draw any conclusions from these results either as both the FC and SW conditions gave similar results.

Based on these results, it is our judgment that hypothesis **H2** is confirmed, because realism is slightly increased with the force cell, based on the analysis of the parameter Mzmax. The difference in the results could be explained by the fact that the movement of the trunk of the user affects the dynamics of the wheelchair-user system. This effect is captured by the force cell, but not by the Smartwheels. However, we would require a statistical analysis based on data collected with at least ten able-bodied subjects to determine rigorously if the difference observed for one able-bodied subject is statistically significant. A further evaluation should be carried out with ten wheelchair-bound individuals. These recommendations are formally stated in the next sections.

The analysis also showed that biomechanical parameters changed between propulsion overground and propulsion on the wheelchair simulator. This is something that was noticed by Lalumière et al. (2014) when they conducted a study to compare overground propulsion to propulsion on the LIO Simulator which used Smartwheels as part of the control system. Their participants were all wheelchair-bound. As they mention in their article, this a phenomenon that has been observed before and may be due to the lack of visual stimulation during simulator propulsion.

The ultimate goal is for the simulator to be so realistic that biomechanical parameters are the same overground and on the simulator. However, should it turn out not to be the case, the differences should be taken into account. This does not dismiss the usefulness of the wheelchair simulator. However, in that case, it should be used with caution, and in combination with overground propulsion training.

5.2.3 2D (curvilinear) manual wheelchair model

The goal of this thesis was to build a stable control system using the force cell as the force sensor. The control system required a mathematical model of the wheelchair. We used a one-dimensional math model because we wanted to concentrate on the development on the control system. A 1-D model is limited in the range of paths that it can model. Curvilinear paths (including turns) require a more complex model (a 2-D wheelchair model). One such model was developed by Chenier (2012) previously and implemented on the LIO Simulator. However, we did not use it in this first study dealing with the force cell, because we did not want to be overwhelmed by the number of variables that we were dealing with.

5.2.4 Dynamic rolling resistance

In section 1.2.2, we derived a one-dimensional mathematical model of overground wheelchair propulsion, described by Eq. (1.11), which takes into account the fact that rolling resistance is not constant during a propulsion cycle, but rather varies with the weight distribution of the user on her/his wheelchair. The implementation of this model would require the use a pressure cushion to determine the center of pressure (COP) of the user. The position of the COP would then be used in a new control loop and with a new mathematical model, both of which would include this information. An overview of a haptic admittance control loop incorporating all these elements is shown on Figure 5.5**Erreur ! Source du renvoi introuvable.**. This improvement of the LIO Simulator should increase its realism.

5.2.5 Validation of the control loop of the force cell with 15 able-bodied subjects

We would suggest a further validation of the force cell control loop by conducting the same comparison done for one subject in the three conditions, for 15 able-bodied subjects. We should note that the experiments should not always occur in the same order. In order to avoid

any type of bias in the results that might be due to the order of experiments, the order of the three conditions should be randomly selected by permutation.

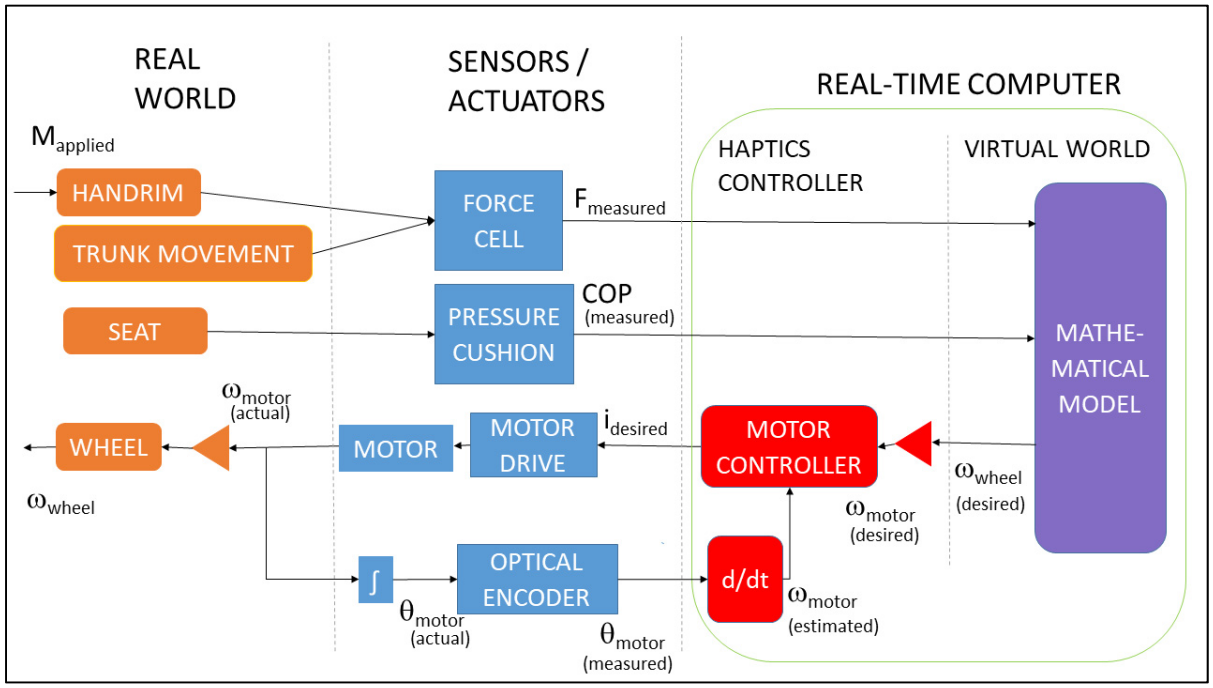

Figure 5.5 Haptic admittance control loop for dynamic rolling resistance (with pressure cushion)

Should the results be similar, it would lend more credence to the results of the experiments performed with the first able-bodied subject. Three sets of data will be obtained for each participant, one set per condition.

For each parameter, the value over the 10 pushes would be averaged to create a value for that user.

For example, for M_{zRmax}, for every user i=1…10,

$$M_{zRmax,i} = \frac{\sum M_{zR,max}\ (of\ every\ push)}{10}$$

We mention here that this further validation was part of the scheduled work that was going to be done in this thesis. The project was awaiting ethics approval by the CRCHUM when the process was delayed significantly due to the covid-19 pandemic.

5.2.6 Validation of the control loop of the force cell with expert MWC users

In a further validation effort, we can try testing the control loop with input data from 15 expert MWC users (regular users of MWCs who have disabilities). A research project was undertaken (Lalumiere et al., 2014) to compare overground propulsion to propulsion on the LIO simulator, with participants who had suffered Spinal Cord Injuries. That study found propulsion on the LIO simulator was similar to that overground.

Since novice users propel differently than experienced users, it might be beneficial to repeat the study by Lalumière but using the force cell to control the simulator. In their research, the variables compared were the total force applied F_{TOT}, the tangential force F_{TAN}, the mechanical effective force (MEF) and power. Those parameters were selected because they were likely related to the development of secondary musculoskeletal impairments affecting the upper limbs among wheelchair users (Paralyzed Veterans of America, 2005).

5.3 Discussion on the study

5.3.1 Objective of the work

The main objective of the present work was to replace the Smartwheels by a force transducer that would meet additional criteria from the list presented in section 1.3. These criteria involved the proper simulation of the influence of the movement of trunk on the dynamics of the MWC-user system, and the respect of the ergonomic properties of the MWC-user interface. The secondary objectives included the validation of the control loop and the evaluation of realism with an individual subject. We have achieved the objectives set out at the beginning of this project.

5.3.2 Perception of realism on the simulator

In previous research efforts, the evaluation of the realism of simulators has also been done by using questionnaires. For example, in a study by Bando et al. (2004), subjects were asked to

rate, on a scale of 1 to 5, how they perceived: the quality of the visual presentation, the feeling of moving on a road, the feeling of ascending a slope, the feeling of collisions. Harrison et al. (2004) asked their subjects to evaluate, on a scale of 1 to 6 (from unable to judge to very realistic): the perception of motion within the environment, level-ground propulsion, freewheel motion, the perception of effort experienced during wheelchair motion. Similar questions could be posed to wheelchair-bound participants in the study to gage the level of realism of the LIO manual wheelchair simulator controlled by the force cell.

5.3.3 Limitations of the study

This was a first attempt at running the manual wheelchair simulator under force cell control. We made several assumptions, which limit the scope of validity of the results. The following limitations of the study can be listed:

- The model of the wheelchair used is one-dimensional (mass and friction). It can only replicate linear paths of a manual wheelchair on the ground.
- The rolling resistance was assumed to be constant, and not vary due to the movement of the user and his trunk
- Regarding biomechanical parameter analysis, if we run the LIO simulator only with a force cell and do not replace the original wheels by the Smartwheels, we do not measure directly the moment applied at the handrim. It can only be estimated from measurement by force cell.

5.3.4 Expected outcomes and importance of the study

The outcomes of this research project will help the development of the haptic interfaces of the high-realism manual wheelchair simulator currently being built for the CRIR Institution. The goal for that simulator is for it to be housed in a rehabilitation center and be used to train new and experienced users on propulsion patterns that are protective of the upper limb and do not lead to injuries.

CONCLUSION

In response to the need for fundamental research on manual wheelchair propulsion and the need for training on manual wheelchair skills for new and experienced users, the team at the ETS Health Technologies laboratory and at the LIO built a manual wheelchair simulator with a high degree of realism in mind: it is able to use a MWCU's own wheelchair and follow a curvilinear path. Using the Smartwheels as force sensors allows the simulator to provide real-time haptic biofeedback, which has been shown to be useful for rehabilitation (Symonds et al., 2018). However, the Smartwheels replace the wheelchair's original wheels, thus changing the wheelchair-user system's mass and rigidity. Therefore, the use of Smartwheels precludes the use of the original wheelchair as is, which could affect the validity of research results and the transfer of skills to real life. A high level of realism is necessary for learnt abilities to be transferred to real life. Full dynamics during the propulsion cycle could not be captured with the Smartwheels.

With the goal of increasing the level of realism, we replaced the Smartwheels with a force cell and built a stable admittance control loop. We then attempted to quantity the degree of improvement of realism when using force cell control instead of Smartwheel control. The parameters chosen for evaluation of manual wheelchair propulsion were maximum propulsion moment (Nm), maximum applied force (N), push time (s) and recovery time (s). A visual and qualitative analysis seems to suggest that the use of a force cell slightly increases the realism of the simulation over that rendered by the Smartwheels.

We discussed the differences in the control of the wheel speed due the input signals coming from the force cell and the Smartwheels and compared our results to those of another manual wheelchair simulator which also used force cells. We also offered several suggestions for further research using the force cell to control the LIO Simulator, such as changing the location of the force cell or adding another force cell. We also suggested using the bidimensional model of overground wheelchair propulsion, as well as using a pressure cushion to calculate the center

of pressure in order to take into account the dynamics rolling resistance. Finally, we listed some limitations of the study and the possible outcomes of this research.

APPENDIX I

FORCE CELL SPECIFICATIONS SHEETS

MC3A Force and Torque Sensor

APPLICATIONS
The MC3A force and torque sensor is particularly suitable for applications requiring simultaneous measurement of several forces and moments, or measurements of forces that change direction and position over time. Common applications for this transducer include research and development in robotics, ergonomics, production processes, biomechanics, and dynamics. A waterproof version is available for use in tow tanks, ocean engineering, and other underwater applications.

DESCRIPTION
AMTI's MC3A force and torque sensor is specifically designed for the precise measurement of forces and moments. The sensor measures the three orthogonal force and moment components along the X, Y, and Z axes, producing a total of six outputs. The characteristics of this strain gage sensor make it ideal for research and testing environments; it has high stiffness, high sensitivity, low cross-talk, excellent repeatability and long term stability. It is simple, easy to use, and is available in either 100, 250, 500, 1000 pound (440, 1100, 2200, 4500 Newton) vertical capacities.

The body of the load cell is manufactured from a high-strength aluminum alloy with an anodized finish to protect the exterior from corrosion. Elastomeric O-ring seals provide internal protection of the strain gages and wiring from industrial environments and moisture exposure.

CALIBRATION
Each sensor is inspected and tested in AMTI's calibration facility. The calibration procedure provides a ten-point calibration of each channel and a complete test of all system components.

AMPLIFICATION
The MC3A force and torque sensor incorporates strain gages mounted on a precision strain element designed to measure forces and moments. As with most conventional strain gage transducers, bridge excitation and signal amplification are required. The MC3A can be used with any strain gage amplifier, including AMTI's product line. AMTI's amplifiers are all high gain devices which provide excitation and amplification for multiple channels in one convenient package to suit different applications.

SOFTWARE
AMTI offers several software packages for use with the multi-component force sensors. Please contact the sales department for more details.

CUSTOM
AMTI also offers other transducers to meet your specific needs. Standard units with a diameter as small as 1 inch (2.25 cm) are available, and sensors with capacities as high as 3,000,000 pounds (13,345,000 Newtons) have also been constructed. Units are available in various sizes, load capacities, sensitivities, materials, and in pressure compensated waterproof versions.

ISO 9001:2000 CERTIFIED

AMTI

Bulletin MC3A-0105 *U.S. Patent # 4493220
Contents of this publication are subject to change without notice.

Figure-A I-1 Force cell specification sheet, page 1

MC3A

Force and Torque Sensor

MC3A Series Specifications	100	250	500	1000
Fz Capacity, lb (N)	100 (440)	250 (1100)	500 (2200)	1000 (4400)
Fx, Fy Capacity, lb (N)	50 (220)	125 (560)	250 (1100)	500 (2200)
Mz Capacity in*lb (Nm)	50 (5.6)	125 (14)	250 (28)	500 (56)
Mx, My Capacity in*lb (Nm)	100 (11)	250 (28)	500 (56)	1000 (110)
Fz Sensitivity, μV/[V*lb] (μV/[V*N])	6.0 (1.35)	3.0 (0.67)	1.5 (0.340	0.75 (0.17)
Fx, Fy Sensitivity, μV/[V*lb] (μV/[V*N])	24.0 (5.4)	12.0 (2.7)	6.0 (1.35)	3.0 (0.67)
Mz Sensitivity, μV/[V*in*lb] (μV/[V*Nm])	24.0 (121.4)	12.0 (106.2)	6.0 (53.1)	3.0 (26.5)
Mx, My Sensitivity, μV/[V*in*lb] (μV/[V*Nm])	30.0 (265.5)	15.5 (137.2)	8.0 (70.8)	4.0 (35.4)
Fz Stiffness, x10^5 lb/in (x10^7 N/m)	1.7 (2.8)	4.5 (7.5)	9.0 (15.0)	18.0 (30.0)
Fx, Fy Stiffness x 10^5 lb/in (x10^7 N/m)	0.12 (0.2)	0.3 (0.5)	0.6 (1.0)	1.2 (2.0)
Mz Stiffness, x10^4 in*lb/radian (x10^4 Nm/radian)	2.0 (0.2)	5.0 (0.5)	10 (1.1)	20 (2.2)
Weight, lb (kg)	2 (0.9)	2 (0.9)	2 (0.9)	2 (0.9)
Mx, My Lowest Resonant Frequency, Hz	300	500	700	1000

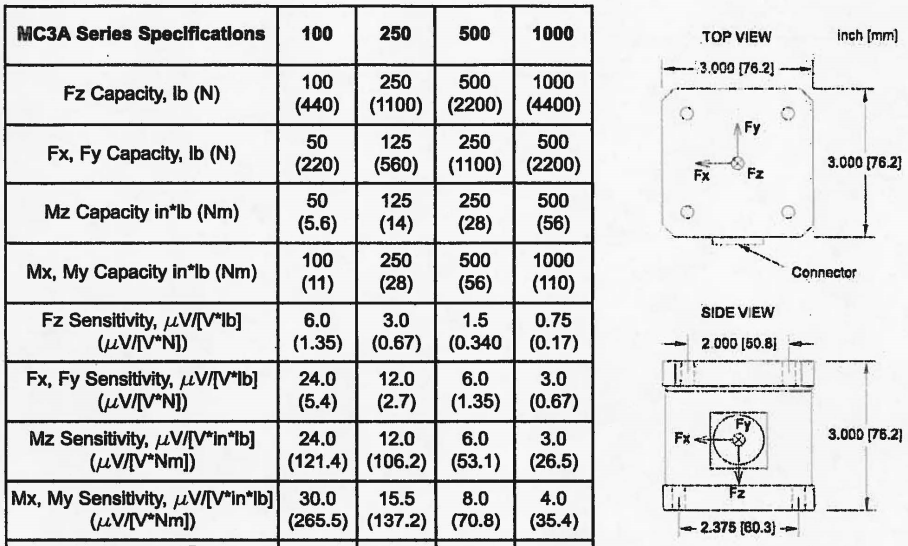

- Four threaded 1/4-20 inserts on 2.000 inch [50.8 mm] centers on top surface.
- Four 0.256 inch [6.5 mm] through holes on 2.375 inch [60.3 mm] centers on bottom surface.
- Metric threaded hold-down inserts available.

CONNECTOR TYPE:
Souriau 851-02E16-26P50-44

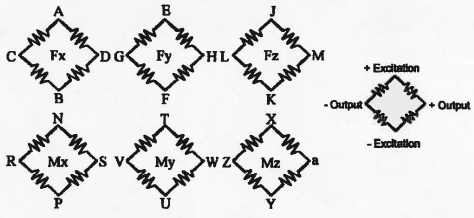

Bridge Fz = 700 ohms
Bridges Fx; Fy; Mx; My; Mz = 350 ohms

GENERAL SPECIFICATIONS
Recommended Excitation: 10V or less
Crosstalk: Less than 2% on all channels
Temperature Range: 0 to 125°F, (-17 to 52°C)
Fx, Fy, Fz hysteresis: ± 0.2 % Full Scale Output
Fx, Fy, Fz non-linearity: ± 0.2% FullScale Output

ISO 9001:2000 CERTIFIED

AMTI
ADVANCED MECHANICAL TECHNOLOGY, INC.
176 WALTHAM STREET WATERTOWN, MA 02472-4800
TEL: (617) 926-6700 • (800) 422-AMTI • FAX: (617) 926-5045
email: sales@amtimail.com • web: www.amti.biz

Figure-A I-2 Force cell specification sheet, page 2

Transducer Load Specification

Rated maximum Loads

Transducer Model MC3A	-100	-250	-500	-1000
Fz	100 lb	250 lb	500 lb	1000 lb
Fx	50 lb	125 lb	250 lb	500 lb
Fy	50 lb	125 lb	250 lb	500 lb
Mx	100 in-lb	250 in-lb	500 in-lb	1000 in-lb
My	100 in-lb	250 in-lb	500 in-lb	1000 in-lb
Mz	50 in-lb	125 in-lb	250 in-lb	500 in-lb

Rated loads are individually applied. The moment origin for load calculations can be taken as located at the geometric center of the transducer. The use of simultaneously applied maximum loads may result in a safety factor lower than recommended. Contact the factory for simultaneous loads above one-half the rated loads or for a check on the safety factor for specific loading conditions.

Transducer Torque Guidelines

The ¼-20 threaded holes are in stainless steel inserts. They have sufficient strength to allow taking grade 8 fasteners up to the yield point. The recommended fastener tightening torque depends upon bolt material and lubrication. To prevent possible galling, a thread lubricant should always be used. If you have bolt tightening specifications or guidelines you should follow these. If not, the following are some recommended tightening torques.

	¼-20
1. Oil Lubricated Grade 8 Bolt	200 in-lb
2. Never Seize Lubricated Grade 8 Bolt	130 in-lb
3. Never Seize Lubricated Austenitic Stainless Bolt	70 in-lb

If you have any questions please contact AMTI for technical support.

AMTI

Figure-A I-3 Force cell specification sheet, page 3

Calibration Loading Diagram

Values of coordinates correspond to Figures 2 and 3 of Section 3.

Component	Actual Max. Load (lb or in-lb)	Load Direction	Moment Arm (in.)	Coordinates of Applied Load x (in.)	y (in.)	z (in.)
Fx	499.6	X	N/A	-1.5	0	0.25
Fy	500.1	Y	N/A	0	-1.5	0.25
Fz	999.1	Z	N/A	0	0	0
Mx	499.7	Z	1	0	1	0
My	499.8	Z	1	-1	0	0
Mz	499.5	Z	1	-1.5	-1	0.25
-Mx	-499.5	Z	1	0	-1	0
-My	-499.7	Z	1	1	0	0

Calibration Load	Actual Max. Load (N or N-m)	Load Direction	Moment Arm (mm)	Coordinates of Applied Load x (mm)	y (mm)	z (mm)
Fx	2222.2	X	N/A	-38.1	0	6.35
Fy	2224.3	Y	N/A	0	-38.1	6.35
Fz	4444.1	Z	N/A	0	0	0
Mx	56.5	Z	25.4	0	25.4	0
My	56.5	Z	25.4	-25.4	0	0
Mz	56.4	X	25.4	-38.1	-25.4	6.35
-Mx	-56.4	Z	25.4	0	-25.4	0
-My	-56.5	Z	25.4	25.4	0	0

Figure-A I-4 Force cell specification sheet, page 4

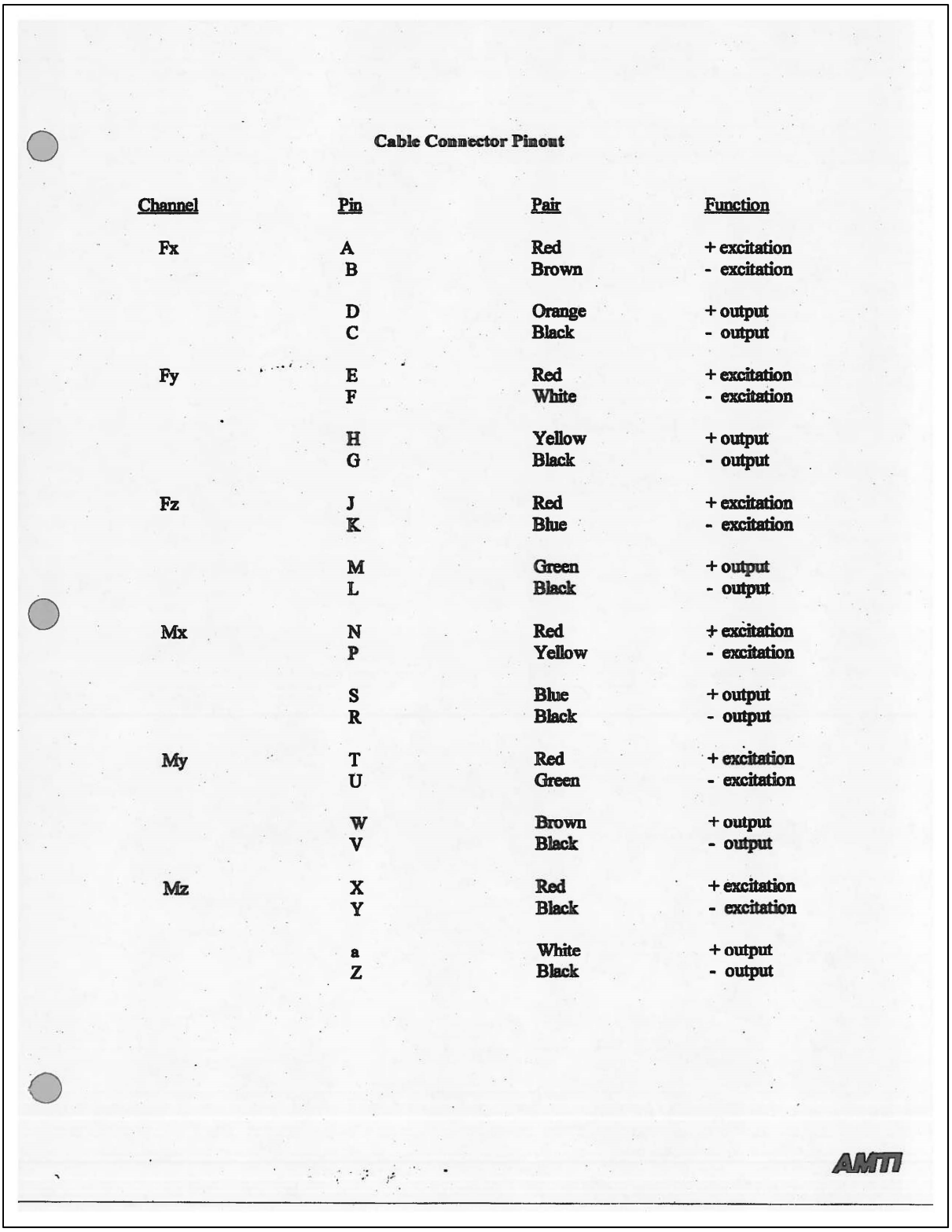

Cable Connector Pinout

Channel	Pin	Pair	Function
Fx	A	Red	+ excitation
	B	Brown	- excitation
	D	Orange	+ output
	C	Black	- output
Fy	E	Red	+ excitation
	F	White	- excitation
	H	Yellow	+ output
	G	Black	- output
Fz	J	Red	+ excitation
	K	Blue	- excitation
	M	Green	+ output
	L	Black	- output
Mx	N	Red	+ excitation
	P	Yellow	- excitation
	S	Blue	+ output
	R	Black	- output
My	T	Red	+ excitation
	U	Green	- excitation
	W	Brown	+ output
	V	Black	- output
Mz	X	Red	+ excitation
	Y	Black	- excitation
	a	White	+ output
	Z	Black	- output

AMTI

Figure-A I-5 Force cell specification sheet, page 5

APPENDIX II

FORCE CELL SUPPORT MANUFACTURING DRAWINGS

II.1 Assembly

The CAD drawing of the assembly (including the force cell) is shown on Figure-A I-1 and its corresponding manufacturing drawing is shown on Figure-A II-2.

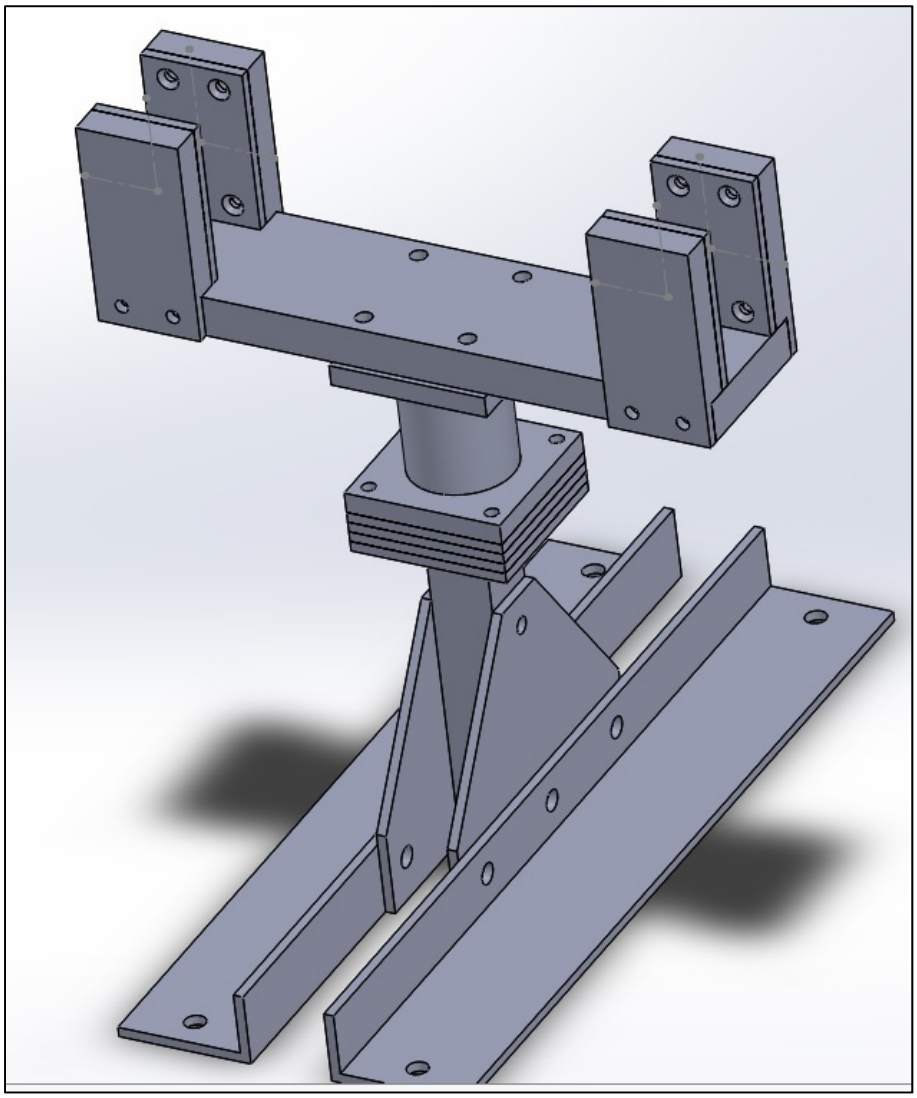

Figure-A II-1 CAD drawing of the assembly

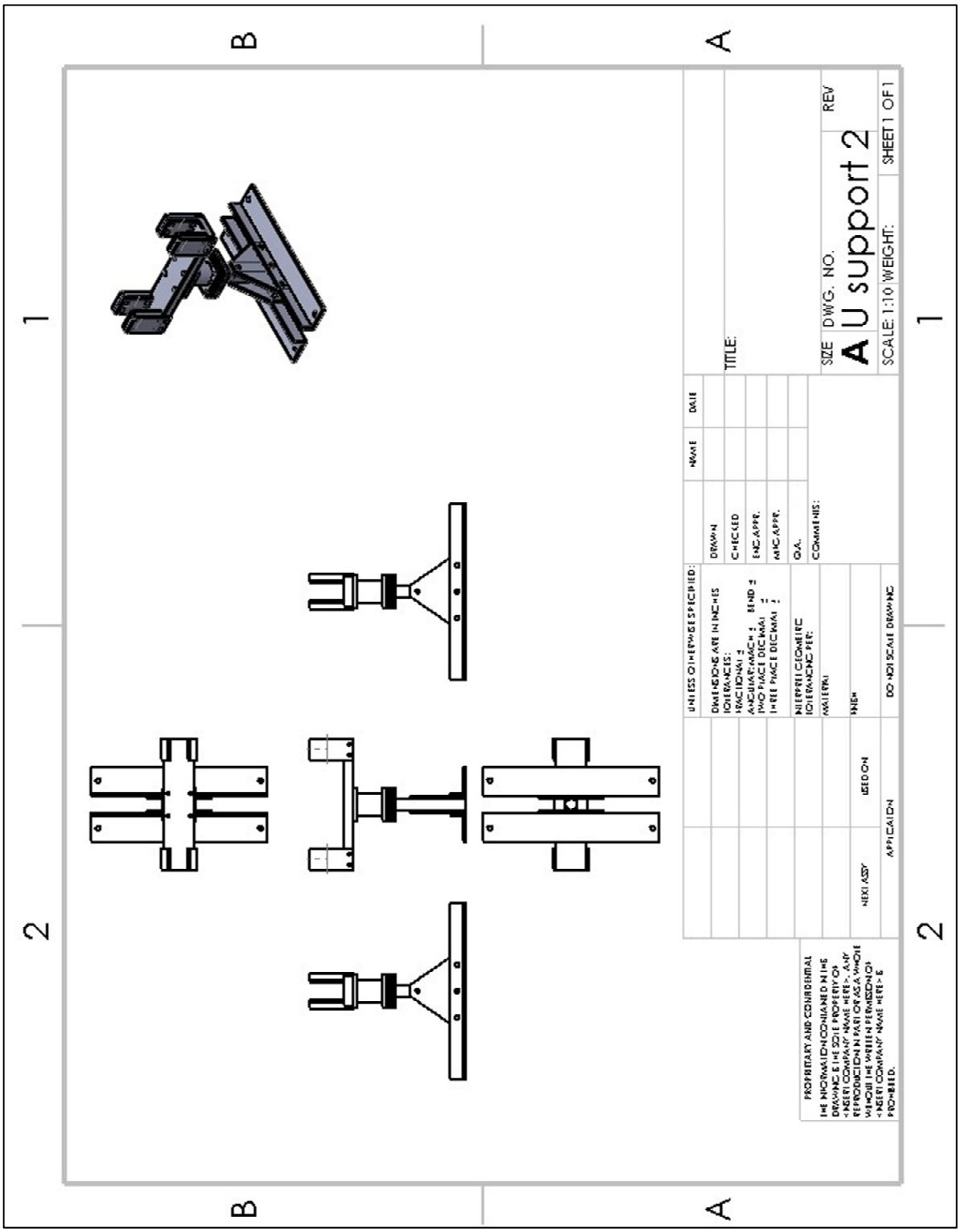

Figure-A II-2 Manufacturing drawing of the assembly

II.2 List of individual parts

The individual parts are listed below, physically from bottom to top. The number of units manufactured is shown in parentheses.

- Support L base (2)
- Base bracket (2)
- Sensor post (1)
- Force sensor base (1)
- Spacer (5)
- Support base (1)
- Lateral supports (4)
- Slider (4)

II.3 CAD drawings and manufacturing drawings of individual parts

II.3.1 Support L base

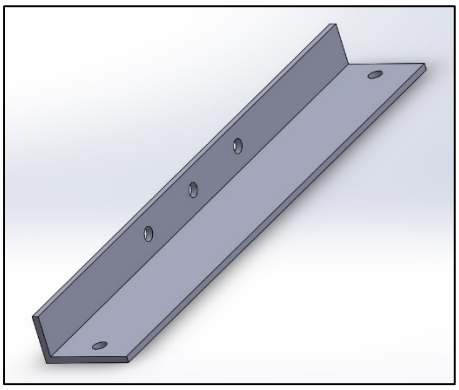

Figure-A II-3 CAD drawing
of the Support L base

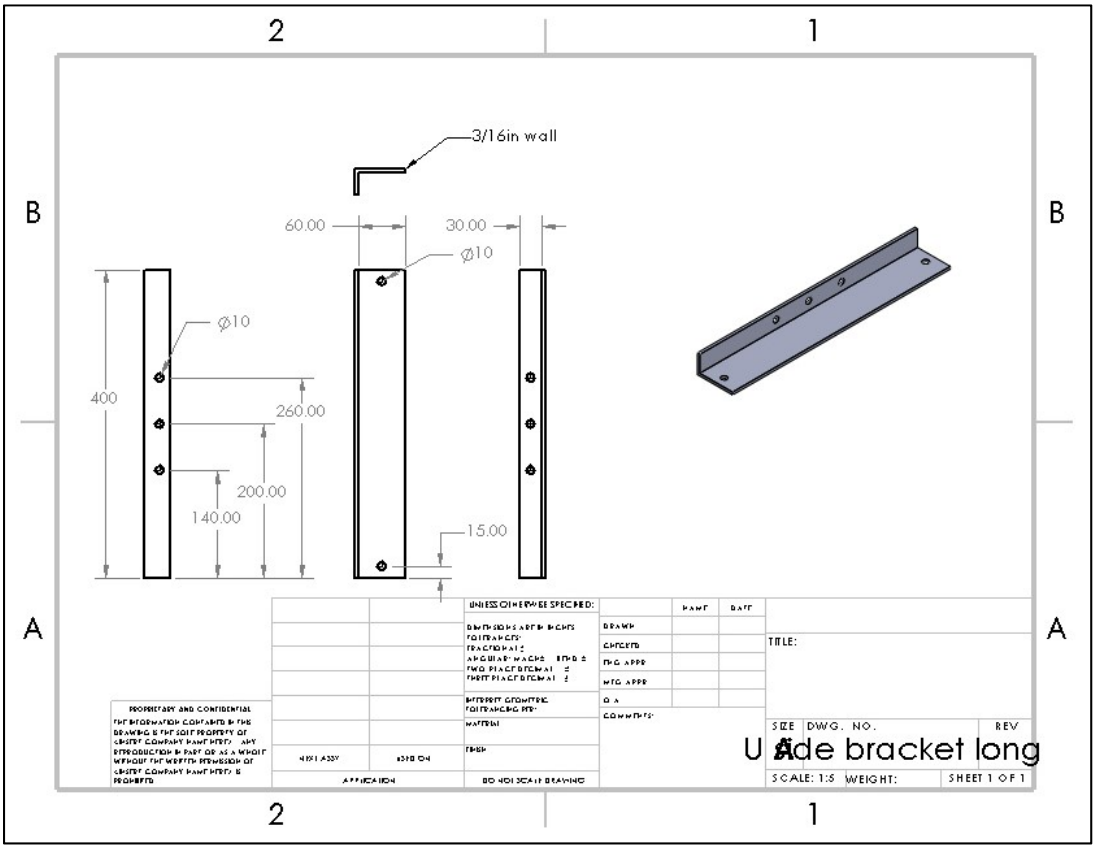

Figure-A II-4 Manufacturing drawing of the Support L base

II.3.2 Base bracket

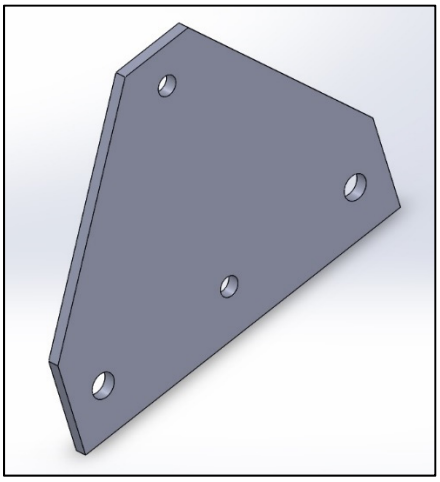

Figure-A II-5 CAD drawing
of the base bracket

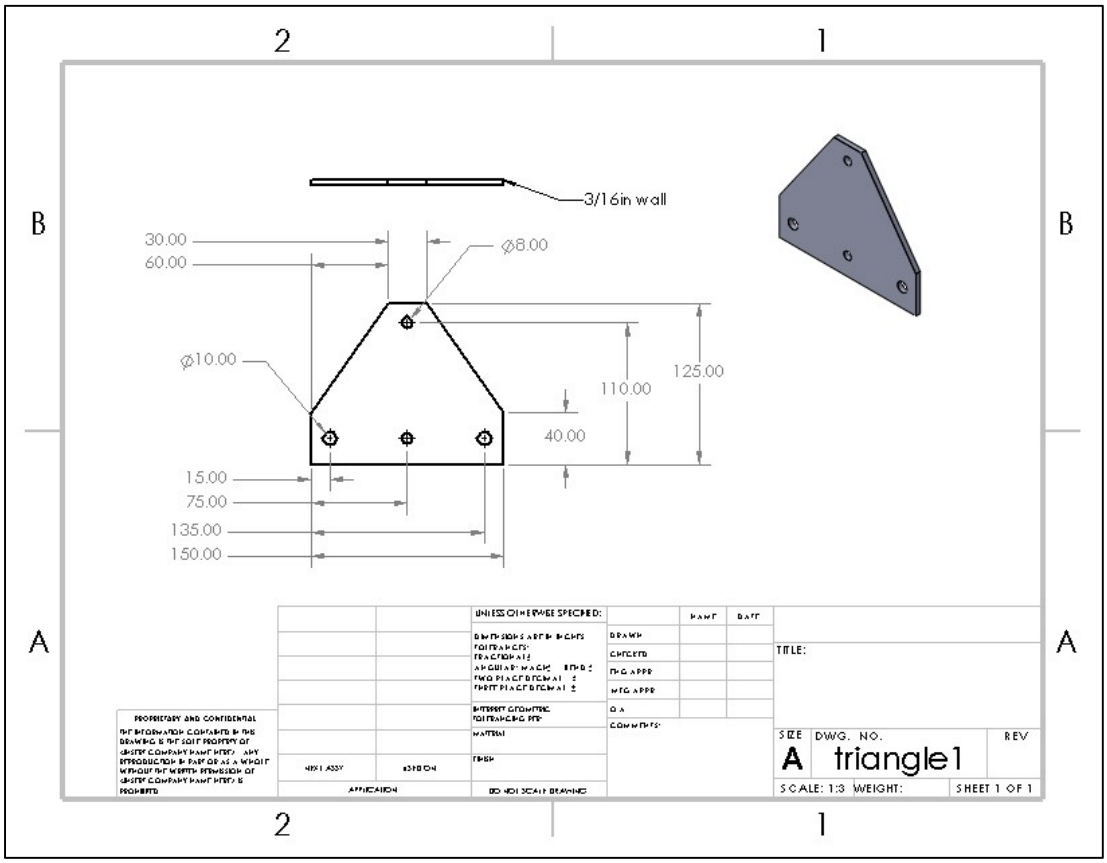

Figure-A II-6 Manufacturing drawing of the base bracket

II.3.3 Sensor Post

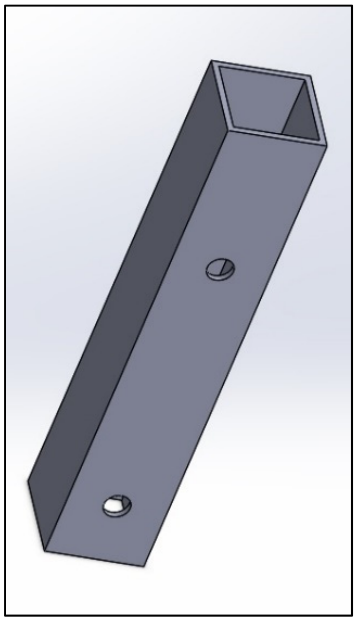

Figure-A II-7 CAD
Drawing of the Sensor Post

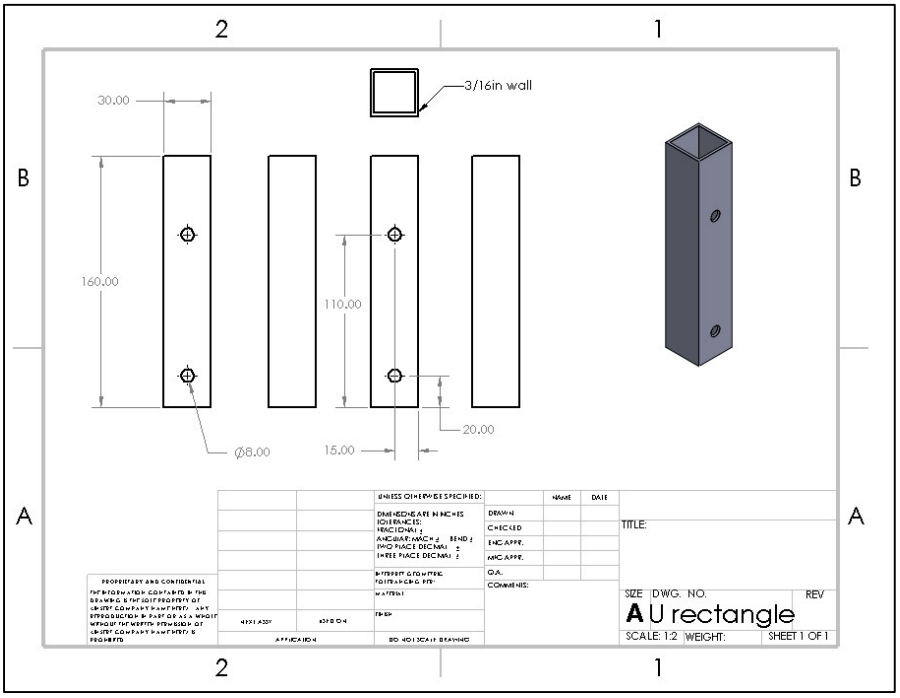

Figure-A II-8 Manufacturing drawing of the Sensor Post

II.3.4 Force sensor base

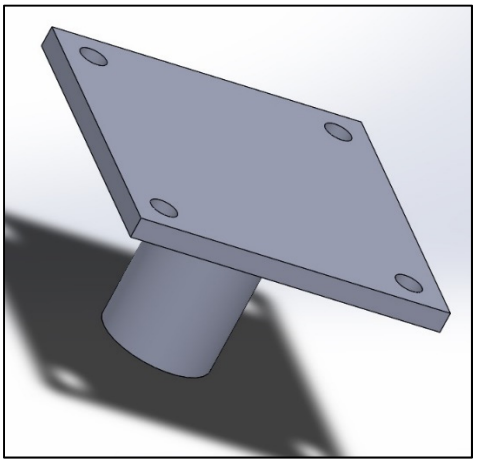

Figure-A II-9 CAD drawing of
the Force sensor base

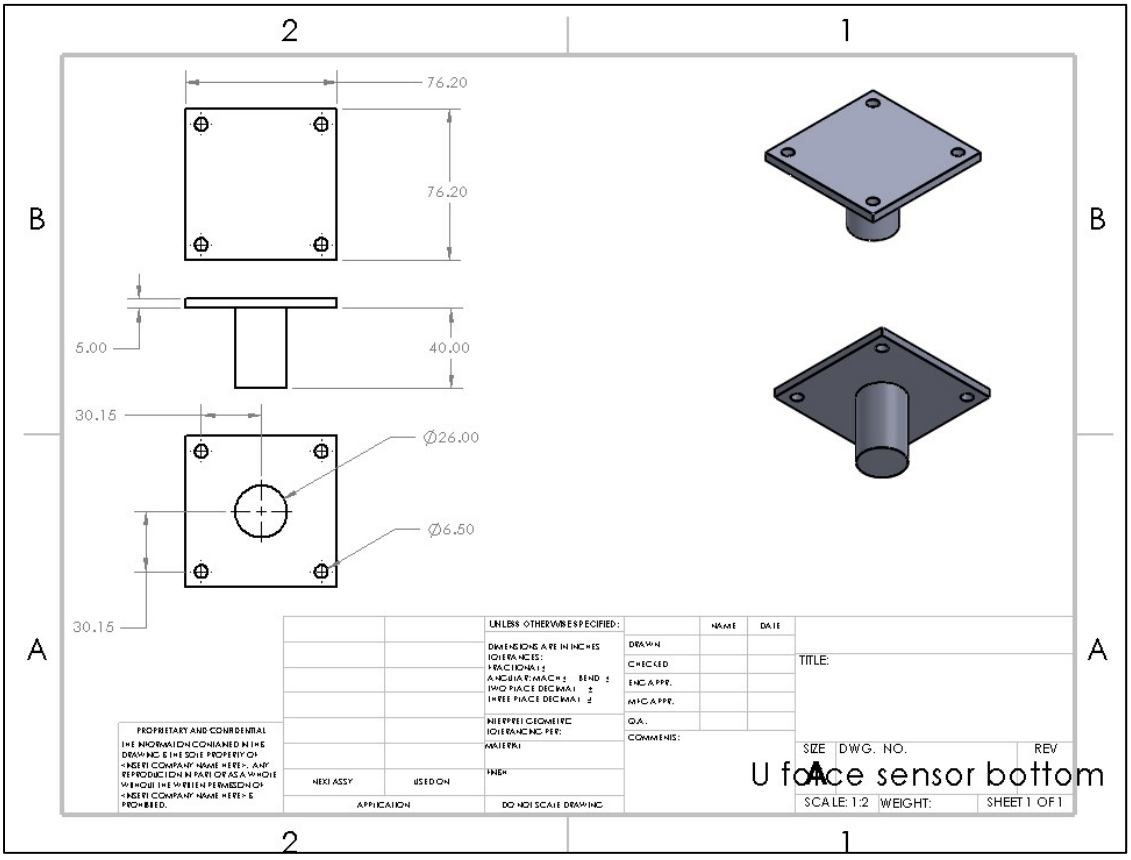

Figure-A II-10 Manufacturing drawing of the Force Sensor Base

II.3.5 Spacer

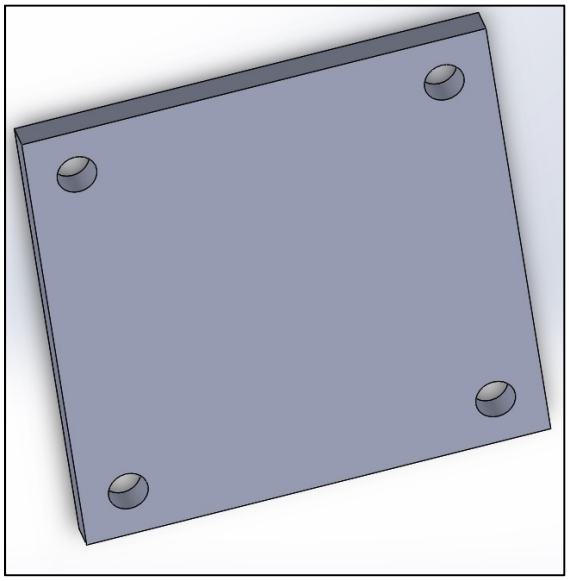

Figure-A II-11 CAD drawing of the Spacer

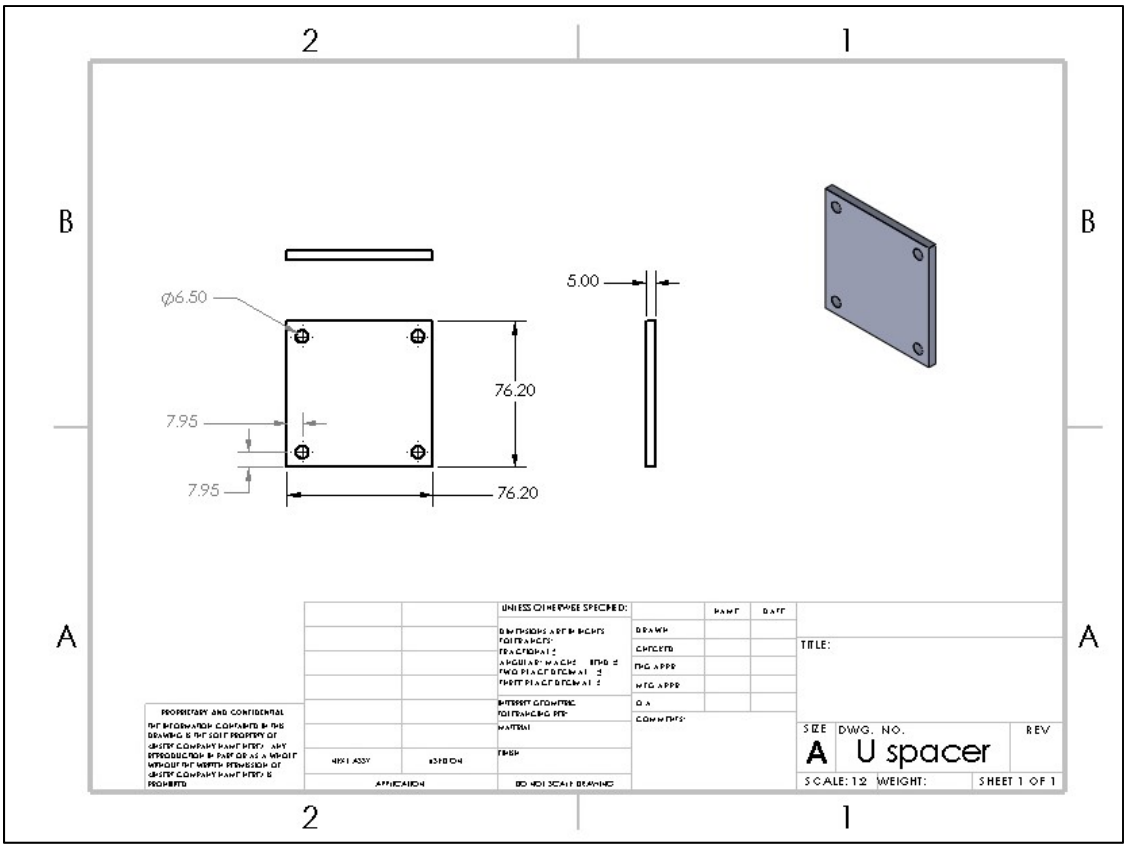

Figure-A II-12 Manufacturing drawing of the Spacer

II.3.6 Support base

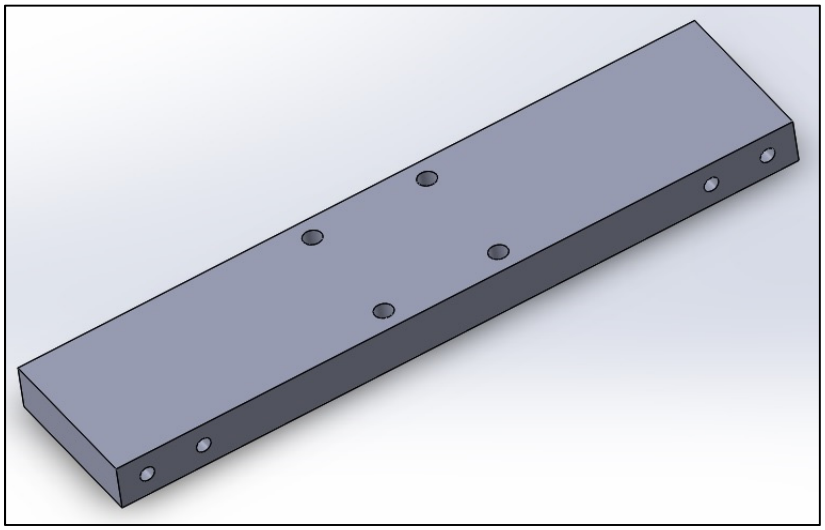

Figure-A II-13 CAD drawing of the Support base

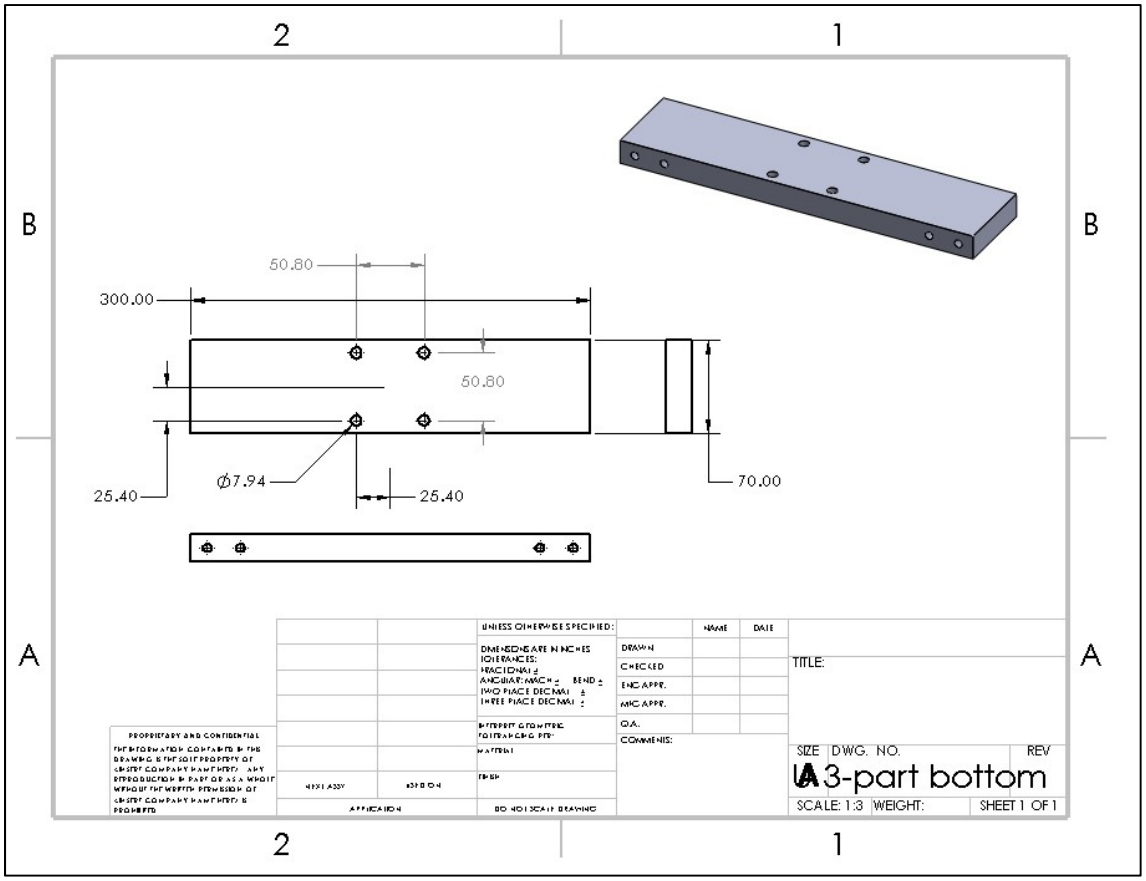

Figure-A II-14 Manufacturing drawing of the Support base

II.3.7 Lateral support

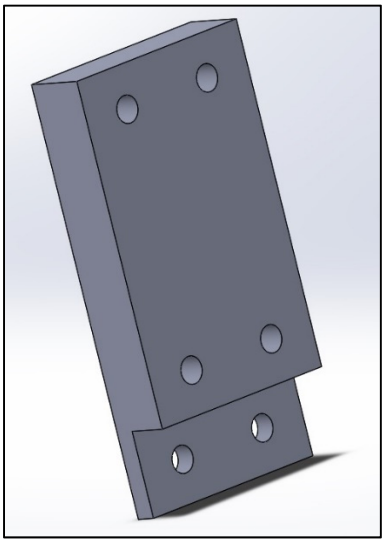

Figure-A II-15 CAD drawing
of the Lateral Support

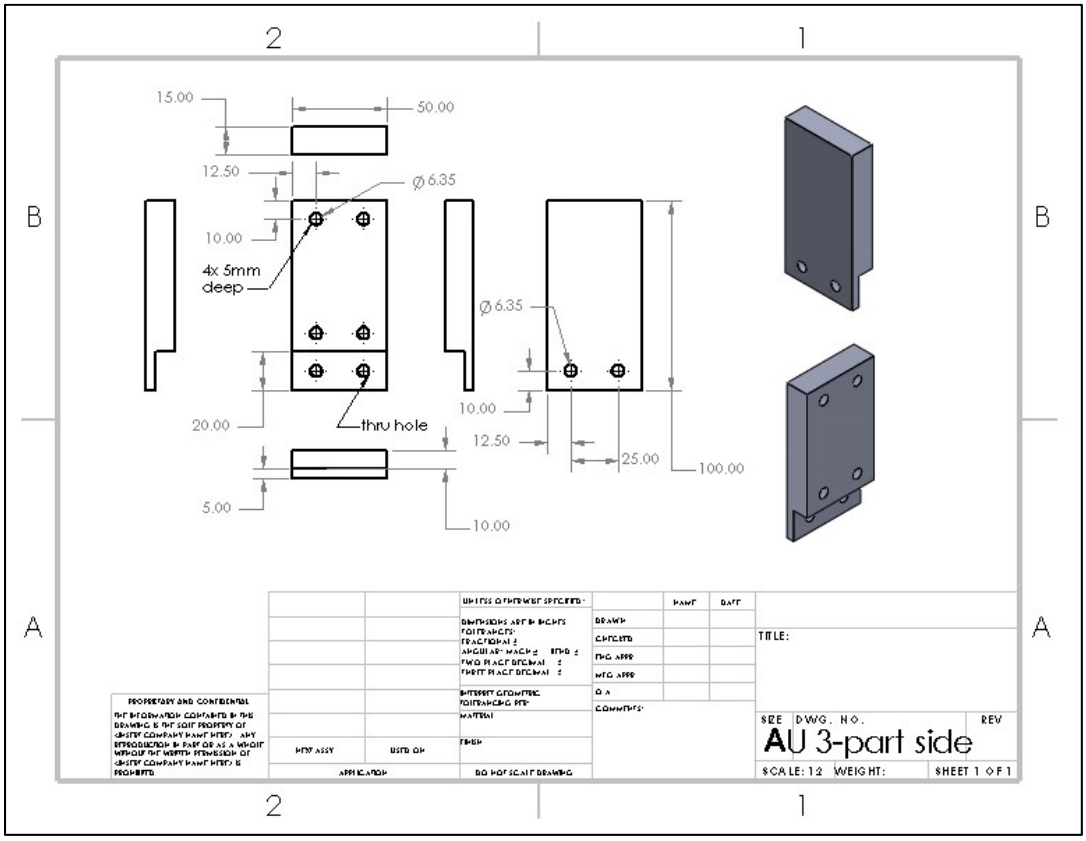

Figure-A II-16 Manufacturing drawing of the Lateral Support

II.3.8 Slider

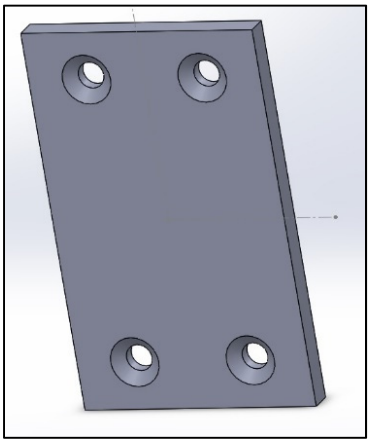

Figure-A II-17 CAD drawing of the Slider

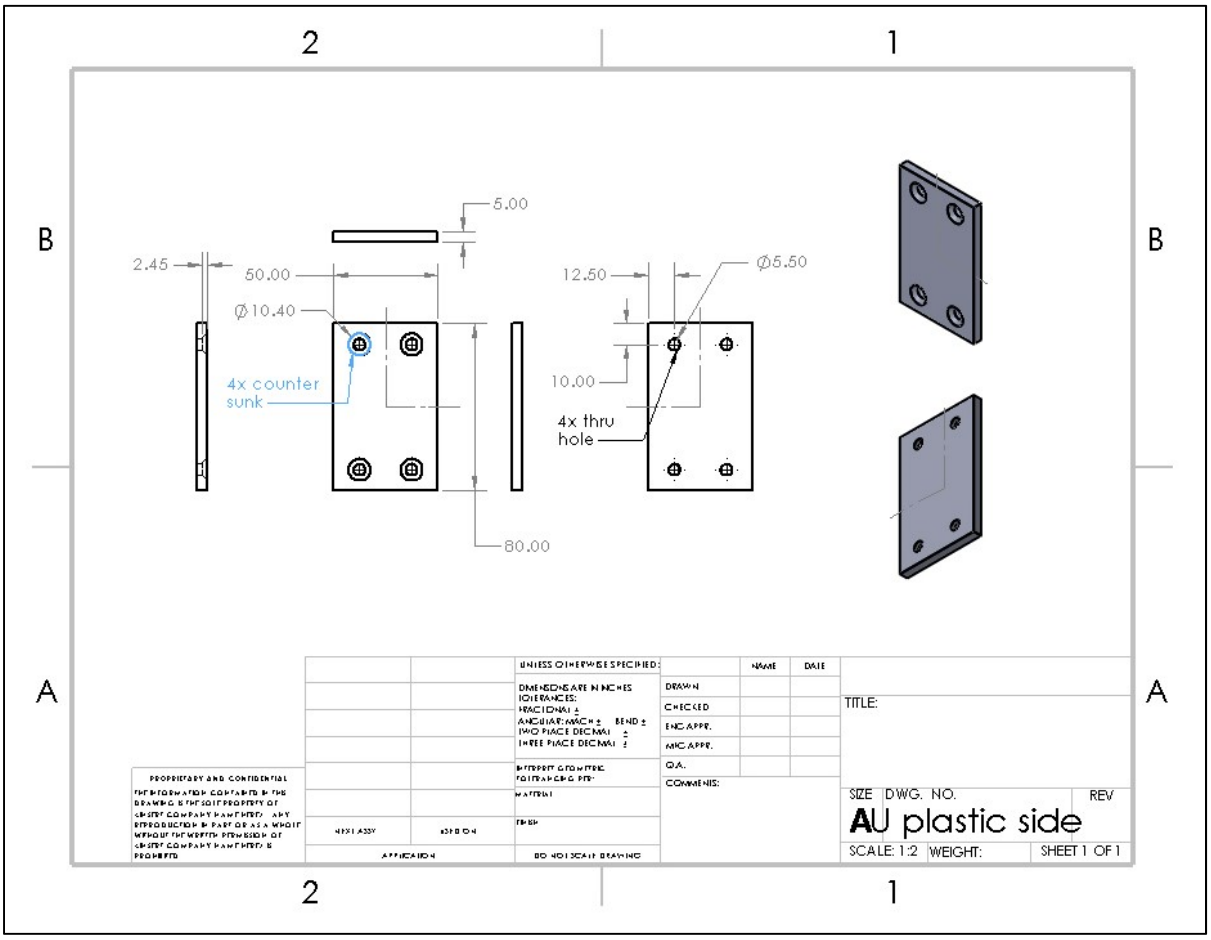

Figure-A II-18 Manufacturing drawing of the Slider

APPENDIX III

VALIDATION OF THE FORCE CELL

III.1. Validation of the multiplication factors with a dynamometer

The output from the force cell is connected to the data acquisition card DAQ PCI-6221 AI (analog inputs), installed in the real-time computer running xPC Target.

The force cell is installed underneath the seat with the output interface facing towards the front of the platform. The output variables are connected in the following way:
- $F_{X,FC}$ on channel 1 (left-right, positive left)
- $F_{Y,FC}$ on channel 2 (front-back, positive back)
- $M_{Z,FC}$ on channel 3 (around z-axis, which is vertical, positive down)

To make sure the multiplication factors used in the MATLAB model were correct, we compared the values obtained with the model to the output of a dynamometer (Shimpo, Cedarhurst, USA). The dynamometer outputs an analog voltage signal proportional to the force applied on it. This signal has a value in the range 0 to 1V, representing a measurement of 0 to 200N. In order to obtain the true measurement and plot it, we multiply the value of the voltage signal by 200.

We first examine the force along the wheelchair axle, denoted $F_{X,FC}$. The signal output by the force cell is multiplied by a gain of 145.022116 to obtain the true value of $F_{X,FC}$ in Newtons. We plot the variable obtained in MATLAB and that output by the Shimpo on Figure-A III-1**Erreur ! Source du renvoi introuvable.**. We perform a visual inspection, and notice that the curves of the two signals overlap.

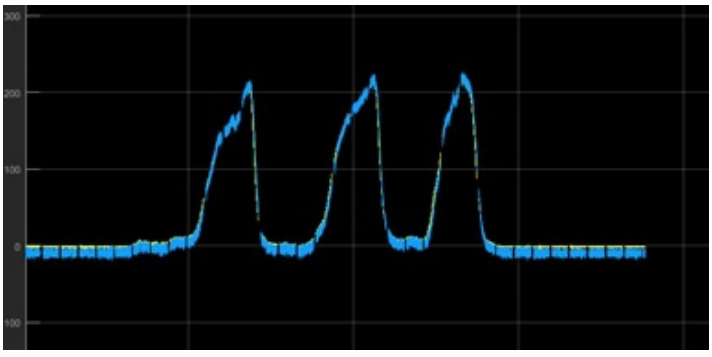

Figure-A III-1 Dynamometer (Shimpo) vs.
force cell (AMTI), $F_{X,FC}$

Now we look at the measurement of $F_{Y,FC}$, the force perpendicular to the wheelchair axle, in the plane parallel to level ground. The force cell outputs an analog voltage signal, which we

multiply by the gain of 144.701048. Once again, we plot both measurements on the same graph, which is shown on Figure-A III-2**Erreur ! Source du renvoi introuvable.**. Upon visual inspection of the graph, we notice that the curves of the two signals basically overlap.

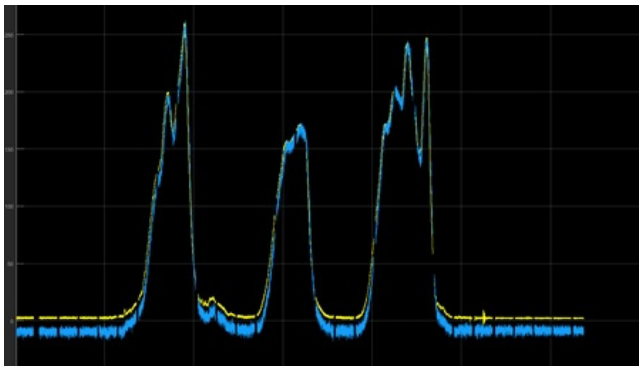

Figure-A III-2 Shimpo vs force cell, $F_{Y,FC}$

III.2 Calculation of moment arms

Using the method described in the experimental methodology, we find that with a moment arm of arm_L = 0.1080m, both curves overlap well, as shown on Figure-A III-**Erreur ! Source du renvoi introuvable.**3.

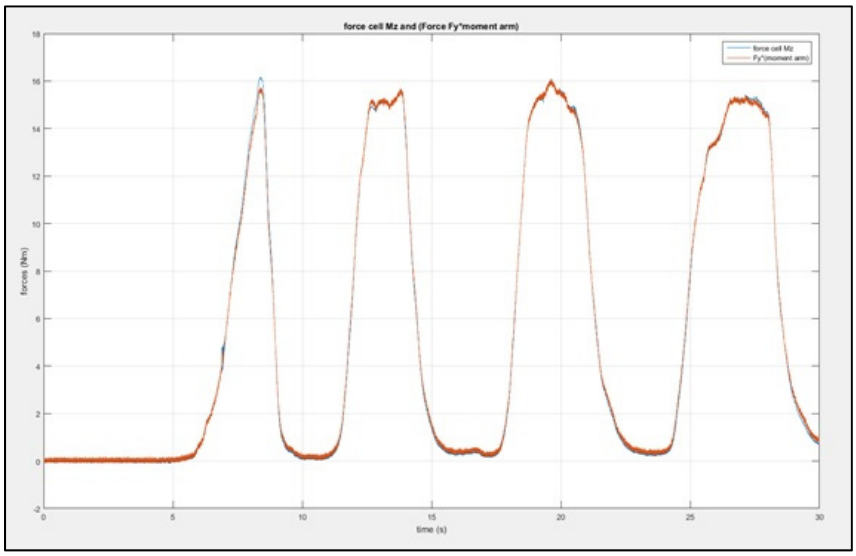

Figure-A III-3 (force $F_{Y,FC}$). (moment arm arm_L) [brown]
and vertical moment $M_{Z,FC}$ [blue]

We run the same procedure on the right side, and find a moment arm of arm_R = 0.1000m. The results are shown on Figure-A III-**Erreur ! Source du renvoi introuvable.**4.

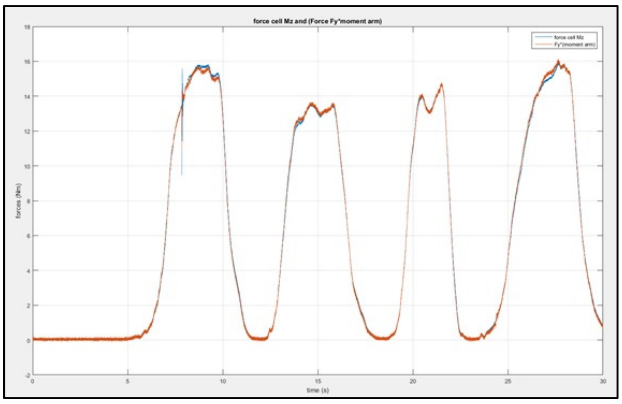

Figure-A III-4 (force $F_{Y,FC}$) . (moment arm arm_R) [brown] and vertical moment $M_{Z,FC}$ [blue]

III.3 Calculation of equivalent left and right-side forces from the antero-posterior force measured by the force cell

We recall here for completeness the equations for calculated forces $F_{yL,FC}$ and $F_{yR,FC}$, Equations (3.29) and (3.30), which are:

$$F_{yL,FC} = \frac{M_{Z,FC} + F_{y,FC}.arm_R}{arm_L + arm_R}$$

$$F_{yR,FC} = F_{y,FC} - F_{yL,FC}$$

The MATLAB model which incorporates analog inputs $F_{X,FC}$, $F_{Y,FC}$, $M_{Z,FC}$ coming from the three channels on the force cell is shown on Figure-A III-5**Erreur ! Source du renvoi introuvable.**.

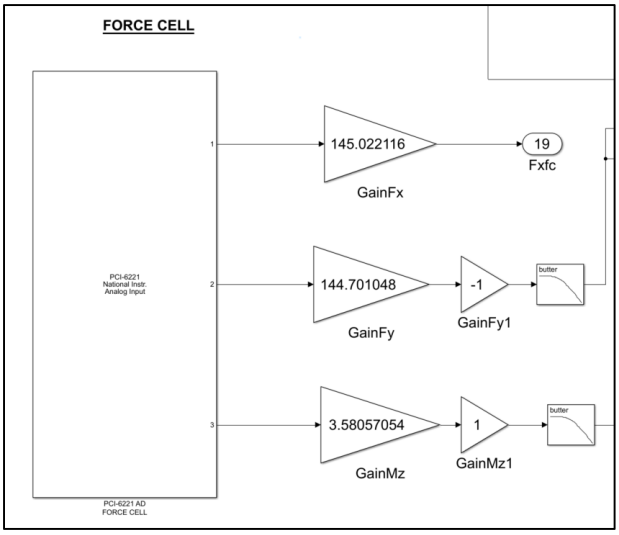

Figure-A III-5 MATLAB model showing outputs
of measurements $F_{X,FC}$, $F_{Y,FC}$ and $M_{Z,FC}$

The MATLAB model where equations **Erreur ! Source du renvoi introuvable.**(3.29) and (3.30)**Erreur ! Source du renvoi introuvable.** are part of a MATLAB function was shown on Figure 4.2**Erreur ! Source du renvoi introuvable.**. This function is called "Force cell forces" in the model.

To show the distribution of force described by equations (3.29)**Erreur ! Source du renvoi introuvable.** and (3.30)**Erreur ! Source du renvoi introuvable.**, we run a 30-second simulation, during which we propel both wheels at constant speed. We record the vertical moment $M_{Z,FC}$ and the antero-posterior force $F_{Y,FC}$, and calculate the distribution of forces $F_{yL,FC}$ and $F_{yR,FC}$. These are shown on Figure-A III-**Erreur ! Source du renvoi introuvable.**6.

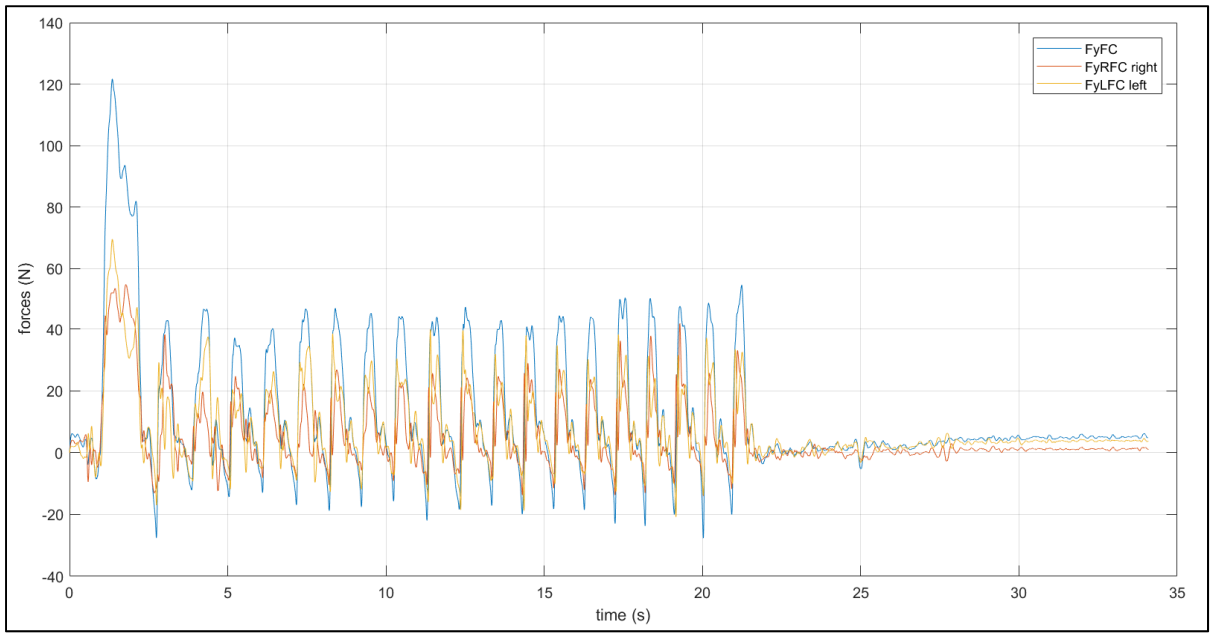

Figure-A III-6 Force cell calculated forces FyL,FC and FyR,FC, and measured force Fy,FC

BIBLIOGRAPHY

Abdossalami, A., & Sirouspour, S. (2008). Adaptive control of haptic interaction with impedance. *Proceedings of the Symposium on Haptics Interfaces for Virtual Environment and Teleoperator Systems*. Symposium on Haptics Interfaces for Virtual Environment and Teleoperator Systems. https://doi.org/10.1109/HAPTICS.2008.4479935

Abel, E., & Frank, T. (1992). A treadmill based wheelchair propulsion simulator for use in biomechanical and ergonomie studies. *Proceedings of the Annual International Conference of the IEEE Engineering in Medicine and Biology Society*, 113–114. https://doi.org/10.1109/IEMBS.1992.5760882

Akbar, M., Balean, G., Brunner, M., Seyler, T. M., Bruckner, T., Munzinger, J., Grieser, T., Gerner, H. J., & Loew, M. (2010). Prevalence of rotator cuff tear in paraplegic patients compared with controls. *Journal of Bone and Joint Surgery*, *92*(1), 23–30. https://doi.org/10.2106/JBJS.H.01373

Alton, F., Baldey, L., Caplan, S., & Morrissey, M. C. (1998). A kinematic comparison of overground and treadmill walking. *Clinical Biomechanics*, *13*(6), 434–440. https://doi.org/10.1016/s0268-0033(98)00012-6

Arlati, S., Colombo, V., Ferrigno, G., Sacchetti, R., & Sacco, M. (2019). Virtual reality-based wheelchair simulators: A scoping review. *Assistive Technology*, 1–12. https://doi.org/10.1080/10400435.2018.1553079

Bando, N., Yamada, H., Nakano, K., & Muto, T. (2004). Development of Wheelchair Simulator Using Virtual Reality. *Proceedings of Virtual Systems and MultiMedia 2004*, 708–713.

Bascou, J., Sauret, C., Pillet, H., Vaslin, P., Thoreux, P., & Lavaste, F. (2013). A method for the field assessment of rolling resistance properties of manual wheelchairs. *Computer Methods in Biomechanics and Biomedical Engineering*, *16*(4), 381–391. https://doi.org/10.1080/10255842.2011.623673

Bentaleb, T., Nguyen, V. T., Sentouh, C., Conreur, G., Poulain, T., & Pudlo, P. (2019). A Real-Time Multi-Objective Predictive Control Strategy for Wheelchair Ergometer Platform. *2019 IEEE International Conference on Systems, Man and Cybernetics (SMC)*, 2397–2404. https://doi.org/10.1109/SMC.2019.8914220

Best, K. L., Miller, W. C., & Routhier, F. (2015). A description of manual wheelchair skills training curriculum in entry-to-practice occupational and physical therapy programs in Canada. *Disability and Rehabilitation. Assistive Technology*, *10*(5), 401–406. https://doi.org/10.3109/17483107.2014.907368

Boninger, M. L., Souza, A. L., Cooper, R. A., Fitzgerald, S. G., Koontz, A. M., & Fay, B. T. (2002). Propulsion patterns and pushrim biomechanics in manual wheelchair propulsion. *Archives of Physical Medicine and Rehabilitation*, *83*(5), 718–723. https://doi.org/10.1053/apmr.2002.32455

Brose, S. W., Boninger, M. L., Fullerton, B., McCann, T., Collinger, J. L., Impink, B. G., & Dyson-Hudson, T. A. (2008). Shoulder Ultrasound Abnormalities, Physical Examination Findings, and Pain in Manual Wheelchair Users With Spinal Cord Injury. *Archives of Physical Medicine and Rehabilitation*, *89*(11), 2086–2093. https://doi.org/10.1016/j.apmr.2008.05.015

Camirand, J., Dugas, L., Cardin, J. F., Dubé, G., Dumitru, V., & Fournier, C. (2010). *Un portrait statistique à partir de l'Enquête sur la participation et les limitations d'activités de 2001 et 2006*. Institut de la statistique du Québec. http://www.stat.gouv.qc.ca/statistiques/sante/etat-sante/incapacite/incapacite-quebec.pdf

Chen, W.-Y., Jang, Y., Wang, J.-D., Huang, W.-N., Chang, C.-C., Mao, H.-F., & Wang, Y.-H. (2011). Wheelchair-Related Accidents: Relationship With Wheelchair-Using Behavior in Active Community Wheelchair Users. *Archives of Physical Medicine and Rehabilitation*, *92*(6), 892–898. https://doi.org/10.1016/j.apmr.2011.01.008

Chénier, F. (2012). *Développement D'un Simulateur De Propulsion En Fauteuil Roulant Manuel Avec Biofeedback Haptique* [Ph.D. thesis]. École de Technologie Supérieure.

Chénier, F., Bigras, P., & Aissaoui, R. (2014). A New Wheelchair Ergometer Designed as an Admittance-Controlled Haptic Robot. *IEEE/ASME Transactions on Mechatronics*, *19*(1), 321–328. https://doi.org/10.1109/tmech.2012.2235079

Chénier, F., Bigras, P., & Aissaoui, R. (2015). A new dynamic model of the wheelchair propulsion on straight and curvilinear level-ground paths. *Comput Methods Biomech Biomed Engin*, *18*(10), 1031–1043. https://doi.org/10.1080/10255842.2013.869318

Chénier, F., Champagne, A., Desroches, G., & Gagnon, D. H. (2018). Unmatched speed perceptions between overground and treadmill manual wheelchair propulsion in long-term manual wheelchair users. *Gait & Posture*, *61*, 398–402.

https://doi.org/10.1016/j.gaitpost.2018.02.009

Chénier, F., Gagnon, D. H., Blouin, M., & Aissaoui, R. (2016). A Simplified Upper-Body Model to Improve the External Validity of Wheelchair Simulators. *IEEE/ASME Transactions on Mechatronics*, *21*(3), 1641–1649. https://doi.org/10.1109/tmech.2016.2527240

Cooper, R. A. (2009). SMARTWheel: From Concept to Clinical Practice. *Prosthetics and Orthotics International*, *33*(3), 198–209. https://doi.org/10.1080/03093640903082126

Crichlow, L. R. (2011). *Development of a Comprehensive Mathematical Model and Physical Interface for Manual Wheelchair Simulation* [Master's thesis]. University of Toronto.

Curtis, K. A., Drysdale, G. A., Lanza, R. D., Kolber, M., Vitolo, R. S., & West, R. (1999). Shoulder pain in wheelchair users with tetraplegia and paraplegia. *Archives of Physical Medicine and Rehabilitation*, *80*(4), 453–457. https://doi.org/10.1016/S0003-9993(99)90285-X

de Groot, S., Vegter, R., Vuijk, C., Dijk, F., Plaggenmarsch, C., Sloots, M., Stolwijk-SwÃ¼ste, J., Woldring, F., Tepper, M., & Woude, L. (2014). WHEEL-I: Development of a wheelchair propulsion laboratory for rehabilitation. *Journal of Rehabilitation Medicine*, *46*(6), 493–503. https://doi.org/10.2340/16501977-1812

de Klerk, R., Vegter, R. J. K., Goosey-Tolfrey, V. L., Mason, B. S., Lenton, J., Veeger, H. E. J., & Van der Woude, L. H. V. (2020). Measuring handrim wheelchair propulsion in the lab: A critical analysis of stationary ergometers. *IEEE Reviews in Biomedical Engineering*, *13*, 199–211. https://doi.org/10.1109/RBME.2019.2942763

de Klerk, R., Vegter, R. J. K., Veeger, H. E. J., & Van der Woude, L. H. V. (2020). Technical note: A novel servo-driven dual-roller handrim wheelchair ergometer. *IEEE Transactions on Neural Systems and Rehabilitation Engineering*, *28*(4), 953–960. https://doi.org/10.1109/TNSRE.2020.2965281

Devillard, X., Calmels, P., Sauvignet, B., Belli, A., Denis, C., Simard, C., & Gautheron, V. (2001). Validation of a new ergometer adapted to all types of manual wheelchair. *European Journal of Applied Physiology*, *85*(5), 479–485. https://doi.org/10.1007/s004210100407

DiGiovine, C. P. (2001). Dynamic calibration of a wheelchair dynamometer. *Journal of Rehabilitation Research and Development*, *38*(1), 41–55.

Ecological Validity in Psychology: Definition & Explanation. (2020). Study.Com. https://study.com/academy/lesson/ecological-validity-in-psychology-definition-lesson-quiz.html

Ellis, R. E., Ismaeil, O. M., & Lipsett, M. G. (1996). Design and evaluation of high-performance haptic interface. *Robotica*, *14*(3), 321–327.

Faulring, E. L., Colgate, J. E., & Peshkin, M. A. (2016). The Cobotic Hand Controller: Design, Control and Performance of a Novel Haptic Display. *The International Journal of Robotics Research*, *25*(11), 1099–1119. https://doi.org/10.1177/0278364906072094

Faupin, A., Gorce, P., & Thevenon, A. (2008). A wheelchair ergometer adaptable to the rear-wheel camber. *International Journal of Industrial Ergonomics*, *38*(7–8), 601–607. https://doi.org/10.1016/j.ergon.2008.01.008

Finley, M. A., & Rodgers, M. M. (2004). Prevalence and identification of shoulder pathology in athletic and nonathletic wheelchair users with shoulder pain: A pilot study. *The Journal of Rehabilitation Research and Development*, *41*(3b), 395–402. https://doi.org/10.1682/JRRD.2003.02.0022

Forte, P., Marinho, D. A., Morouco, P. G., & Barbosa, T. (2016). CFD analysis of head and helmet aerodynamic drag to wheelchair racing. *2016 1st International Conference on Technology and Innovation in Sports, Health and Wellbeing (TISHW)*, 1–6. https://doi.org/10.1109/TISHW.2016.7847775

Frank, T., & Abel, E. W. (1991). Drag forces in wheelchairs. In *Ergonomics of manual wheelchair propulsion: State of art* (pp. 255–267).

Gagnon, D. H., Jouval, C., & Chénier, F. (2016). Estimating pushrim temporal and kinetic measures using an instrumented treadmill during wheelchair propulsion: A concurrent validity study. *Journal of Biomechanics*, *49*(9), 1976–1982.

Gauthier, C., Arel, J., Brosseau, R., Hicks, A. L., & Gagnon, D. H. (2017). Reliability and minimal detectable change of a new treadmill-based progressive workload incremental test to measure cardiorespiratory fitness in manual wheelchair users. *The Journal of Spinal Cord Medicine*, *40*(6), 759–767. https://doi.org/10.1080/10790268.2017.1369213

Grant, M., Harrison, C., & Conway, B. (2004). Wheelchair simulation. *Proceedings of the 2nd Cambridge Workshop on Universal Access and Assistive Technology*, 101–109.

Guo, L., Kwarciak, A. M., Rodriguez, R., Sarkar, N., & Richter, W. M. (2011). Validation of a biofeedback system for wheelchair propulsion training. *Rehabilitation Research and Practice*, *2011*. https://doi.org/10.1155/2011/590780

Harrison, C. S., Grant, M., & Conway, B. A. (2004). Haptic Interfaces for Wheelchair Navigation in the built environment. *Presence*, *13*(5), 520–534. https://doi.org/10.1162/1054746042545265

Hoenig, H., Landerman, L. R., Shipp, K. M., Pieper, C., Pieper, C., Richardson, M., Pahel, N., & George, L. (2005). A Clinical Trial of a Rehabilitation Expert Clinician Versus Usual Care for Providing Manual Wheelchairs: Clinical Trial of Two Ways to Provide Wheelchairs. *Journal of the American Geriatrics Society*, *53*(10), 1712–1720. https://doi.org/10.1111/j.1532-5415.2005.53502.x

Hosseini, S. M., Oyster, M. L., Kirby, R. L., Harrington, A. L., & Boninger, M. L. (2012). Manual Wheelchair Skills Capacity Predicts Quality of Life and Community Integration in Persons With Spinal Cord Injury. *Archives of Physical Medicine and Rehabilitation*, *93*(12), 2237–2243. https://doi.org/10.1016/j.apmr.2012.05.021

Hwang, S., Kim, S., Son, J., & Kim, Y. (2012). Torque and power outputs on different subjects during manual wheelchair propulsion under different conditions. *Journal of the Korean Physical Society*, *60*(3), 540–543. https://doi.org/10.3938/jkps.60.540

Johansson, C., & Chinworth, S. A. (2012). *Mobility in Context: Principles of Patient Care Skills*. F. A. Davis Company. https://fadavispt.mhmedical.com/content.aspx?bookid=1866&sectionid=139615808

Kaye, H. S., Kang, T., & LaPlante, M. P. (2000). Mobility Device Use in the United States. *Disability Statistics*, *14*, 66.

Kirby, R. L., Miller, W. C., Routhier, F., Demers, L., Mihailidis, A., Polgar, J. M., Rushton, P. W., Titus, L., Smith, C., McAllister, M., Theriault, C., Thompson, K., & Sawatzky, B. (2015). Effectiveness of a Wheelchair Skills Training Program for Powered Wheelchair Users: A Randomized Controlled Trial. *Archives of Physical Medicine and Rehabilitation*, *96*(11), 2017-2026.e3. https://doi.org/10.1016/j.apmr.2015.07.009

Kirby, R. L., Wang, S., Thompson, K., & Theriault, C. (2015). Proportion of Wheelchair Users Who Receive Wheelchair Skills Training During an Admission to a Canadian Rehabilitation Center. *Topics in Geriatric Rehabilitation*, *31*(1), 58–66. https://doi.org/10.1097/TGR.0000000000000046

Klaesner, J., Morgan, K. A., & Gray, D. B. (2014). The Development of an Instrumented Wheelchair Propulsion Testing and Training Device. *Assistive Technology*, *26*(1), 24–32. https://doi.org/10.1080/10400435.2013.792020

Koontz, A. M., Worobey, L. A., Rice, I. M., Collinger, J. L., & Boninger, M. L. (2012). Comparison Between Overground and Dynamometer Manual Wheelchair Propulsion. *Journal of Applied Biomechanics*, *28*(4), 412–419. https://doi.org/10.1123/jab.28.4.412

Kurt, M., Geyik, H., & Mutlu, B. (2008). Design, prototype and experimental evaluation of a wheelchair treadmill. *Acta Mechanica et Automatica*, *2*, 71–75.

Kwarciak, A. M., Turner, J. T., Guo, L., & Richter, W. M. (2011). Comparing handrim biomechanics for treadmill and overground wheelchair propulsion. *Spinal Cord*, *49*(3), 457–462. https://doi.org/10.1038/sc.2010.149

Lakomy, H. K., Campbell, I., & Williams, C. (1987). Treadmill performance and selected physiological characteristics of wheelchair athletes. *British Journal of Sports Medicine*, *21*(3), 130–133. https://doi.org/10.1136/bjsm.21.3.130

Lalumiere, M., Blouin, M., Chénier, F., Aissaoui, R., & Gagnon, D. (2014). To what extent are spatiotemporal and handrim kinetic parameters comparable between overground and wheelchair simulator propulsions among long-term manual wheelchair users? *Proceedings of RESNA 2014*. Rehabilitation Engineering and Assistive Technology of North America Annual Conference 2014.

MacPhee, A. H., Kirby, R. L., Coolen, A. L., Smith, C., MacLeod, D. A., & Dupuis, D. J. (2004). Wheelchair skills training program: A randomized clinical trial of wheelchair users undergoing initial rehabilitation. *Archives of Physical Medicine and Rehabilitation*, *85*(1), 41–50. https://doi.org/10.1016/S0003-9993(03)00364-2

Mason, B., Lenton, J., Leicht, C., & Goosey-Tolfrey, V. (2014). A physiological and biomechanical comparison of over-ground, treadmill and ergometer wheelchair propulsion. *Journal of Sports Sciences*, *32*(1), 78–91. https://doi.org/10.1080/02640414.2013.807350

Morgan, K. A., Engsberg, J. R., & Gray, D. B. (2017). Important wheelchair skills for new manual wheelchair users: Health care professional and wheelchair user perspectives. *Disability and Rehabilitation: Assistive Technology*, *12*(1), 28–38. https://doi.org/10.3109/17483107.2015.1063015

New Disability. (2002). *Wheelchair Statistics: How Many Wheelchair Users Are There?* http://www.newdisability.com/wheelchairstatistics.htm

Niesing, R., Eijskoot, F., Kranse, R., den Ouden, A. H., Storm, J., Veeger, H. E. J., van der Woude, L. H. V., & Snijders, C. J. (1990). Computer-controlled wheelchair ergometer. *Medical & Biological Engineering & Computing*, *28*(4), 329–337. https://doi.org/10.1007/BF02446151

Paralyzed Veterans of America, C. for S. C. M. (2005). Preservation of Upper Limb Function Following Spinal Cord Injury: A Clinical Practice Guideline for Health-Care Professionals. *The Journal of Spinal Cord Medicine*, *28*(5), 434–470. https://doi.org/10.1080/10790268.2005.11753844

Peer, A., & Buss, M. (2008). A New Admittance-Type Haptic Interface for Bimanual Manipulations. *IEEE/ASME Transactions on Mechatronics*, *13*(4), 416–428. https://doi.org/10.1109/tmech.2008.2001690

Phang, S. H., Martin Ginis, K. A., Routhier, F., & Lemay, V. (2011). The role of self-efficacy in the wheelchair skills-physical activity relationship among manual wheelchair users with spinal cord injury. *Disability and Rehabilitation*, *34*(8), 625–632. https://doi.org/10.3109/09638288.2011.613516

Pithon, T., Weiss, T., Richira, S., & Klingera, E. (2009). Wheelchair simulators: A review. *Technology and Disability*, *21*, 1–10. https://doi.org/10.3233/TAD-2009-0268

Pouvrasseau, F., Monacelli, E., Charles, S., Schmid, A., Goncalves, F., Leyrat, P.-A., Coulmier, F., & Malafosse, B. (2017). Discussion about functionalities of the Virtual Fauteuil simulator for wheelchair training environment. *2017 International Conference on Virtual Rehabilitation (ICVR)*, 1–7. https://doi.org/10.1109/ICVR.2017.8007509

Rankin, J. W., Richter, W. M., & Neptune, R. R. (2011). Individual muscle contributions to push and recovery subtasks during wheelchair propulsion. *Journal of Biomechanics*, *44*(7), 1246–1252. https://doi.org/10.1016/j.jbiomech.2011.02.073

Riley, P. O., Paolini, G., Della Croce, U., Paylo, K. W., & Kerrigan, D. C. (2007). A kinematic and kinetic comparison of overground and treadmill walking in healthy subjects. *Gait & Posture*, *26*(1), 17–24. https://doi.org/10.1016/j.gaitpost.2006.07.003

Rizzo, A. "Skip," & Kim, G. J. (2005). A SWOT Analysis of the Field of Virtual Reality Rehabilitation and Therapy. *Presence: Teleoperators and Virtual Environments*, *14*(2), 119–146. https://doi.org/10.1162/1054746053967094

Rushton, P. W., Miller, W. C., Mortenson, W. B., & Garden, J. (2010). Satisfaction with participation using a manual wheelchair among individuals with spinal cord injury. *Spinal Cord*, *48*(9), 691–696. https://doi.org/10.1038/sc.2009.197

Sauret, C., Bascou, J., Rmy, N. de S., Pillet, H., Vaslin, P., & Lavaste, F. (2012). Assessment of field rolling resistance of manual wheelchairs. *The Journal of Rehabilitation Research and Development*, *49*(1), 63. https://doi.org/10.1682/JRRD.2011.03.0050

Sauret, C., Vaslin, P., Lavaste, F., de Saint Remy, N., & Cid, M. (2013). Effects of user's actions on rolling resistance and wheelchair stability during handrim wheelchair propulsion in the field. *Medical Engineering & Physics*, *35*(3), 289–297. https://doi.org/10.1016/j.medengphy.2012.05.001

Shields, M. (2004). Use of wheelchairs and other mobility support devices. *Health Reports - Statistics Canada*, *15*(3), 37–41.

Stephens, C. L., & Engsberg, J. R. (2010). Comparison of overground and treadmill propulsion patterns of manual wheelchair users with tetraplegia. *Disability and Rehabilitation: Assistive Technology*, *5*(6), 420–427. https://doi.org/10.3109/17483101003793420

Symonds, A., Barbareschi, G., Taylor, S., & Holloway, C. (2018). A systematic review: The influence of real time feedback on wheelchair propulsion biomechanics. *Disability and Rehabilitation: Assistive Technology*, *13*(1), 47–53. https://doi.org/10.1080/17483107.2016.1278472

Symonds, A., Taylor, S. J. G., & Holloway, C. (2016). Sensewheel: An adjunct to wheelchair skills training. *Healthcare Technology Letters*, *3*(4), 269–272. https://doi.org/10.1049/htl.2016.0056

Three Rivers Holdings LLC. (2010). *Smartwheel User's Guide*. Three Rivers.

van der Woude, L. H. V., de Groot, S., & Janssen, T. W. J. (2006). Manual wheelchairs: Research and innovation in rehabilitation, sports, daily life and health. *Medical Engineering & Physics*, *28*(9), 905–915. https://doi.org/10.1016/j.medengphy.2005.12.001

van der Woude, L. H. V., Veeger, H. E. J., Dallmeijer, A. J., Janssen, T. W. J., & Rozendaal, L. A. (2001). Biomechanics and physiology in active manual wheelchair propulsion. *Medical Engineering & Physics*, *23*(10), 713–733. https://doi.org/10.1016/S1350-4533(01)00083-2

Vanlandewijck, Y. C., Verellen, J., Beckman, E., Connick, M., & Tweedy, S. M. (2011). Trunk Strength Effect on Track Wheelchair Start: Implications for Classification. *Medicine & Science in Sports & Exercise*, *43*(12), 2344–2351. https://doi.org/10.1249/MSS.0b013e318223af14

Vanlandewijck, Y., Theisen, D., & Daly, D. (2001). Wheelchair Propulsion Biomechanics: Implications for Wheelchair Sports. *Sports Medicine*, *31*(5), 339–367. https://doi.org/10.2165/00007256-200131050-00005

Velzen, J., Leeuwen, C., Groot, S., Woude, L., Faber, W., & Post, M. (2012). Return to work five years after spinal cord injury inpatient rehabilitation: Is it related to wheelchair capacity at discharge? *Journal of Rehabilitation Medicine*, *44*(1), 73–79. https://doi.org/10.2340/16501977-0899

Warms, C. A., Whitney, J. D., & Belza, B. (2008). Measurement and description of physical activity in adult manual wheelchair users. *Disability and Health Journal*, *1*(4), 236–244. https://doi.org/10.1016/j.dhjo.2008.07.002

World Health Organization. (2008). *Guidelines on the provision of manual wheelchairs in less-resourced settings*. https://www.who.int/disabilities/publications/technology/wheelchairguidelines/en/

Worobey, L. A., Kirby, R. L., Heinemann, A. W., Krobot, E. A., Dyson-Hudson, T. A., Cowan, R. E., Pedersen, J. P., Shea, M., & Boninger, M. L. (2016). Effectiveness of Group Wheelchair Skills Training for People With Spinal Cord Injury: A Randomized Controlled Trial. *Archives of Physical Medicine and Rehabilitation*, *97*(10), 1777-1784.e3. https://doi.org/10.1016/j.apmr.2016.04.006

Wu, J. (2013). *Comparison of Manual Wheelchair Propulsion in "Real-world" and Computer Simulated Environments* [Master's thesis]. University of Alberta.

Yamada, H., & Muto, T. (2004). Using Virtual Reality to Assess Factors Affecting Shipboard Accessibility for Wheelchair Users. *Control and Intelligent Systems*, *32*(1), 52–57. https://doi.org/10.2316/Journal.201.2004.1.201-1343